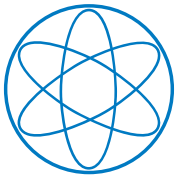

Relativistic Continuum Random Phase Approximation in Spherical Nuclei

Dissertation
von
Ioannis Daoutidis

Institut für Theoretische Physik T30
Physik Department
Technische Universität München

Physik–Department der Technischen Universität München
Theoretische Physik T30

Relativistic Continuum Random Phase Approximation in Spherical Nuclei

Ioannis Daoutidis

Vollständiger Abdruck der von der Fakultät für Physik der Technischen Universität München zur Erlangung des akademischen Grades eines

Doktors der Naturwissenschaften (Dr. rer. nat.)

genehmigten Dissertation.

Vorsitzender:		Univ.-Prof. Dr. F. von Feilitzsch
Prüfer der Dissertation:	1.	Univ.-Prof. Dr. P. Ring
	2.	Univ.-Prof. Dr. W. Weise

Die Dissertation wurde am 15.09.2009 bei der Technischen Universität München eingereicht und durch die Fakultät für Physik am 01.10.2009 angenommen.

Abstract

Covariant density functional theory is used to analyze the nuclear response in the external multipole fields. The investigations are based on modern functionals with zero range and density dependent coupling constants. After a self-consistent solution of the Relativistic Mean Field (RMF) equations for the nuclear ground states multipole giant resonances are studied within the Relativistic Random Phase Approximation (RRPA), the small amplitude limit of the time-dependent RMF. The coupling to the continuum is treated precisely by calculating the single particle Greens-function of the corresponding Dirac equation. In conventional methods based on a discretization of the continuum this was not possible. The residual interaction is derived from the same RMF Lagrangian. This guarantees current conservation and a precise decoupling of the Goldstone modes. For nuclei with open shells pairing correlations are taken into account in the framework of BCS theory and relativistic quasiparticle RPA. Continuum RPA (CRPA) presents a robust method connected with an astonishing reduction of the numerical effort as compared to conventional methods. Modes of various multipolarities and isospin are investigated, in particular also the newly discovered Pygmy modes in the vicinity of the neutron evaporation threshold. The results are compared with conventional discrete RPA calculations as well as with experimental data. We find that the full treatment of the continuum is essential for light nuclei and the study of resonances in the neighborhood of the threshold.

Kovariante Dichtefunktionaltheorie wird herangezogen um den nuklearen Response von Kernen in äusseren Multipol-Feldern zu untersuchen. Ausgangspunkt dazu bilden moderne Funktionale mit verschwindender Reichweite und dichteabhängigen Kopplungskonstanten. Zunächst wird der Grundszustand im Rahmen der relativistischen Mittelfeld-Näherung (RMF) behandelt. Darauf aufbauend werden elektrische Multipole-Resonanzen im Rahmen der relativistischen Random-Phase-Näherung (RPA) untersucht, der sich im Limes kleiner Amplituden aus der zeitabhängigen RMF-Theorie ergibt. Entscheidend ist dabei die Kopplung an das Kontinuum, die durch die Berechnung der Greens-Funktion der zugehörigen Dirac-Gleichung exakt behandelt wird. Dies war in den konventionellen Methoden, die auf einer Diskretisierung des Kontinuums beruhten, nicht möglich. Die Restwechselwirkung in den RPA-Rechnungen wird selbst-konsistent aus dem Dichtefunktional abgeleitet. Das garantiert Strom-Erhaltung und eine exakte Entkopplung der Goldstone-Moden. Zur Behandlung von Kernen mit offenen Schalen wird die BCS-Methode und die entsprechende Quasiteilchen-RPA herangezogen. Kontinuum-RPA (CRPA) stellt eine sehr robuste Methode dar, die im Vergleich zu den bisher üblichen Methoden der diskreten RPA zu einer erheblichen Reduktion des numerischen Aufwands führt. Moden mit verschiedenem Drehimpuls und Isospin werden untersucht, insbesondere auch die kürzlich gefundene Pygmy-Resonanz an der Neutronen-Schwelle. Die Resultate werden mit Rechnungen im Rahmen der diskreten RPA und mit Experimenten verglichen. Es ergibt sich, dass eine exakte Behandlung des Kontinuums zur Beschreibung leichter Kerne und an der Schwelle zum Teilchen-Kontinuum von entscheidender Bedeutung ist.

Acknowledgements

First and foremost I would like to thank my supervisor, Prof. Dr. Peter Ring, not only for stimulating discussions and timely advice, but also for his support throughout the various phases of the work presented in this document. His understanding and experience in many areas has made a pleasure working with him. I am particularly grateful for his optimism and overall confidence in the project, always trying to point me on the right direction.

Many thanks go also to Prof. Dr. George Lalazissis, who has always been a source of interesting conversations and important advice. It is a pleasure for me to thank all my colleagues and friends who have provided support and company during my time in Munich, with a special mention to Daniel Arteaga, Ignacio W. Rae, Javier Madronero, Aykut Erbas, Immanuel Kalcher and Douwe Bonthuis but also to my greek friends Kyriaki Kosma, Kalatzantonaki Pano, Kitsiki Agi, Tsipouridi Maki and Matiaki Tilemacho.

A great deal of joy came from my Greek buddies Stelios and Peter who always made me forget my difficult times in Germany specially during the unforgettable nights of endless nargile and Whishkey. Their support was the dopping I needed to continue through.

Finally, I should like to thank my family for support and understanding whilst I have been away from home. Mama, Mpampa, Zwi, mou peire enan aiona alla ta katafera. Sas Euxaristw poli gia ola. Above all, the most important "thanks" goes to Jenny Manolopoulou for her love, patience and encouragement.

Contents

List of used Acronyms **xi**

1 Introduction **1**

2 Nuclear Density Functional Theories **9**
2.1 Basic concepts of DFT 9
2.1.1 Hohenberg Kohn Theorems 9
2.1.2 Self Consistent Kohn-Sham Equations 12
2.1.3 Nuclear Density Functional Theory 14
2.2 Relativistic Mean Field Theory of Finite Range 16
2.2.1 Equations of Motion 18
2.2.2 Extended versions and Medium Dependences 19
2.3 Relativistic MFT of Zero Range (Point Coupling) 21
2.4 PC-RMF Parameterizations 25

3 Random Phase Approximation **29**
3.1 Matrix Representation of RPA 30
3.2 Linear response theory 33
3.2.1 The strength function 35
3.2.2 Sum Rules 36
3.2.3 Separability and Channel Representation 37
3.3 The Point coupling Effective Interaction 38
3.3.1 Relativistic Free Response Function 43
3.3.2 Bethe-Salpeter Equation 45
3.4 Achievements and Limitations of Discretization Methods 47
3.5 Continuum RPA 49
3.5.1 Green's Function Formalism 50

4 Results **55**
4.1 Numerical Details 56
4.2 Multipole Resonances 57
4.2.1 Isoscalar Giant Monopole Resonances 57
4.2.2 Isovector Giant Dipole Resonances 61
4.2.3 Isoscalar Giant Dipole Resonances 67
4.2.4 Isoscalar Giant Quadrupole Resonances 71

5 Quasiparticle continuum RPA **73**

5.1 The RMF plus BCS Model 74
5.2 Linear Response Theory with Pairing 77
5.3 Dynamical Pairing 80
5.4 CQRPA Calculations and the Spurious State 82
5.4.1 Tin Isotopes 84

6 Conclusion and outlook **87**

A Rearrangement terms of the residual Interaction **91**
A.1 PC-F1 92
A.2 DD-PC1 97

B Derivative Terms in the Point-Coupling Interaction **99**

List of used Acronyms

BCS Bardeen-Cooper-Schrieffer

CRPA Continuum RPA

CRRPA Continuum Relativistic Random Phase Approximation

DB Dirac Brueckner

DD-ME1 Parametrization of the relativistic density dependent meson exchange functional

DD-ME2 Parametrization of the relativistic density dependent meson exchange functional

DD-PC1 Parametrization of the relativistic density dependent point coupling functional

DFT Density Functional Theory

DRPA Discrete RPA

E1 Electric $J^\pi = 1^+$ transitions

EFT Effective Field Theory

EWSR Energy Weighted Sum Rule

GDR Giant Dipole Resonance

GMR Giant Monopole Resonance

HF Hartree Fock

HFB Hartree Fock Bogoliubov

HK Hohenberg-Kohn

ISGMR Isoscalar Giant Monopole Resonance

ISGQR Isoscalar Giant Quadrupole Resonance

ISGDR Isoscalar Giant Dipole Resonance

IVGDR Isovector Giant Dipole Resonance

KS Kohn-Sham

LDA Local Density Approximation

M1 Magnetic $J^\pi = 1^+$ transitions

MF Mean Field

NL3 Parametrization of Relativistic Mean Field non linear model

PC-F1 Parametrization of relativistic density dependent point coupling functional

PDR Pygmy Dipole Resonance

QCD Quantum Chromodynamics

QRPA Quasiparticle Random Phase Approximation

RDFT Relativistic Density Functional Theory

RHB Relativistic Hartree Bogoliubov

RMF Relativistic Mean Field

RPA Random Phase Approximation

RQRPA Relativistic Quasiparticle Random Phase Approximation

RRPA Relativistic Random Phase Approximation

TDDFT Time Dependent Density Functional Theory

TRK Thomas-Reiche-Kuhn

Chapter 1

Introduction

With the construction of new facilities using radioactive beams the investigation of nuclei far from stability has gained considerable interest in recent years. Knowledge of such exotic nuclei may improve our present insight, not only into the origin of element abundances on the earth, but also into the processes leading to the formation of matter in the universe. The most prospective paths for the formation of heavy elements are the s-process (slow neutron capture), the r-process (rapid neutron capture) and the rp-process(rapid proton capture). It is assumed that the rapid processes run in environments with high isospin asymmetry, and that the subsequent-decays are slower than the captures, resulting in the production of elements heavier than iron. Complex nuclear reaction networks used in the study of these phenomena need the input of nuclear data, as far as possible from experiment but in most of the cases, where experiments are not available, from calculations based on the theory of nuclear structure.

The majority of theories of nuclear structure which have been developed so far are based on the simple argument that the nucleus consists of point-like protons and neutrons. For a long time, this assumption was also the only one available since, after their discovery, these two particles were identified as the elementary constituents of the nucleus.

Today we know, of course, that this is not true and that these two kind of nucleons - unlike the electron - do have inner structure, created by combinations of quarks, gluons, and anti-quarks. Therefore, it is legitimate to think that a theory that includes quarks and gluons as the main degrees of freedom in a unique way should be the starting point towards a description of the nuclear phenomena over the entire nuclear chart. Indeed, such an idea has turned into one of the most successful theories, the Quantum Chromodynamics (QCD).

However, the link between QCD and the bare nucleon-nucleon force remains one of

the long-term goals of nuclear theory. The difficulty in describing quantitatively the structure of the interaction between nucleons in this way is due to its non-perturbation character at low energies. Even though, to date, only a qualitative understanding of nucleons in terms of full QCD has been possible. Efforts that take the underlying symmetries as a basis and exploit the separation of scales in terms of the relevant degrees of freedom in the framework of effective field theories (EFT) [1] look very promising. Other new approaches start with phenomenological two-nucleon potentials adjusted to the nucleon-nucleon scattering data and take advantage of the relatively low energy dynamics of the nucleus to extract a universal potential that cuts out the high momentum part of the interaction.

Our main goal is, of course, to achieve a global description of nuclear systems ranging in size from the deuteron to nuclear matter and to neutron stars using a single parameterization of the nuclear forces. Historically, the idea of employing a bare nucleon-nucleon interaction from ab-initio calculations had always been in quest. Improvements in this direction through the last decades have been able to provide us with a series of quite remarkable realistic two- and three-nucleon potential models, such as Argonne v18 [2], Illinois IL2 [3, 4], or N^{3}LO [5]. Several methods have been developed upon these forces to perform exact solutions of the nuclear many-body problem for very light nuclei, such as the Green's Function Monte Carlo (GFMC) method [3], the No-core Shell Model (NCSM) [6], or Coupled Cluster (CC) methods [7]. One also hopes to calculate saturation properties of dense nuclear matter. However, the complexity of these calculations renders the method practically unfeasible for cases beyond p-shell nuclei.

For somewhat heavier nuclei configuration mixing (CI) calculations are possible. In nuclear physics they are usually called Shell Model (SM) calculations. In this case one concentrates on a limited configuration space, as for instance the sd-shell in an harmonic oscillator basis and diagonalizes the full nuclear hamiltonian within this limited basis [8]. Of course the corresponding hamiltonian is an effective one. It depends on the underlying configuration space and the matrix elements are usually adjusted to experimental data. For nuclei beyond A=40 the configuration spaces grow quickly to astronomical numbers. By now, one has techniques to diagonalize matrices of dimension 10^{10}, which corresponds to the full pf-shell [9]. Such calculations are also possible for heavier nuclei, but only in the vicinity of closed shells.

For that purpose, alternative methods have been developed, usually in the form of self-consistent mean field theories. Their starting point is the assumption that, in first order, the nucleons inside the nucleus can be considered as independent particles moving in an average field generated by the other nucleons. Phenomenological in nature, these methods are very successful in describing bulk nuclear properties all across the nuclear chart, which makes them a very powerful tool for the study of nuclear phenomena.

Their principles are based on the Density Functional Theory (DFT), which is widely used in many-body systems dominated by the Coulomb force, such as atomic physics,

molecular physics, quantum chemistry, or solid state physics. It has been introduced by Kohn and Sham [10, 11] in the sixties and is based on an energy functional $E[\rho]$ [12] which depends on the local single particle density which is in principle exact. It avoids the use of complicated many-body wave functions and explicit matrix elements of the underlying hamiltonian.

A few years after DFT had been known in other areas of physics, a similar idea was introduced in nuclear physics. It was based on the idea of Brueckner that, due to the Pauli principle and the uncertainty relation, the nuclear interaction is considerably modified in the nuclear interior [13, 14]. In particular it depends strongly on the density. This effective density-dependent interaction was used for density dependent Hartree-Fock (DDHF) calculations [15, 16]. It was quickly recognized that this method is more or less equivalent to density functional theory in the sense of Kohn and Sham where the energy density $E[\rho]$ is the HF-energy calculated with these density dependent forces.

Nuclear density functional theory does not depend on any bare two-nucleon or three-nucleon-interaction, rather it uses effective density-dependent forces, which are adjusted to experimental data in nuclear matter and finite nuclei. It has turned out that these phenomenological methods are extremely successful in describing many nuclear properties all over the periodic table.

The first approaches of this type used a non-relativistic framework. This can be understood, if one considers that nuclear structure phenomena were limited to nucleon velocities small compared to the speed of light and to energy scales considerably smaller than the nucleon rest mass.

It is evident that one does not have to consider relativistic kinematics in the nuclear system. However, during the last decades [17, 18, 19], it has turned out that even without relativistic kinematics there are several properties which can be understood only in terms of very strong relativistic potentials in the nucleus and that a relativistic description has many advantages. Within this framework, the average nuclear potential in the nuclear interior is a sum of a very strong attractive scalar potential $S(r)$ of roughly 400 MeV depth and a nearly as strong repulsive vector potential $V(r)$ of roughly 350 MeV. The size of both potentials is no longer small against the rest mass of the nucleons, but in the nuclear interior they cancel more or less and one is left with a slightly attractive potential of roughly 50 MeV leading to relatively small momenta and allowing a non-relativistic approximation. On the other side these two strong potentials add up in the spin orbit term, leading to the very strong spin-orbit splitting which was well known (but not understood) since the early days of the nuclear shell model [20].

The idea to describe the nucleus as a relativistic system has been pushed much by Walecka [21], who developed a relativistic quantum field theory Quantum Hadrodynamics (QHD) based on the Lagrangian description of the nuclear systems rather than on the NN-potentials. In the framework of this unique approach, the nuclear proper-

ties are described by point-like nucleons interacting through the exchange of mesons. QHD puts nuclear theory on a qualitatively new level, at which it can be regarded as a relativistic quantum field theory. Of course, the exact relativistic quantum-field description corresponding to Walecka Lagrangian is very complicated. In particular, despite the fact that it can be shown formally by power counting that it is a renormalisable model [19], one meets serious problems using perturbation theory in practice because of the large values of the coupling constants. For example, it has been shown that loop expansions do not converge [22]. Therefore the idea of a fully fledged quantum field theory has been given up.

However, it turns out that in the framework of this model it is possible to obtain many important results by using the *mean-field approximation*, i.e. by treating the meson fields that occur in the Walecka approach as classical fields[1]. So the Lagrangian of the relativistic mean-field theory (RMF) may be considered as an effective Lagrangian for relativistic calculations in the same sense as the Skyrme potential is an effective force for classical non-relativistic mean-field calculations.

In the basis of RMF, one considers that the meson fields are purely phenomenological. By adjusting only a few model parameters (coupling constants and effective masses) to global properties of spherical nuclei, it has been possible to describe many nuclear structure phenomena, not only in nuclei along the valley of stability, but also in exotic nuclei with extreme isospin values and nuclei close to the particle drip lines. The theory is based on the following assumptions: i) nucleons are treated as point particles, ii) relativity is fully taken into account and iii) nucleons move as independent particles in the corresponding mean fields. The nuclear many body problem is described by Dirac equations containing a mass operator and including meson fields with different spin, parity and isospin properties. In almost all implementations for nuclear matter and finite nuclei, RMF is treated in the no-sea approximation: the Dirac sea is assumed to be empty, hence the negative energy states do not contribute to the calculation of the local densities and currents.

Besides the proper treatment of the spin-orbit splitting, relativistic mean field models have a number of additional advantages as compared to the corresponding non-relativistic methods, as for instance the interpretation of pseudo-spin symmetry in the nuclei [23, 24, 25, 26], or the proper description of currents and nuclear magnetism in nuclear systems with time-reversal breaking in the intrinsic frame as in odd-mass nuclei or in rotating nuclei [27, 28, 29, 30]. Already, the relativistic treatment provides good description of the experimental data for the total binding energy of nuclei, the charge distribution radii and the separation energies, competing successfully the Skyrme and Gogny forces. The binding energies and the charge radii are reproduced to an accuracy of less than a percent. Finally, kink effect in the r.m.s. charge radii behavior in the Ph-isotopic chain appears also to be an inherent feature of a relativistic treatment of

[1] Although this approximation was provided by Walecka only in the limit of high densities, its use also at observed nuclear densities is justified by the large number of experimental results that are nicely reproduced.

the system [31], since they cannot be predicted by the conventional non-relativistic models.

After it had been realized that the Walecka model [18] with all its nice properties was not able to reproduce the surface properties of nuclei in a satisfactory way, Boguta and Bodmer [32] introduced a density dependence by non-linear meson couplings. This was the real break through for the relativistic description of high precision of many nuclear properties. It was recognized that this density dependent version of the Walecka model was a covariant version of nuclear density functional theory [33, 34, 35, 36, 37, 38]. The mesonic degrees of freedom have little to do with mesons in free space. They only are considered in the framework of fields with relativistic quantum numbers. The classical Lagrangians of such models provide a Lorentz-invariant framework for a relativistic density functional theory and the resulting Dirac-equations are equivalent to the non-relativistic effective potential of Kohn and Sham.

In recent years, an alternative RMF model has appeared, the flexibility of which has gained many credits, as compared to non-linear models. Firstly introduced by Brockmann and Toki [39], it is based on the ansatz that no higher order terms are needed, once the meson coupling constants are density dependent. This idea had good reasons to succeed, since it is consistent with the relativistic approaches constrained by QCD and chiral symmetries [40]. Of course, the credibility of this model relies on the form of this density dependance and on the correct choice of the required parameters. The DD-ME1 [41, 42] and even more the DD-ME2 [43] parameter sets have reached the highest level of accuracy even on exotic nuclei and nuclei close to the drip lines.

A question arises on whether one can do better than that. The answer can be positive if we proceed not only in terms of quantitative agreement with experimental data, but also in terms of simplicity and efficiency of the equations. All the previous approaches have in common finite-range meson fields. However, a zero-range or point coupling model, which has to be seen as the relativistic equivalent to the non-relativistic Skyrme interaction, has been proven to reach the same level of accuracy by using a very simple zero-range Lagrangian. This point coupling RMF had been introduced by Manakos et.al. [44, 45] and later on by Bürvenich et. al. [46], who also proposed a new phenomenological set, capable of achieving a very nice agreement with the experimental data.

The above RMF approaches should be able to give a quantitative agreement with the ground state properties of wide majority of nuclei. In practice, in their initial form, they are restricted to spherical double-closed nuclei. In spherical open shell nuclei and in particular in nuclei where spherical symmetry is not preserved, pairing between nucleons play a very important role and certain correlations must be taken into account. In this direction, the BCS approximation which reconstructs the single particle spectrum by applying finite occupation probabilities, has been a very simple and successful scheme for treating those correlations [47, 48]. However, it faces severe problems in nuclei close to the drip lines, where the Fermi level is very close to the

continuum. In these cases, one has to use the Relativistic Hartree (RHB) model [49, 50, 37] that treats pairing correlations in a more consistent way. In the latter model, an explicit pairing channel is included and often expressed by a non-relativistic Gogny interaction. Since this force has a finite range, one obtains a natural cutoff, avoiding in this way one of the most important problems that plague BCS and other schemes involving artificial pairing windows.

Summarizing, the relativistic mean field approaches are effective models that give a very nice overview of the ground state properties of light and heavy nuclei, such as binding energies, radii, density distributions, deformation parameters, moments of inertia, and with some restrictions [51] also to single particle energies. However, static single particle models fail to describe collective phenomena of nuclei, such as rotations or surface and multipole oscillations, known as giant resonances. We call them collective because many nucleons are participating in these excitations in a coherent way. In order to investigate these nuclear properties, one needs to go beyond the ground state and consider oscillations around the self-consistent static solution. This can be done by solving the time-dependent relativistic mean field equations (TDRMF) [52] or the relativistic Random Phase Approximation (RRPA) [53, 54, 55, 56] that is the small amplitude limit of the time-dependent RMF. RRPA and RQRPA * has proven itself as a very powerful tool in providing high level of quantitative agreement. In addition, it is based on a fully self-consistent solution of the time-dependent mean field equations and therefore one does not need any additional parameter to describe the dynamical problem.

The concept of resonance appears everywhere in the dynamics of physical systems. All isolated multi-particle systems have natural vibrational frequencies, and the resonance phenomenon describes how these modes couple to the surrounding environment. There is such a mode in almost any multipolarity and isospin channel. The most prominent resonances are the Isovector Giant Dipole Resonance (IVGDR) which to a first approximation is a collective vibration of protons against neutrons, the Isoscalar Giant Monopole Resonance (ISGMR), which describes an isoscalar breathing of the nucleus as a whole, and the Isoscalar Giant Quadrupole Resonance (ISQR) which corresponds to small collective quadrupole oscillations with T=0. These modes show up in an energy range of $10 - 30$ MeV and they exhaust a dominant portion of the corresponding sum rule.

There is a long standing history of microscopic calculations of giant resonances and nowadays, one faces a world of valuable information in the resonance excitation spectra [52, 59, 60, 61]. For instance, it is known that the asymmetry parameter α_{sym} of the empirical mass formula, as well as the sum rule enhancement κ are closely related to the excitation energy of the GDR. In addition, the nuclear matter incompressibility is proportional to the position of the isoscalar monopole resonance, where the correct position of the quadrupole resonance is an indication of an effective mass of the field

*Relativistic Quasiparticle RPA (RQRPA) [57, 58] is a straightforward generalization of the RPA to include pairing correlations

close to $m^*/m = 0.8$ etc.

The position and the transition strength of the giant resonances can be determined either by diagonalizing the RRPA equations in an appropriate basis or by solving the linear response equations in a time-dependent external field. However, these models treat another important quantity in a very different way, namely the coupling to the continuum inducing a width to the resonances. The treatment of the continuum is a very important issue, particularly for the study of exotic nuclei, where the Fermi level is close to the continuum limit. Almost all the successful RRPA and RQRPA methods, so far, have been treating the continuum by expansion of the *ph*-wave functions in an appropriate basis, given for instance by a finite number of eigenfunctions of a harmonic oscillator [62] or of a Saxon-Woods potential in a finite box [63]. In such a way, RPA fails to provide a mechanism to produce continuous spectrum of the strength distribution.

In non-relativistic systems a solution to those problems has been achieved with the exact coupling to the continuum. Already in the seventies a series of non-relativistic models has been developed to include this mechanism. They are usually known under the name continuum RPA (CRPA) [64, 65].The treatment of the continuum single-particle states as scattering waves is clearly a more realistic picture and in addition, it is capable of reproducing that part of the width of the resonances, which comes form coupling to the continuum and which was missing in the former RPA approaches.

Unfortunately, in many of these these models, important facts, such as full self-consistency have been neglected, due to their complexity. Thus, the explicit treatment of the continuum for modern relativistic point coupling models with density dependent coupling constants in the framework of RRPA, is a challenging work and will be attempted in this thesis.

Therefore, it is the aim of this work to formulate the general framework, under which the coupling to the continuum is properly included in the relativistic models which study nuclear collective phenomena and at the same time compare with other methods which treat the continuum approximately by discretization.

This work is organized as follows: In the Chapter 2 we give a short introduction to the basic ideas of Density Functional Theory in general and to the concept of covariant DFT for nuclear systems in particular. This method provides a very powerful framework in revealing the static properties of nuclei. The basic equations of Relativistic Mean Field theory are formulated, where we pay attention to non-linear, density dependent and point coupling forces, which are three alternative approaches within RMF. In the next Chapter 3, the Random Phase Approximation in terms of relativistic and non-relativistic considerations is presented. The mechanism of the continuum coupling, as well as some of the key points of its numerical implementation is described in details in the same chapter. In Chapter 4 we present some results of this method with a direct comparison to discrete method and, of course, to experimental data. The extension of the model to include pairing correlations allows us to describe spherical open shell

nuclei. It is discussed together with several applications in Chapter 5. We end the thesis with some conclusive remarks and a brief outlook for future investigations and improvements in Chapter 6.

Chapter 2

Nuclear Density Functional Theories

2.1 Basic concepts of DFT

Density Functional Theory (DFT) is a quantum mechanical method used in many areas of physics to investigate many-body systems. DFT is among the most popular and versatile methods available in condensed matter physics, computational chemistry, and, of course, nuclear physics. Novel applications relevant to fields traditionally considered more distant from quantum mechanics, like biology and mineralogy, are beginning to appear.

DFT owes this versatility to the generality of its fundamental concepts and the flexibility with which it can be implemented, despite being based on quite a rigid conceptual framework. Traditional methods in many-body quantum theory are based on complicated many-particle wave functions $\Psi(\mathbf{r}_1, \ldots, \mathbf{r}_A)$. DFT promotes the local particle density $\rho(\mathbf{r})$ from just one of many observables to the status of a key variable, on which the calculation of all the other observables can be based. In principle, it is a simpler quantity to deal with, both conceptually and practically.

2.1.1 Hohenberg Kohn Theorems

The idea of expressing the expectation values of observables, such as energy, as a function of the ground state density of the system is not new. Already by the year 1927, Thomas and Fermi developed a simple atomic model, under which the total energy of the system could be described by the knowledge of the density alone. However, the Fermi model could no longer give quantitative results, when attempting to move to

nuclear dimensions, thus being practically unusable. Only forty years later by the work of Kohn and Sham, this was finally possible. Based on two fundamental theorems, Hohenberg and Kohn [12] proved that it is possible to replace the N-particle wave function by the ground state density $\rho_0(\mathbf{r})$, or in other words, from a quantity of $4N$ degrees of freedom (three spatial coordinates and one spin) to a quantity of only three degree of freedom. In first glance, this looks impossible, but one needs to keep in mind that the ground state density is not just a simple density of the system but has rather unique properties. More analytically, the two theorems indicated that:

- **Theorem 1:** *Every observable quantity of a stationary quantum mechanical system is determined by the ground-state density alone.*

In other words, the aim of DFT is not to obtain a good approximation for the ground state wave function of the system, but rather to find the energy of the system as a functional of the density, without any reference to the wave function. In a sense, this argument transforms the initial idea of Thomas and Fermi from a simple model into a basic theorem. The argument that all observables of a many-body system are unique functionals of the density, provides the theoretical basis for DFT. For the first theorem, referring always to an electron system in an external potential $\upsilon_{ext}(\mathbf{r})$, one can write:

$$E_\upsilon[\rho(\mathbf{r})] \;=\; F[\rho(\mathbf{r})] \;+\; V_{ext}[\rho(\mathbf{r})] \tag{2.1}$$

with

$$V_{ext}[\rho] = \int d^3r\, \upsilon_{ext}(\mathbf{r})\rho(\mathbf{r}). \tag{2.2}$$

$F[\rho(\mathbf{r})]$ is an unknown, but otherwise universal functional of the electron density $\rho(\mathbf{r})$ only, including kinetic and interaction terms.

- **Theorem 2:** *The exact ground-state density $\rho_0(\mathbf{r})$ of a system in a particular external potential can be found by minimization of the energy functional.*

This was a rather important statement, since until that time, the total energy, which is the most important property of an electronic ground state could only be calculated by means of wave function methods, e.g. either by the direct solution of the Schrödinger equation $H\Psi = E\Psi$ or by means of the Reyleigh Ritz variational principle $E = min_{\tilde{\Psi}}(\tilde{\Psi}, H\tilde{\Psi})$.

In the present case however, the minimization procedure is done in a similar fashion, but with respect to a trial density:

$$E = min_{\tilde{\rho}} E_\upsilon[\tilde{\rho}(r)], \tag{2.3}$$

where the structure of $E_\upsilon[\rho]$ is described in Eq. (2.1).

Therefore, the general idea of the second theorem can be summarized in the inequality:

$$E[\rho(\mathbf{r})] > E[\rho_0(\mathbf{r})] \tag{2.4}$$

which can be easily proven [10]. In other words, the above theorem indicates that one can use a simple variational principle with respect to the density in order to derive the ground state energy.

However it was soon realized that the situation was little improved. Suppose for instance that one starts with an energy functional in the simple form (2.1) with:

$$F[\rho(\mathbf{r})] = T[\rho(\mathbf{r})] + V_H[\rho(\mathbf{r})] + E_{xc}[\rho(\mathbf{r})] \tag{2.5}$$

where $T[\rho]$ is the kinetic energy and $V_H[\rho]$ the Hartree term

$$V_H[\hat{\rho}] = \frac{e^2}{2}\int d^3r \int d^3r' \frac{\rho(\mathbf{r})\rho(\mathbf{r}')}{|\mathbf{r}-\mathbf{r}'|}, \tag{2.6}$$

and the exchange-correlation term $E_{xc}[\rho(\mathbf{r})]$ contains all the rest. Of course, the knowledge of these terms as functions of ρ would immediately solve the problem since the variational principle, applied on the sum (2.1) would lead to the exact density ρ_0, according to the second Hohenberg-Kohn theorem:

$$0 = \frac{\delta E[\rho]}{\delta\rho(\mathbf{r})} = \frac{\delta T_s[\rho]}{\delta\rho(\mathbf{r})} + \frac{\delta V_H[\rho]}{\delta\rho(\mathbf{r})} + \frac{\delta V_{ext}[\rho]}{\delta\rho(\mathbf{r})} + \frac{\delta E_{xc}[\rho]}{\delta\rho(\mathbf{r})}.$$

But obviously we do not know the functional dependence of all these terms. Despite the fact that the density dependent terms $V_{ext}[\rho]$ in Eq. (2.2) and $V_H[\rho]$ in Eq. (2.6) are explicit functions of ρ this is unfortunately not true for the other two terms. For the kinetic term, the expression:

$$T_{TF}[\rho] = \frac{3}{10}(3\pi^2)^{2/3}\int \rho^{5/3}(\mathbf{r})d\mathbf{r} \tag{2.7}$$

of Thomas and Fermi would in principle be a good choice, specially for infinite particle systems, but as Kohn recognized, this functional is problematic and incapable of reproducing shell effects, an important phenomenon with a single-particle origin. In addition, the exchange-correlation $E_{xc}[\rho]$, which was defined to include all the remaining terms of the energy functional, is a rather complicated term and although the first Hohenberg-Kohn theorem shows the existence of such a functional it does not give any hint, how it can be derived from the Coulomb interaction.

As a conclusion, the direct minimization of the energy functional could not be considered as the most efficient way to implement DFT; in particular, since orbital-based approaches such as Hartree-Fock theory appeared to perform much better in this respect. This would mean that although the Hohenberg-Kohn theorem is exact, it is also practically useless.

The solution to this problem was given soon thereafter by Kohn and Sham [10, 11] who realized that one needs a single particle Schrödinger equation in order to obtain shell effect. Therefore they introduced an auxiliary single particle potential $\upsilon_{eff}(\mathbf{r})$ in one-to-one correspondence with the exact density $\rho(\mathbf{r})$. Today, when one says DFT, he is likely talking about the Kohn-Sham method.

2.1.2 Self Consistent Kohn-Sham Equations

Kohn and Sham did not exclusively work in terms of the particle density, but instead, they introduced an auxiliary single particle potential $v_{eff}(\mathbf{r})$, which defines the Kohn-Sham equations:

$$\left(-\frac{\hbar^2}{2m}\frac{d^2}{dr^2} + v_{eff}(\mathbf{r})\right)\psi_i(\mathbf{r}) = \varepsilon_i\psi_i(\mathbf{r}). \tag{2.8}$$

The single particle energies ε_i and the single particle wave functions $\psi_i(\mathbf{r})$ are auxiliary quantities with no specific physical meaning at this point. The effective Kohn-Sham potential $v_{eff}(\mathbf{r})$ is defined by the requirement that the local density obtained from these single particle wave functions

$$\rho(\mathbf{r}) = \sum_{i=1}^{N}\psi_i(\mathbf{r})\psi_i(\mathbf{r}) \tag{2.9}$$

is identical to the exact local density. Eq. (2.9) is a valid representation [66] of the exact density and there is a one to one correspondence between the two functions $\rho(\mathbf{r})$ and $v_{eff}(\mathbf{r})$.

In this way Kohn and Sham mapped the exact many-body problem onto an effective single-particle problem with the orbitals $\psi_i(\mathbf{r})$. They ingeniously introduced a fictitious non-interacting reference system and created the link to the interacting many-body problem.

Next Kohn and Sham defined an approximation for the kinetic energy:

$$T_{KS} = \frac{\hbar^2}{2m}\sum_{i=1}^{N}\int d\mathbf{r}|\nabla\psi_i(\mathbf{r})|^2 = -\frac{\hbar^2}{2m}\sum_{i=1}^{N}\int d\mathbf{r}\psi_i^*(\mathbf{r})\Delta\psi_i(\mathbf{r}), \tag{2.10}$$

because for non-interacting particles, the total kinetic energy is just the sum of the individual kinetic energies. Since all $\psi_i(\mathbf{r})$ are functionals of ρ, this expression for T_{KS} is an explicit orbital functional with an implicit density dependence $T_{KS}[\rho] = T_{KS}[\{\psi_i[\rho]\}]$. The expression (2.10) is an approximation to the exact kinetic energy $T[\rho]$ The difference between the $T[\rho]$ and $T_{KS}[\rho]$ is small and can be absorbed by the exchange-correlation term. We thus obtain the Kohn-Sham energy

$$E_{KS}[\rho(\mathbf{r})] \;=\; T_{KS}[\rho(\mathbf{r})] \;+\; V_H[\rho(\mathbf{r})] \;+\; V_{ext}[\rho(\mathbf{r})] \;+\; E_{xc}[\rho(\mathbf{r})]. \tag{2.11}$$

The idea of Kohn and Sham was then to carry out the variation of the this energy functional by performing variations with respect to the orbitals $\psi(\mathbf{r})$ entering Eq. (2.9)

$$\frac{\delta E}{\delta\psi_i^*(\mathbf{r})} = 0. \tag{2.12}$$

This variation is quite straightforward and yields Eq. (2.8) with the effective Kohn-Sham potential

$$v_{eff}(\mathbf{r}) = v_H(\mathbf{r}) + v_H(\mathbf{r}) + v_{xc}(\mathbf{r}) \tag{2.13}$$

with

$$v_H(\mathbf{r}) = e \int d^3r \, \frac{\rho(\mathbf{r}')}{|\mathbf{r} - \mathbf{r}'|}, \qquad \text{and} \qquad v_{xc}(\mathbf{r}) = \frac{\delta E_{xc}[\rho]}{\delta \rho(\mathbf{r})}. \tag{2.14}$$

Of course at this stage one needs an explicit expression for the density dependence of the exchange-correlation term $E_{xc}[\rho]$. Therefore in the past 40 years much effort has been put into the determination of this term for Coulomb systems [67]. Starting from gradient expansions with phenomenological parameters one nowadays has rather successful expressions for this term derived completely from the Coulomb interaction.

Since the potentials v_H and v_{xc} depend on $\rho(\mathbf{r})$, which itself depends on the orbitals ψ_i, which in turn depend on v_{eff}, the problem of solving the Kohn-Sham equations is highly non-linear. Therefore, it must be solved self consistently, that is, we start from an initial guess for $\rho(\mathbf{r})$ and proceed to the above steps till convergence is achieved. Using the single particle orbitals, one gets in this way the exact ground state density we defined in Eq. (2.9). The most visible consequence is the appearance of shell structure effects as well as correct treatment of the density in the asymptotic region.

Once we have a convergence solution ρ_0, the exact ground state energy of Eq. (2.5) can be calculated:

$$E_0 = \sum_i^N \varepsilon_i - \frac{e^2}{2} \int d^3r \int d^3r' \frac{\rho_0(\mathbf{r})\rho_0(\mathbf{r}')}{|\mathbf{r} - \mathbf{r}'|} - E_{xc}[\rho_0(\mathbf{r})]. \tag{2.15}$$

This equation shows that E_0 is not simply the sum of all ε_i. In fact, it should be clear from the derivation of Eq. (2.8) that the ε_i are completely artificial objects. They are the eigenvalues of an auxiliary single-particle Schrödinger equation whose eigenfunctions yield the correct density. It is only this density, and of course the total energy and its derivatives, that have a strict physical meaning in the Kohn-Sham equations. The Kohn-Sham eigenvalues, on the other hand, bear only a semi-quantitative resemblance with the true single particle energy spectrum, but are not to be trusted quantitatively*.

Finally, we notice that the Kohn-Sham equations (2.8) look much like the Hartree-Fock (where basically v_{xc} appears to replace the Fock term), or even more the simple Hartree equation. However, there are two important differences: (i) the Kohn-Sham theory is in principle exact, if one has the exact expression for the exchange-correlation energy $Exc[\rho]$. It includes many more correlations than Hartree-Fock and (ii) the Kohn-Sham potential $v_{eff}(\mathbf{r})$ is local and therefore one avoids the numerical complexity of the non-local exchange terms in the Hartree-Fock equations.

*There is however a small exception, regarding the ionization (Fermi) energy ε_F, since the condition that the exact particle number is contained in the density, allows for the constraint equation:

$$\delta \left[E[\rho] - \mu \left(\int d^3r \, \rho(\mathbf{r}) - N \right) \right] = 0 \tag{2.16}$$

which gives the chemical potential μ.In other words, the fermi energy is the only one to have a physical meaning.

2.1.3 Nuclear Density Functional Theory

After its success in Coulomb systems, i.e. in atomic, molecular and solid state physics, density functional theory appeared to be the most notable tool in the development of the nuclear models as well. In fact shortly after the Kohn and Sham have introduced density functional theory in Coulomb systems, a similar method has been developed in nuclear physics. Goldstone [13] and Brueckner [14] realized that because of the Pauli principle and the uncertainty relation the effective interaction in the nuclear interior is very different from the bare nucleon-nucleon interaction determined from scattering experiments in the vacuum. In particular, it depends strongly on the density. Early attempts to use this effective interaction in the framework of the local density approximation for Hartree-Fock calculations in finite nuclei failed [68], because it was not clear at that time that tree-body forces play an important role in nuclear systems. However, the idea of phenomenological density dependent interactions introduced by Vautherin and Brink [15] turned out to be very successful. It soon became clear that these density dependent Hartree-Fock calculations (DDHF) were closely related to density functional theory in Coulomb systems. In fact, the energy functional $E[\rho]$ is nothing but the Hartree-Fock energy calculated with the corresponding density dependent force. This functional was introduced in a completely phenomenological way by adjusting the parameters of the model to binding energies and radii in finite nuclei. Vautherin and Brink used the model of Skyrme [69, 15, 70, 71] with zero range forces. Gogny [16, 72] developed a phenomenological model with finite range forces of Gaussian type and a similar density dependence. It was able to include at the same time pairing correlations in the density dependent Hartree-Fock-Bogoliubov framework. Covariant density functional theories in nuclear physics based on the Walecka model [73, 17, 74, 18, 32] allow a consistent description of the spin degree of freedom[19, 33, 35]. All these three models have been applied with great success in reproducing data all over the periodic table [75, 37].

There are howevwe essential differences between DFT in Coulomb systems and in nuclear systems:

- The theorems of Hohenberg and Kohn are based on a many-body system in an external potential. However, nuclei are self-bound systems and an external potential does not exist. The Hohenberg-Kohn theorem is still valid, but useless, because as a consequence of translational invariance the exact single particle-density is a constant [76]. In fact the densities used in DDHF theory are intrinsic densities. Of course, the Hohenberg-Kohn theorems can be generalized to any Hermitian operator, thus including the intrinsic density. However, the problem is that the intrinsic density depends on the center of mass coordinate and therefore this quantity is an A-body operator [77]. A possible solution to this problem would include some approximations regarding an "adiabatic" treatment of the center of mass coordinate managing to recover the Kohn-Sham equations in the $1/A$-limit of large nucleon numbers [78]. In any case, regarding the problem from a realistic point of view, at present the exact density functional cannot be de-

rived from first principles anyhow. Therefore it is an academic question, whether density functional theory in nuclei is exact or only an excellent approximation.

- In Coulomb systems in most cases one can neglect the spin degrees of freedom as a small effect. This is not true in nuclear systems. Here one has additional degrees of freedom which cannot be neglected, such as spin and isospin. Therefore, calculations must include besides the usual density with $(S = 0, T = 0)$ the spin density $(S = 1, T = 0)$, the isospin density $(S = 0, T = 1)$ etc. This leads to an increasing number of phenomenological parameters which are difficult to adjust to experimental data and this is the reason, why most of the present functionals contain redundant parameters. It is the advantage of covariant density functionals, that the spin degree of freedom is taken into account automatically in a proper way and therefore they usually contain a smaller number of phenomenological parameters.

- Pairing correlations play an essential role in nuclear systems. Apart from the few cases with doubly magic shells closures, the large majority of nuclei are superfluid systems. BCS and HFB theory allow an elegant description of these phenomena, which is based on a generalized mean field approximation and provides a vehicle to implement density functional theory for superfluid systems. Here the density functional $E[\mathcal{R}]$ depends on the generalized Valatin density [79]

$$\mathcal{R} = \begin{pmatrix} \rho & \kappa \\ \kappa^* & 1-\rho^* \end{pmatrix} \tag{2.17}$$

  which contains the normal density ρ and the pairing density κ. In this way pairing correlations have been introduced in non-relativistic [16] as well as in relativistic [80, 50] density functionals with great success.

- Conventional density functional theory is based on the well know Coulomb force and therefore over the years one has developed very successful "ab-initio" functionals. They are based on exact numerical solutions of the homogeneous electron gas and do not contain any phenomenological parameter. The situation in nuclear physics is much more complicated. The basic theory is QCD. Because of its non-perturbative character one is far from an exact solution of nuclear matter. So far, one usually starts with the bare nucleon-nucleon force, which is nowadays well known, but our knowledge on tree-body forces is still very limited and exact solutions of the nuclear matter problems are in their infancy. It also turns out that there is a considerable cancellation of the contributions of the kinetic energy and the two-body interaction and therefore small effects, such as three-body forces, play an essential role. Therefore one probably will need always some additional parameters for fine tuning in order to achieve the high accuracy of present days phenomenological density functionals in nuclear physics.

This work is based on covariant density functional theory. In the next section we therefore discuss the essential properties of nuclear density functionals based on the Lorentz invariance.

2.2 Relativistic Mean Field Theory of Finite Range

The Walecka model is used as a vehicle to implement relativity in DFT. Following the idea of Kohn and Sham, one needs a relativistic one-body potential and in order to implement self-consistency (Hartree term), one needs a simple relativistic interaction. Because of the requirement of causality, two body interactions can only be formulated in a relativistic way by zero-range forces or by forces caused by an exchange of particles.

Historically, the meson coupling model has been introduced first in the framework of the Walecka model [74, 18]. In such an approach, one considers that the protons and neutrons in a nucleus interact with each other in a relativistic covariant manner through the exchange of various mesons (carrying different spin, isospin and angular momentum), as we discussed in the introduction. This model should not be considered as a fully fledged quantum field theory but rather a possible way to implement relativity in the framework of a mean field theory. The mesons are only auxiliaries quantities. They are treated only on the classical level, defining fields with the proper relativistic quantum numbers. They have little to do with mesons in free space.

The most important meson that exists in free space is the pion. However, the pion has a pseudo-scalar nature, which means that in the Hartree level, it produces a field that violates parity. This comes in full contradiction to all experimental observations which state that the parity is conserved on the level of the strong interaction. This fact was probably the reason why relativistic mean field models after their first discovery in the fifties [73, 17, 74] had not been considered more seriously in nuclear physics for many years.

However, this is all occurring in the nuclear interior where interactions between nucleons are far more complicated than the bare nucleon-nucleon interaction in free space. Since we are bound to stay within the mean field approximation, there should be no restriction on using any kind of mesons, even those that are not observed in free space. The idea was encouraging and a minimal number of two mesons was finally able to describe the saturation properties of infinite nuclear matter and binding properties of finite nuclei quite well. These mesons are the σ-meson, which has an isoscalar-scalar nature and the isoscalar vector ω-meson. Their strength and mass parameters are chosen in such a way as to reproduce observed phenomena. For instance, the choice of a larger mass and a stronger coupling for the ω meson against the σ is responsible for the short range repulsion, familiar from standard nucleon-nucleon interactions.

The first RMF approximation was nothing but a simple $\sigma - \omega$ model. Later on, another meson was considered necessary, carrying isospin [33, 34] and thus providing in a reasonable way the asymmetry energy term. This was the isovector-vector ρ-meson, the quantum numbers of which are given in Eq. (2.18), together with those of

the other mesons.

$$J^\pi, T = \begin{cases} 0^+, \ 0, & \sigma \text{ meson} \\ 1^-, \ 0, & \omega \text{ meson} \\ 1^-, -1, & \rho \text{ meson} \end{cases} \tag{2.18}$$

Of course, there is also the possibility to consider scalar isovector meson fields with $S = 0, T = 1$. They are usually associated with the δ-meson. However, it turns out that present data on ground state properties of nuclei do not allow the corresponding parameters of the Lagrangian with reasonable accuracy. All the present attempts to fit these parameters lead to highly redundant parameter sets and unstable fits. The scalar isoscalar δ-fields are therefore neglected in all present successful parameterizations.

In order to derive the RMF equations, it is reasonable to start with a relativistic covariant Lagrangian which is composed by the meson and nucleon degrees of freedom plus the electromagnetic field:

$$\mathcal{L} = \mathcal{L}_N + \mathcal{L}_m + \mathcal{L}_{int}. \tag{2.19}$$

The nucleon part describes free nucleons with mass m:

$$\mathcal{L}_N = \bar{\psi} \left(i\gamma^\mu \partial_\mu - m \right) \psi. \tag{2.20}$$

In addition, the meson part describes the motion of σ, ω and ρ mesons with the corresponding masses m_σ, m_ω and m_ρ, and the photon:

$$\begin{aligned} \mathcal{L}_m &= \frac{1}{2}\partial_\mu\sigma\partial^\mu\sigma - \frac{1}{2}m_\sigma^2\sigma^2 - \frac{1}{4}\Omega_{\mu\nu}\Omega^{\mu\nu} + \frac{1}{2}m_\omega^2\omega_\mu\omega^\mu \\ &\quad -\frac{1}{4}\vec{R}_{\mu\nu}\vec{R}^{\mu\nu} + \frac{1}{2}m_\rho^2\vec{\rho}_\mu\vec{\rho}^\mu - \frac{1}{4}F_{\mu\nu}F^{\mu\nu} \end{aligned} \tag{2.21}$$

where the field tensors for the vector mesons (ω,ρ) and photon fields are defined as*

$$\Omega_{\mu\nu} = \partial_\mu\omega_\nu - \partial_\nu\omega_\mu \tag{2.22}$$

$$\vec{R}_{\mu\nu} = \partial_\mu\vec{\rho}_\nu - \partial_\nu\vec{\rho}_\mu \tag{2.23}$$

$$F_{\mu\nu} = \partial_\mu A_\nu - \partial_\nu A_\mu. \tag{2.24}$$

Finally, the nucleon-meson interaction is described by the minimal coupling and is given by the sum:

$$\mathcal{L}_{int} = -\bar{\psi}\Gamma_m\phi_m\psi = -\bar{\psi}\Gamma_\sigma\sigma\psi - \bar{\psi}\Gamma_\omega^\mu\omega_\mu\psi - \bar{\psi}\vec{\Gamma}_\rho^\mu\vec{\rho}_\mu\psi - \bar{\psi}\Gamma_\gamma^\mu A_\mu\psi, \tag{2.25}$$

where the index m runs over different mesons ϕ_m and vertices Γ_m, given by

$$\Gamma_\sigma = g_\sigma, \quad \Gamma_\omega^\mu = g_\omega\gamma^\mu, \quad \vec{\Gamma}_\rho^\mu = g_\rho\vec{\tau}\gamma^\mu, \quad \Gamma_\gamma^\mu = e\frac{1+\tau_3}{2}\gamma^\mu, \tag{2.26}$$

with the coupling constants g_σ, g_ω, g_ρ and e.

*The units $\hbar = c = 1$ are used in the present discussion and isovectors are characterized by arrows.

2.2.1 Equations of Motion

According to the initial approximation of Walecka, the RMF equations can be provided by replacing the field operators of the mesons and the photon by their expectation values, formally by setting $\hat{\sigma} \rightarrow \sigma \rightarrow \langle\hat{\sigma}\rangle$ etc. Then, the role of the meson fields reduces to that of potentials generated by the appropriate nucleon densities, so that the nucleons would behave as non-interacting particles moving in these mean fields.

The Dirac equations for the nucleons are derived from the Lagrangian by the classical variational principle. Considering time-reversal symmetry and charge conservation we obtain the Dirac equation for the nucleons:

$$\left[i\gamma^{\mu}\partial_{\mu} + V + \beta(M - S)\right]\psi_i = \varepsilon_i\psi_i, \tag{2.27}$$

with the fields

$$S = g_{\sigma}\sigma, \qquad V = g_{\omega}\omega_0 + g_{\rho}\tau_3\rho_0 + eA_0, \tag{2.28}$$

and the Klein-Gordon equations for the mesons:

$$\left[\partial^{\mu}\partial_{\mu} + m_m^2\right]\phi_m = \pm\left\langle\bar{\psi}\Gamma_m\psi\right\rangle \tag{2.29}$$

where, the positive (negative) sign holds for vector (scalar) fields while the photon mass vanishes ($m_{\gamma} = 0$).

In Eq. (2.28) one introduces the attractive scalar field $S(r)$ and the repulsive vector field $V(r)$ which appear to be very large in absolute value (≈ 400 and 350 MeV respectively). However, for the large components we deal only with the difference $V - S \approx 50$ MeV, meaning that the Fermi energies are less than $50\,MeV$ and hence small compared to the rest mass. In other words, we have to deal with non-relativistic kinematics. On the other hand, in the second equation that includes the small components, a very large potential $V + S \approx 750MeV$ appears. This implies that whenever these potentials add up, in a constructive way, the relativistic effects are non-negligible. This has multiple consequences, as for example the fact that the spin-orbit coupling has the right magnitude naturally and without requiring additional fitting parameters.

The sources of the inhomogeneous equations (2.29) are given by various densities and currents

$$\left\langle\bar{\psi}\Gamma_m\psi\right\rangle = \sum_{i=1}^{A}\bar{\psi(}\mathbf{r})\Gamma_m\psi(\mathbf{r}). \tag{2.30}$$

Here the sum runs only over the occupied states in the Fermi sea. This is known as the "no-sea approximation" and is used in almost all practical applications of RMF in nuclear matter and finite nuclei. Of course, in order to be complete, we would have to include also the negative energy states in the Dirac sea. However, this would lead to divergent terms, which have to be removed by a proper renormalization. In finite systems this is very complicated, since the corresponding equations can be solved only numerically [81]. An analytical solution is possible for infinite nuclear matter [82]. In

approximate numerical studies of the vacuum polarization in spherical [22, 83] and deformed nuclei [84], the renormalization effects appear to be of the order of 20-30%. However, if the vacuum polarization is taken into account, the parameter set of the effective Lagrangian has to be re-adjusted to the experimental data, leading to a new force with approximately the same results as in the case when the vacuum polarization is neglected. Therefor the "no-sea approximation" is not really an approximation. In such calculations effects of vacuum polarization are not neglected, but rather taken into account in a global phenomenological way by adjusting the corresponding parameters to data.

2.2.2 Extended versions and Medium Dependences

Extensive studies have shown that a quantitative treatment of nuclear matter and finite nuclei necessitates a medium dependence of effective mean-field interactions, which take into account higher order many body effects. This can be achieved either by including non-linear meson self-interaction terms on the Lagrangian (2.19) or by assuming an explicit density dependence for the meson-nucleon coupling, as we briefly discussed in the introduction.

In the first case, non linear terms have been adopted in the construction of several very successful phenomenological RMF interactions, where the prediction of many nuclear properties can reach high level of accuracy. In particular, the mass term of free mesons is replaced by a non-linear potential including higher order terms

$$\frac{1}{2}m_\sigma^2\sigma^2 \qquad \rightarrow \qquad U(\sigma) = \frac{1}{2}m_\sigma^2\sigma^2 + \frac{g_2}{3}\sigma^3 + \frac{g_3}{4}\sigma^4. \tag{2.31}$$

This ansatz was first introduced by Boguta and Bodmer [32] and was widely accepted since. Later on, a self-coupling of the vector field, i.e. a quadratic ω^4 term was added [85] in order to soften the equation of state for neutron matter. It was shown, that models linear in ω are responsible for a very steep neutron matter equation of state, hence being incompatible with the observed spectrum of neutron star masses, whereas the addition of the vector self-coupling of ω has the advantage of "softening" the above effect. Recently, another model including a sophisticated meson-meson coupling between σ and ω, in a similar fashion to the non linear terms, has been introduced [86] and, although it slightly overestimates the charge radii of several closed shell nuclei, it gives a nice prediction of the binding energies as well as the compressibility of nuclear matter. The Lagrangian parameters are usually obtained, as in the case of non-relativistic mean field calculations, by using fitting procedures on bulk properties of several spherical nuclei [33]. The most widely used parameter sets [87, 88, 89] that determine the RMF equations are listed in the Table 2.1.

More modern models avoid the somewhat unphysical non-linear terms and introduce a density dependence of the meson-nucleon vertex functions. This density dependence can be determined either from "ab-initio" calculations based on Dirac-Brueckner theory

parameters	NL1	NL3	$NL3^*$
m	938.0	939.0	939.0
m_σ	492.25	508.194	502.5742
m_ω	795.359	782.501	782.6
m_ρ	763.0	763.0	763.0
	.	.	.
g_σ	10.138	10.217	10.0944
g_ω	13.285	12.868	12.8065
g_ρ	4.976	4.474	4.5748
g_2	-12.172	-10.431	-10.8093
g_3	-36.265	-28.885	-30.1486

Table 2.1: RMF parameterizations NL1 [87], NL3 [89] and NL3* [90]. K_{nm} corresponds to the incompressibility of the nuclear matter for each set of parameters. The masses m are given in MeV, while the coupling constants are dimensionless, except g_3 which is given in fm^{-1}.

in nuclear matter [39, 91, 92, 93], or it can be completely phenomenological [94, 95, 43], with parameters adjusted to data of finite nuclei and empirical properties of symmetric and asymmetric nuclear matter. One obtains a Lagrangian with density dependent coupling constants $g_m(\rho)$, where ρ is either the scalar density ρ_s or the Lorentz invariant form $\sqrt{j^u j_\mu}$ of the baryon density, $j_\mu = \bar{\psi}\gamma_\mu\psi$ [42]. In particular, one often uses the Typel and Wolter ansatz [94] with the following density dependence:

$$g_i(\rho) = g_i(\rho_{\rm sat}) f_i\left(\frac{\rho}{\rho_{\rm sat}}\right) \quad \text{for} \quad i = \sigma, \omega \ . \tag{2.32}$$

Here, $\rho_{\rm sat}$ denotes the baryon density at saturation in symmetric nuclear matter and

$$f_i(x) = a_i \frac{1 + b_i(x + d_i)^2}{1 + c_i(x + d_i)^2} \tag{2.33}$$

is a function of $x = \rho/\rho_{\rm sat}$. The eight real parameters (a_i, b_i, c_i, d_i for $i = 1, 2$) in Eq. (2.33) are not independent. The five constraints $f_i(1) = 1$, $f_i''(0) = 0$ ($i = 1, 2$) and $f_\sigma''(1) = f_\omega''(1)$ reduce the number of independent parameters to three. Three additional parameters in the isoscalar channel are: $g_\sigma(\rho_{\rm sat})$, $g_\omega(\rho_{\rm sat})$, and m_σ - the mass of the phenomenological sigma-meson. For the ρ-meson coupling the functional form of the density dependence is suggested by Dirac-Brueckner calculations of asymmetric nuclear matter [93]

$$g_\rho(\rho) = g_\rho(\rho_{\rm sat}) \exp\left[-a_\rho(x - 1)\right] \ . \tag{2.34}$$

The parameter set DD-ME2, from Lalazissis et al. [96](Table 2.2.2) has lead to one of the most successful nuclear description, ranging all over the periodic table.

In addition, when compared with standard nonlinear meson-exchange effective Lagrangians, interactions with an explicit density dependence on the meson-nucleon couplings are more flexible and provide an improved description of asymmetric nuclear matter, neutron matter and finite nuclei far from stability.

m_σ	=	550.1238	m_ω	=	783.000	m_ρ	=	763.000
$g_\sigma(\rho_{\rm sat})$	=	10.5396	$g_\omega(\rho_{\rm sat})$	=	13.0189	$g_\rho(\rho_{\rm sat})$	=	3.6836
a_σ	=	1.3881	a_ω	=	1.3892	a_ρ	=	0.5647
b_σ	=	1.0943	b_ω	=	0.9240			
c_σ	=	1.7057	c_ω	=	1.4620			
d_σ	=	0.4421	d_ω	=	0.4775			

Table 2.2: The parameter set DD-ME2. Masses are given in MeV and the remaining parameters are dimensionless. The nucleon mass is M=939 MeV and the saturation density is $\rho_{\rm sat} = 0.152$ fm^{-3} (from Ref. [96]).

2.3 Relativistic MFT of Zero Range (Point Coupling)

The previous versions of RMF approaches have been able to describe the static nuclear system starting from different descriptions of the medium dependence (non-linearities, density dependencies). Their common basis was the agreement that the nucleons interact via the exchange of meson fields with finite range. An idea of implementing a zero-range counterpart of these fields would in principle be very enterprizing, since such a simplified approach could not beat the predicting power of the FR-RMF. However, intensive studies have proved that this idea is not only a possible scenario but it has turned into a powerful and numerically preferable RMF approach.

Under this framework, a zero range or contact interaction can be used (Fig. 2.1), instead of the virtual meson fields, in order to represent the system of interacting Dirac nucleons.

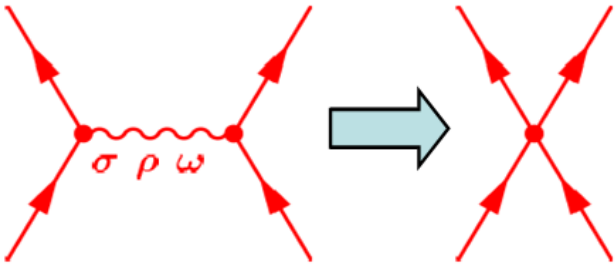

Figure 2.1: Diagrammatic structure of the meson exchange (a) and the point coupling (b) interaction for two nucleons

A general point-coupling effective Lagrangian must be constructed to be consistent

with the underlying symmetries of QCD (e.g., Lorentz covariance, gauge invariance, and chiral symmetry), just as in the case of the meson-exchange model. It should in principle contain every possible term, allowed by these symmetries, but at the same time should also be described by the least possible parameters in order to give a quantitative solution.

Under such a concept, we construct the point coupling Lagrangian as an expansion in powers of the nucleon scalar, vector and isovector-vector densities. Here, finite-range phenomenology and experience with meson-exchange RMF models are useful guides. Thus, we follow the reasoning of Ref. [97] to make an one to one correspondence between the new Lagrangian and the meson exchange one (2.19), through a simple leading-order analysis. For example, the scalar field, ϕ_σ is proportional to the scalar density ρ_s; the term cubic in the scalar density in the point-coupling model corresponds to the term cubic in the non-linear scalar field, and so on.

In addition, the Klein-Gordon equations (2.29) of the meson-exchange model with meson masses m_m and couplings g_m are replaced by two point coupling interaction terms, via the expansion of the Yukawa potential in terms of $1/m_m^2$:

$$\frac{g_m}{-\Delta + m_m^2} \approx \frac{g_m}{m_m^2} + g_m \frac{\Delta}{m_m^4} + \dots \tag{2.35}$$

In the case of infinite nuclear matter, the two models give the same results because the gradient terms in Eq. (2.35) vanish in this case. For finite nuclei, however, the central potentials $S(r)$ and $V(r)$ are very large and the gradients appear to be essential in a quantitative theory.

In this work we use the point coupling Lagrangian of Ref. [46]. It presents an expansion in powers of the nucleon scalar, vector and isovector-vector densities.

$$\mathcal{L} = \mathcal{L}_{\text{free}} + \mathcal{L}_{\text{4f}} + \mathcal{L}_{\text{hot}} + \mathcal{L}_{\text{der}} + \mathcal{L}_{\text{em}} \tag{2.36}$$

with the Lagrangian for free nucleons:

$$\mathcal{L}_{\text{free}} = \bar{\psi}(i\gamma_\mu \partial^\mu - m_N)\psi, \tag{2.37}$$

the Lagrangian for normal four-fermion interactions

$$\mathcal{L}_{\text{4f}} = -\frac{\alpha_S}{2}(\bar{\psi}\psi)(\bar{\psi}\psi) - \frac{\alpha_V}{2}(\bar{\psi}\gamma_\mu\psi)(\bar{\psi}\gamma^\mu\psi) - \frac{\alpha_{TV}}{2}(\bar{\psi}\vec{\tau}\gamma_\mu\psi)(\bar{\psi}\vec{\tau}\gamma^\mu\psi), \tag{2.38}$$

the Lagrangian for higher order terms leading in mean field approximation to a density dependence

$$\mathcal{L}_{\text{hot}} = -\frac{\beta_S}{3}(\bar{\psi}\psi)^3 - \frac{\gamma_S}{4}(\bar{\psi}\psi)^4 - \frac{\gamma_V}{4}[(\bar{\psi}\gamma_\mu\psi)(\bar{\psi}\gamma^\mu\psi)]^2, \tag{2.39}$$

the Lagrangian containing derivative terms which simulate in a simple way the finite range of the forces:

$$\mathcal{L}_{\text{der}} = -\frac{\delta_S}{2}(\partial_\mu\bar{\psi}\psi)(\partial^\mu\bar{\psi}\psi) - \frac{\delta_V}{2}(\partial_\mu\bar{\psi}\gamma_\nu\psi)(\partial^\mu\bar{\psi}\gamma^\nu\psi) - \frac{\delta_{TV}}{2}(\partial_\mu\bar{\psi}\vec{\tau}\gamma_\nu\psi)(\partial^\mu\bar{\psi}\vec{\tau}\gamma^\nu\psi), \tag{2.40}$$

and the electro-magnetic part of the Lagrangian

$$\mathcal{L}_{\rm em} = -\frac{1}{4}F_{\mu\nu}F^{\mu\nu} - \frac{e}{2}(1+\tau_3)A_\mu\bar{\psi}\gamma^\mu\psi \tag{2.41}$$

In these equations the subscripts S and V are attributed to scalar and vector fields, while the subscript T is attributed to isovector fields. As usual, vectors in isospin space are denoted by arrows, where symbols in bold indicate vectors in ordinary three-dimensional coordinate space. The scalar-isovector channel is again neglected.

As it stands, the Lagrangian contains the nine coupling constants α_S, α_V, α_{TV}, β_S, γ_S, γ_V, δ_S, δ_V and δ_{TV}. Hence, the model contains more or less the same number of free parameters as the analogous RMF-FR models.

From the Lagrangian (2.36) and the corresponding energy momentum tensor we can derive the RMF equations using either the classical Euler-Lagrange equation, as we did in the meson-exchange version, or a relativistic energy density functional. This energy functional has the form:

$$\mathcal{E}_{\rm RMF}[\rho,t] = \int d^3r\ H(\mathbf{r},t), \tag{2.42}$$

where the energy density

$$H(\mathbf{r},t) = H_{\rm kin}(\mathbf{r},t) + H_{\rm int}(\mathbf{r},t) + H_{\rm em}(\mathbf{r},t) \tag{2.43}$$

consists of a kinetic part

$$H_{\rm kin}(\mathbf{r},t) = \sum_i^A \bar{\psi}_i(\mathbf{r},t)\left(\alpha\mathbf{p} + \beta m - m\right)\psi_i(\mathbf{r},t), \tag{2.44}$$

an interaction part

$$\begin{aligned} H_{\rm int}(\mathbf{r},t) = {} & \frac{\alpha_S}{2}\rho_S^2 + \frac{\beta_S}{3}\rho_S^3 + \frac{\gamma_S}{4}\rho_S^4 + \frac{\delta_S}{2}\rho_S\Delta\rho_S \\ & + \frac{\alpha_V}{2}j_\mu j^\mu + \frac{\gamma_V}{4}(j_\mu j^\mu)^2 + \frac{\delta_V}{2}j_\mu\triangle j^\mu \\ & + \frac{\alpha_{TV}}{2}\vec{j}^\mu_{TV}\cdot\vec{j}_{TV\mu} + \frac{\delta_{TV}}{2}\vec{j}^\mu_{TV}\cdot\triangle(\vec{j}_{TV})_\mu, \end{aligned} \tag{2.45}$$

and an electromagnetic part

$$H_{\rm em}(\mathbf{r},t) = \frac{1}{4}F_{\mu\nu}F^{\mu\nu} - F^{0\mu}\partial_0 A_\mu + eA_\mu j_p^\mu. \tag{2.46}$$

The interaction part depends on the local densities:

$$\rho_S(\mathbf{r},t) = \sum_i^A \bar{\psi}_i(\mathbf{r},t)\psi_i(\mathbf{r},t), \tag{2.47}$$

$$\rho_V(\mathbf{r},t) = \sum_i^A \bar{\psi}_i(\mathbf{r},t)\gamma_0\psi_i(\mathbf{r},t), \tag{2.48}$$

$$\rho_{TV}(\mathbf{r},t) = \sum_i^A \bar{\psi}_i(\mathbf{r},t)\vec{\tau}\gamma_0\psi_i(\mathbf{r},t), \tag{2.49}$$

and currents

$$j_V^{\mu}(\mathbf{r},t) = \sum_i \bar{\psi}_i(\mathbf{r},t)\gamma^{\mu}\psi_i(\mathbf{r},t), \tag{2.50}$$

$$\vec{j}_{TV}^{\mu}(\mathbf{r},t) = \sum_i \bar{\psi}_i(\mathbf{r},t)\vec{\tau}\gamma^{\mu}\psi_i(\mathbf{r},t). \tag{2.51}$$

As in all relativistic mean field models, the *no-sea* approximation is used in the calculations of the nuclear densities.

The self energy, i.e. the single particle Hamiltonian is obtained as the functional derivative of the energy density functional with respect to the relativistic density matrix:

$$h_D(t) = \frac{\delta E[\hat{\rho}]}{\delta \hat{\rho}}. \tag{2.52}$$

This yields the Dirac Hamiltonian: h_D:

$$h_D = \alpha[-i\nabla - \mathbf{V}(\mathbf{r},t)] + V(\mathbf{r},t) + \beta(m + S(\mathbf{r},t)) \tag{2.53}$$

with the self-consistent scalar and vector potentials

$$S(\mathbf{r},t) = \Sigma_S(\mathbf{r},t) \tag{2.54}$$

$$V^{\mu}(\mathbf{r},t) = \Sigma_V^{\mu}(\mathbf{r},t) + \vec{\tau}\cdot\vec{\Sigma}_{TV}^{\mu}(\mathbf{r},t). \tag{2.55}$$

The nucleon isoscalar-scalar, isovector-scalar, isoscalar-vector and isovector-vector self-energies are density dependent and defined by the following relations:

$$\Sigma_S = \alpha_S\rho_S + \beta_S\rho_S^2 + \gamma_S\rho_S^3 - \delta_S\Delta\rho_S \tag{2.56}$$

$$\Sigma_V^{\mu} = \alpha_V\rho_V + \gamma_V\rho_V^3 - \delta_V\Delta\rho_V - eA^{\mu}\frac{1+\tau_3}{2} \tag{2.57}$$

$$\vec{\Sigma}_{TV}^{\mu} = \alpha_{TV}\rho_{TV} - \delta_{TV}\Delta\rho_{TV}. \tag{2.58}$$

Here we have neglected retardation effects, i.e. second derivatives with respect to the time for the various densities.

The problem of the RMF equations is solved self-consistently. An initial guess of the fields (usually of Woods-Saxon character) is enough to give us an explicit form of the Hamiltonian (2.53), which in tern, solves the Dirac equation. The resulting wave-functions are the tool to construct the single-particle densities and, through them, a new set of field functionals.

$$\psi_i^{(1)} \rightarrow \hat{\rho} \rightarrow \Sigma_{\mu} \rightarrow \{S, V^{\mu}\} \rightarrow h_i \rightarrow \psi_i^{(2)} \rightarrow \dots \tag{2.59}$$

The same procedure continues until a convergence in the field structure is achieved.

2.4 PC-RMF Parameterizations

PC-F1

The point coupling Lagrangian PC-F1 of Ref. [46] contains nine coupling constants. Based on an extensive multi parameter χ^2 minimization procedure, Bürvenich et al. have adjusted the parameters to reproduce ground state properties of infinite nuclear matter and spherical double closed nuclei. This set is listed in Table 2.3 and it has been tested in the calculation of many ground state properties of spherical and deformed nuclei all over the periodic table. The results are very well comparable with reasonable effective meson-exchange interactions.

PC-F1	$\alpha_i\,[fm^{-2}]$	$\beta_i\,[fm^{-5}]$	$\gamma_i\,[fm^{-8}]$	$\delta_i\,[fm^{-4}]$
S	-14.935894	22.994736	-66.769116	-0.634576
V	10.098025	0.0	-8.917323	-0.180746
TV	1.350268	0.0	0.0	-0.063680

Table 2.3: The coupling constants in the parameter set PC-F1 resulting from the fitting procedure in Ref. [46].

DD-PC1

Quite recently, there has been developed a new parameter set for the point coupling Lagrangian by T. Nikšić et al [98] with the name DD-PC1. The main peculiarity of this parameterization is that the linear term as well as the medium dependence are all included in a density dependent coupling constant $\alpha(\rho)$, in a similar way to the DD-ME1 and DD-ME2 cases of the meson-exchange approaches [95, 96]. In addition, these coupling constants strictly depend on the baryon density $\rho = \rho_v$ and not on the local densities that correspond to the various spin-isospin channels. The effective Lagrangian in this case would be:

$$\begin{aligned}\mathcal{L} &= \bar{\psi}(i\gamma\cdot\partial - m)\psi \\ &- \frac{1}{2}\alpha_S(\rho)(\bar{\psi}\psi)(\bar{\psi}\psi) - \frac{1}{2}\alpha_V(\rho)(\bar{\psi}\gamma^\mu\psi)(\bar{\psi}\gamma_\mu\psi) - \frac{1}{2}\alpha_{TV}(\rho)(\bar{\psi}\vec{\tau}\gamma^\mu\psi)(\bar{\psi}\vec{\tau}\gamma_\mu\psi) \\ &- \frac{1}{2}\delta_S(\partial_\nu\bar{\psi}\psi)(\partial^\nu\bar{\psi}\psi) - e\bar{\psi}\gamma\cdot A\frac{(1+\tau_3)}{2}\psi. \end{aligned} \tag{2.60}$$

For the functional form of the coupling constants, one chooses the following practical ansatz:

$$\alpha_i(\rho) = a_i + (b_i + c_i x)e^{-d_i x}, i = \{S, V, TV\} \tag{2.61}$$

where $x = \rho/\rho_{sat}$ and ρ_{sat} is the saturation density of nuclear matter, which is set to $\rho_{sat} = 0.152\,fm^{-3}$.

The self-energies which are used to determine the self-consistent scalar and vector potentials $S(\mathbf{r})$ and $V(\mathbf{r})$ of Eq. (2.54) are defined by the following equations:

$$\Sigma_S = \alpha_S(\rho)\rho_s - \delta_S\Delta\rho_s \tag{2.62}$$

$$\Sigma_V^\mu = \alpha_V(\rho)j^\mu + e\frac{(1+\tau_3}{2}A^\mu + \Sigma_R^\mu \tag{2.63}$$

$$\Sigma_{TV}^\mu = \alpha_{TV}(\rho)\vec{j}^\mu. \tag{2.64}$$

with the rearrangement term

$$\Sigma_R^\mu = \frac{1}{2}\frac{j^\mu}{\rho_v}\left\{\frac{\partial\alpha_S}{\partial\rho}\rho_s^2 + \frac{\partial\alpha_V}{\partial\rho}j_\mu j^\mu + \frac{\partial\alpha_{TV}}{\partial\rho}\vec{j}_\mu\vec{j}^\mu\right\} \tag{2.65}$$

The parameters of this functionals will have to be adjusted to structure data of finite nuclei. For the majority of the functionals used in previous approaches, this tuning has been performed on a relatively small set of spherical closed-shell nuclei, mainly because they are simple to calculate and can therefore be easily included in multi-parameter least-squares fits.

A problem arises, however, because ground-state data of closed-shell nuclei include long-range correlations that cannot really be absorbed into mean-field functionals. Generally this will affect the predictive power of energy density functionals when they are used in the description of phenomena related to the evolution of shell structure. For instance, soft potential energy surfaces or small energy differences between coexisting minima in deformed nuclei, are often difficult to describe using functionals adjusted solely to data of spherical nuclei, even when sophisticated models are employed that include angular momentum and particle number projection, as well as intrinsic configuration mixing. As a consequence, the parameters of the set DD-PC1, which are shown in Table 2.4, are adjusted to 64 axially deformed nuclei in the mass regions $A \approx 150 - 180$ and $A \approx 230 - 250$.

The undeniable advantage of the point coupling scheme is of course the ability to predict the ground state properties of nuclei with a much simpler approach, as compared to the finite range ones and using the same number of parameters. From a different perspective, RMF-PC model allows one to investigate its relationship to non-relativistic point-coupling approaches, such as the Skyrme-Hartree-Fock (SHF) theory, which is also a well-developed self-consistent mean-field model that performs very well. One

DD-PC1	$a_i\,[fm^2]$	$b_i\,[fm^2]$	$c_i\,[fm^2]$	d_i	$\delta_i\,[fm^4]$
S	-10.0462	-9.1504	-6.4273	1.3724	-0.815
V	5.9195	8.8637	0.0	0.6584	0.0
TV	0.0	2.2657	0.0	0.9214	0.0

Table 2.4: The coupling constants in the parameter set DD-PC1 resulting from the fitting procedure in Ref. [98].

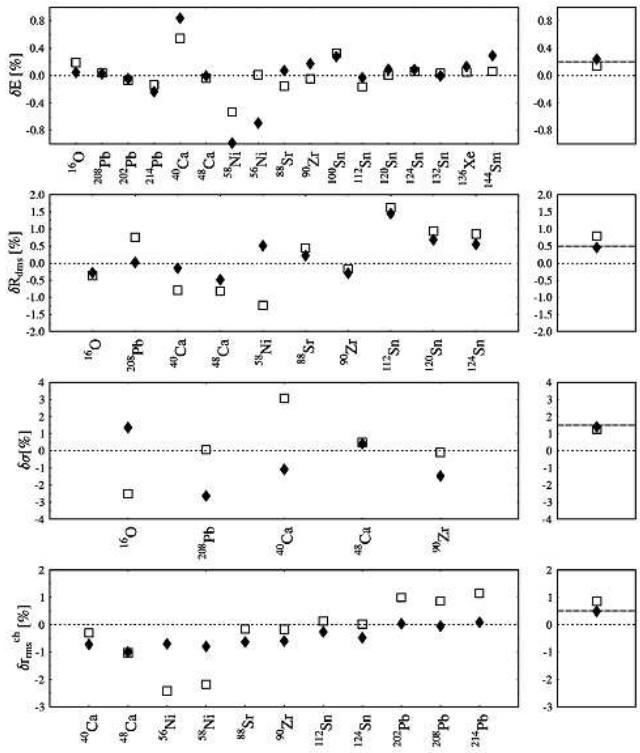

Figure 2.2: Errors (in %) for the observables binding energy, diffraction radius, surface thickness, and rms charge radius for PC-F1 (filled diamonds) and NL-Z2 (open squares) are seen on the left. The right panels show the absolute mean errors for the corresponding observables, where the dashed lines indicate the relative error ΔO in the fitting procedure [46]

can hence view RMF-PC as an approach that lies between the RMF-FR and the nonrelativistic SHF approach. In particular, a comparison of RMF-PC and SHF would address the differences between in-medium Dirac and Schrödinger nucleons, that is, in kinetic and spin-orbit components, whereas a comparison of RMF-PC and RMF-FR would address the absence versus presence of finite range and the different treatments of density dependence.

Summarizing, we can say that in a qualitative level, the point coupling approach is more general and the interaction terms are not restricted by the constraints imposed by the finite range of meson exchange. Furthermore, with the point coupling RMF, the need of virtual mesons, which do not exist in free space, is avoided.

In a quantitative level, the efficiency of the point coupling model can be seen in Fig. 2.2, where the performance of the parameter set PC-F1 is demonstrated and compared with the finite range force NL-Z2 [46].

In Fig. 2.3 we plot for the Pb and Sn isotopic chains the absolute deviations of the calculated binding energies from the experimental values, as functions of the mass number. The binding energies are calculated using the RMF+BCS model with the

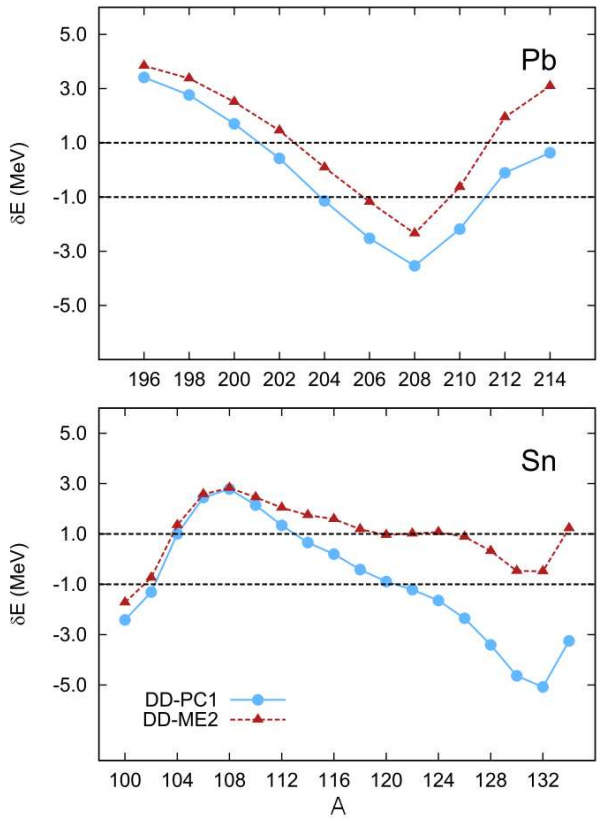

Figure 2.3: Absolute deviations of the calculated binding energies from the experimental values for the Pb (upper panel) and Sn (lower panel) isotopic chains, as functions of the mass number. The theoretical binding energies are calculated using the RMF+BCS model with the point-coupling effective interaction DD-PC1 [98] and the finite-range meson exchange interaction DD-ME2 [96].

functional DD-PC1 are also compared to those obtained with the meson-exchange interaction DD-ME2 [96]. In this case, we see that the variance between calculated masses and the corresponding experimental values is somewhat larger. We have to keep in mind however that the set DD-ME2, like most of the modern self-consistent mean-field nonrelativistic and relativistic interactions, was adjusted to reproduce the binding energies of doubly closed-shell nuclei, including ^{132}Sn and ^{208}Pb. It is thus not surprising that DD-ME2 goes better than DD-PC1 in the vicinity of the double closed nuclei while the opposite is happening outside this area.

The nuclear ground state is defined as the equilibrium point of the functional (2.42), thus, is associated with the density which minimizes $E_{\rm RMF}[\hat{\rho}]$. Furthermore, small oscillations around this equilibrium point correspond to the vibrational nuclear states. They are usually described within the harmonic approximation, that is, using linear response theory. In nuclear physics, this is the so called Random Phase Approximation (RPA) which has been already mentioned in our discussion and will be described in more detail in the next section.

Chapter 3

Random Phase Approximation

So far, we have seen that on the mean field level, protons and neutrons inside the nuclear interior are considered as non-interacting (uncorrelated) particles moving in an average mean field potential. The occupation of the lowest single-particle levels up to, and not beyond, the Fermi energy describes the ground state of the system. This simple model can successfully describe the shell structure of the nucleus, as well as general bulk properties, such as binding energies and nuclear radii. However, in order to go a step further and explain the collective properties of a nucleus, one needs to consider the residual two-body interaction between the nucleons which is not accounted for in the mean-field potential. It is this residual interaction which give rise to the collectivity of the nucleus.

Excitations of the ground state are described in terms of particle-hole transitions where a nucleon in some state below the Fermi surface (hole) is promoted to a state above it (particle). These excitations can be handled with relative ease. This is a blessing, since $1p1h$ excitations are the dominant components in a variety of processes. For example, nuclear states that have large $1p1h$ components are strongly excited by electromagnetic processes, such as inelastic electron scattering, and by strong interaction probes in the form of intermediate energy nucleon scattering. In a study of the properties of such states, one of our primary concerns is to establish the correct correlation between different $1p1h$ components, in order to produce, for example, the observed strong enhancement in strengths. The Random Phase Approximation solves that problem by allowing only certain types of correlations and is thus able to account for the strong $1p1h$ excitations observed in many nuclei with a relatively simple calculation.

The Random Phase Approximation (RPA) is a theory of small-amplitude vibrations in the quantum many-body system. The name was originated in the first application of the method by Bohm and Pines referring to the plasma oscillations of an electron gas [99]. The theory is equivalent to the time dependent mean field theory, at the limit where the amplitude of the motion is small. Consequently, the applicability of

the theory is restricted to systems where an effective mean-field theory provides a good description of the ground state of the nucleus.

With improved interactions and present computer resources, RPA has proven itself to be a robust theory, capable of predicting and describing in detail many properties of collective excitations.

There are two quite different mathematical representations of the RPA, namely the **configuration space formalism** or *A-B matrix diagonalization* and the **response function formalism**. In a brief outlook, the configuration space formalism diagonalizes a non-hermitian matrix which are constructed in the configuration space of $1p1h$ excitations. In contrast, in the response function formalism, ones solves the linear response equations in a time dependent external field. This requires a matrix inversion for given frequency ω.

The above two methods are in principle equivalent, but in practise, one or the other way may be better suited to the problem at hand. For instance, the response function formalism allows excitations to be calculated in very large spaces of configurations; the computational effort is only linear in the number of configurations. However, the residual interaction must have a simple form, with very restricted possibilities for non-locality. In particular, the exchange interaction can only be calculated approximately, in a zero-range approximation. In contrast, the matrix diagonalization puts no limitation on the interaction, but the computational effort is cubic in the number of configurations included in the space.

Another important difference is that the response-function formalism is capable of treating the coupling to the positive energy continuum exactly, as we will extensively discuss later. It is much harder to deal with this coupling, by using the matrix diagonalization method. In the following, the details of these two formalisms are unfolded.

3.1 Matrix Representation of RPA

In any of the cases discussed above, one starts from a ground state described in a mean field theory and considers small amplitude fluctuations around its equilibrium configuration. For the sake of simplicity, we describe here only spherical, double closed nuclei. In a microscopic picture, all states below fermi surface are fully occupied and all states above the fermi surface are empty. However, they are all calculated in the same basis, regardless the fact that some of them may belong to the positive energy continuum. The latter are determined by expansion in an appropriate basis, given for instance by a finite number of eigenfunctions of a harmonic oscillator [62] , or of a Woods-Saxon potential in a finite box [63].

In order to describe excited states, we start from the same relativistic energy density functional $E[\rho]$ that was used to determine the nuclear ground states in the last section. In an arbitrary representation indicated by the Greek indices $\alpha, \beta, \ldots$ (e.g. the $(\mathbf{r}, s, d, t)$-representation) this functional depends on the single particle density matrix:

$$\rho_{\alpha\beta} = \langle 0|a_\beta^+ a_\alpha|0\rangle. \tag{3.1}$$

The same functional can be used for the description of excited states by considering the time-dependent single particle density:

$$\rho_{\alpha\beta}(t) = \langle \Phi(t)|a_\beta^+ a_\alpha|\Phi(t)\rangle \tag{3.2}$$

With the help of the time-dependent variational principle

$$\delta \int_{t_1}^{t_2} dt \left\{\langle \Phi|i\partial_t|\Phi\rangle - E\left[\rho(t)\right]\right\} = 0, \tag{3.3}$$

we can derive the equation of motion for the density matrix:

$$i\partial_t \rho(t) = \left[h(\rho(t)), \rho(t)\right]. \tag{3.4}$$

These are the time-dependent relativistic mean field equations and the single-particle Dirac-Hamiltonian h is obtained from the functional derivative of the energy with respect to the single-particle density matrix ρ

$$h = \frac{\delta E}{\delta \rho}. \tag{3.5}$$

The static solution is immediately deduced if we neglect the time-dependance in Eq. (3.4):

$$[h_0, \rho_0] = 0 \tag{3.6}$$

and it describes the nuclear ground state as discussed in the last section. This means that $h_0 = h(\rho_0)$ and ρ_0 can be diagonalized at the same time and in the static basis. h_0 is diagonal and the matrix ρ_0 has the form:

$$\rho_{0,kl} = \delta_{kl} n_k \tag{3.7}$$

where the occupation numbers are:

$$\begin{array}{ll} n_i = 1 & \text{for occupied states} \\ n_m = 0 & \text{for unoccupied states} \end{array} \tag{3.8}$$

That means that, besides the occupied states (hole states (h)), we have in the relativistic case two types of unoccupied states. These are the positive energy solutions (particle states (p)) with eigenvalues $\varepsilon_p > \varepsilon_F$ and negative energy solutions (anti-particle states (a)) due to the no-sea approximation.

The numerical solution of the time-dependent RMF equations [100, 52] requires not only a tremendous numerical effort, but it is also connected with additional problems. For instance, their solutions break symmetries and they are connected with a spurious

channel mixing (see Ref. [101]). In order to avoid these problems, we consider in this section excited states in the small amplitude limit, that is, we concentrate on vibrations around the ground state density by ρ_0:

$$\rho(t) = \rho_0 + \delta\rho(t). \tag{3.9}$$

In the mean field approximation we assume that the many-body wave function $|\Phi(t)\rangle$ stays at all times a Slater determinant, i.e.

$$\rho^2(t) = \rho(t), \tag{3.10}$$

In first order in $\delta\rho$, the equation of motion of Eq. (3.4 becomes:

$$i\partial_t \delta\rho(t) = [h_0, \delta\rho(t)] + \left[\left.\frac{\partial h}{\partial \rho}\right|_{\rho_0} \delta\rho(t), \rho_0 \right] \tag{3.11}$$

$$= [h_0, \delta\rho(t)] + [V\delta\rho(t), \rho_0] \tag{3.12}$$

with the effective interaction:

$$V_{\alpha\beta,\alpha'\beta'} = \left.\frac{\delta h_{\alpha\beta}}{\delta\rho_{\alpha'\beta'}}\right|_{\rho_0} = \left.\frac{\delta^2 E(\rho)}{\delta\rho_{\alpha\beta}\delta\rho_{\alpha'\beta'}}\right|_{\rho_0}. \tag{3.13}$$

Decomposing the full time-dependent solution $|\Phi(t)\rangle$ in terms of the eigenstates (the ground state $|0\rangle$ and the excited states $|\mu\rangle$) of the nuclear Hamiltonian we get

$$|\Phi(t)\rangle = e^{-iE_0 t}|0\rangle + \sum_\mu c_\mu e^{-iE_\mu t}|\mu\rangle \tag{3.14}$$

and find in first order in c_μ:

$$\delta\rho_{\alpha\beta}(t) = \sum_\mu c_\mu \langle 0|a^+_\beta a_\alpha|\mu\rangle e^{-i\Omega_\mu t} + (h.c.) \tag{3.15}$$

with the transition densities:

$$\rho^{(\mu)}_{\alpha\beta} = \langle 0|a^+_\beta a_\alpha|\mu\rangle \tag{3.16}$$

which connect the ground state $|0\rangle$ and the excited state $|\mu\rangle$. Because of the relation (3.10) we find in the static basis that the only non-vanishing matrix elements of $\delta\rho$ are $\delta\rho_{mi}$ and $\delta\rho_{im}$ connecting occupied and unoccupied states and the transition densities have in this basis the form:

$$\delta\rho_{ab} = \begin{pmatrix} 0 & \delta\rho_{mi} \\ \delta\rho_{im} & 0 \end{pmatrix}. \tag{3.17}$$

For convenience, we transform the above expression so that the *ph*-space is characterized by the vectors

$$\delta\rho = \begin{pmatrix} \delta\rho_{mi} \\ \delta\rho_{im} \end{pmatrix}. \tag{3.18}$$

Inserting the expression (3.15) for $\delta\rho$ into equation (3.11) and considering only components oscillating with the frequency Ω_μ we find in the static basis the linear eigenvalue problem:

$$\Omega_\mu \rho^\mu_{mi} = (\varepsilon_m - \varepsilon_i)\rho^\mu_{mi} + \sum_{nj} V_{mi,nj}\rho^\mu_{nj} + V_{mi,jn}\rho^\mu_{jn} \tag{3.19}$$

$$-\Omega_\mu \rho^\mu_{im} = (\varepsilon_m - \varepsilon_i)\rho^\mu_{im} + \sum_{nj} V^*_{mi,jn}\rho^\mu_{nj} + V^*_{mi,nj}\rho^\mu_{jn}. \tag{3.20}$$

Introducing the ph-amplitudes:

$$X^\mu_{mi} = \langle 0|a^+_i a_m|\mu\rangle, \qquad \text{and} \qquad Y^\mu_{mi} = \langle 0|a^+_m a_i|\mu\rangle, \tag{3.21}$$

the RPA equations are given using the following matrix formulation:

$$\begin{pmatrix} A & B \\ B^* & A^* \end{pmatrix} \begin{pmatrix} X^\mu \\ Y^\mu \end{pmatrix} = \Omega_\mu \begin{pmatrix} 1 & 0 \\ 0 & -1 \end{pmatrix} \begin{pmatrix} X^\mu \\ Y^\mu \end{pmatrix}, \tag{3.22}$$

with the RPA matrices:

$$A_{mi\,nj} = (\varepsilon_m - \varepsilon_i)\delta_{mn}\delta_{ij} + V_{mi,nj}, \tag{3.23}$$

$$B_{mi\,nj} = V_{mi,jn}. \tag{3.24}$$

As was discussed before, this is a linear eigenvalue problem describing small amplitudes vibrations $|\mu\rangle$ of the nuclear many-body problem, The eigenmodes Ω_μ of the RPA equations correspond to the excitation energies of the system, while the transition densities

$$\rho^\mu = \begin{pmatrix} X^\mu_{mi} \\ Y^\mu_{mi} \end{pmatrix}, \tag{3.25}$$

are the eigenvectors of the RPA equations.

The RPA-equations (3.22) are usually solved in a discrete basis, i.e. the eigenfunctions of the static basis are expanded in terms of a complete set of harmonic oscillator functions of the eigenfunctions of a Saxon-Woods potential within a finite box of Radius R. In this case one needs a discrete ph-basis of relatively large dimension. This requires a considerable numerical effort, in particular in the relativistic case, where one has to consider also a very large number of (ah)-configurations including a hole in the Fermi sea and a particle in the Dirac sea.

3.2 Linear response theory

So far, we considered eigen-modes $|\mu\rangle$ of the system and found in Eq. (3.22) a linear eigenvalue problem. In the linear response formalism, we start from a totally different

ansatz. We now consider the system in an external time-dependent field with small amplitudes:

$$F(t) = \sum_{\alpha\beta} f_{\alpha\beta}(t) a^\dagger_\alpha a_\beta e^{-i\omega t} + f^*_{\beta\alpha} a^\dagger_\alpha a_\beta e^{+i\omega t}. \tag{3.26}$$

oscillating with the frequency ω. This external field F leads to a change in the density, similar to the Eq. (3.9). The basic assumption in this formalism is the assumption that the transition density $\delta\rho$ is linear in the external field:

$$\delta\rho_{\alpha\beta}(\omega) = \sum_{\alpha'\beta'} R_{\alpha\beta\alpha'\beta'}(\omega) f_{\alpha'\beta'}. \tag{3.27}$$

The matrix $R_{\alpha\beta\alpha'\beta'}(\omega)$ is called response function and describes the response of the system to the external field. With the help of time-dependent perturbation theory in first order in the external field, this function can be written in the general form:

$$R_{\alpha\beta\alpha'\beta'}(\omega) = \sum_\mu \frac{\langle 0|a^+_\beta a_\alpha|\mu\rangle\langle\mu|a^+_{\alpha'} a_{\beta'}|0\rangle}{\omega - E_\mu + E_0 + i\eta} - \frac{\langle\mu|a^+_\beta a_\alpha|0\rangle\langle 0|a^+_{\alpha'} a_{\beta'}|\mu\rangle}{\omega + E_\mu - E_0 + i\eta}. \tag{3.28}$$

However, the above expression is not really helpful for the calculation of $R(\omega)$, because the energies E_μ are not known quantities. In the other hand, this function can be derived from the time-dependent mean field equation

$$i\partial_t \rho(t) = [h(\rho(t)) + f(t), \rho(t)] \tag{3.29}$$

of a nuclear system in the external field $F(t)$. In the limit of a small external field, we find:

$$i\partial_t \delta\rho(t) = [h_0, \delta\rho(t)] + [V\delta\rho(t), \rho_0] + [f(t), \rho_0] \tag{3.30}$$

and for the vectors (3.18) we obtain in analogy the RPA equation (3.22) the linear response equation:

$$\left[\omega \begin{pmatrix} 1 & 0 \\ 0 & -1 \end{pmatrix} - \begin{pmatrix} A & B \\ B^* & A^* \end{pmatrix}\right] \begin{pmatrix} \delta\rho_{mi} \\ \delta\rho_{im} \end{pmatrix} = \begin{pmatrix} f_{mi} \\ f_{im} \end{pmatrix}. \tag{3.31}$$

By inverting this equation we obtain for the response function of Eq. (3.27) in the static basis

$$R_{klk'l'}(\omega) = \left[\omega \begin{pmatrix} 1 & 0 \\ 0 & -1 \end{pmatrix} - \begin{pmatrix} A & B \\ B^* & A^* \end{pmatrix}\right]^{-1}_{klk'l'}. \tag{3.32}$$

Neglecting the residual interaction between the ph-pairs we find the free response function

$$R^0_{klk'l'}(\omega) = \frac{n_k - n_l}{\omega - \varepsilon_k + \varepsilon_l + i\eta} \delta_{kk'}\delta_{ll'} \tag{3.33}$$

and using the expressions (3.23) and (3.24) for the RPA matrices we obtain for the full response

$$R(\omega) = \left[(R^0(\omega))^{-1} - V^{\mathrm{ph}}\right]^{-1}, \tag{3.34}$$

where the ph-interaction is given by the matrix

$$V^{\mathrm{ph}} = \begin{pmatrix} V_{minj} & V_{mijn} \\ V^*_{im,nj} & V^*_{imjn} \end{pmatrix} \tag{3.35}$$

Eq. (3.34) can be written in the standard form of the linearized Bethe Salpeter equation:

$$R(\omega) = R^0(\omega) + R^0(\omega)V^{\rm ph}R(\omega). \tag{3.36}$$

This means, that a local external field $F(\mathbf{r})$ induces in r-space a transition density $\delta\rho(\mathbf{r};\omega)$ which obeys the equation

$$\delta\rho(\mathbf{r};\omega) = \delta\rho^0(\mathbf{r};\omega) + \int d^3r' d^3r'' R^0(\mathbf{r}\mathbf{r}',\omega)V^{\rm ph}(\mathbf{r}'\mathbf{r}'')\delta\rho(\mathbf{r}'';\omega), \tag{3.37}$$

where

$$\delta\rho^0(\mathbf{r};\omega) = \int d^3r' R^0(\mathbf{r}\mathbf{r}',\omega)f(\mathbf{r}') \tag{3.38}$$

3.2.1 The strength function

We now consider the excitation of the system in an external field $F(t)$ of the form (3.26) and calculate the strength function function:

$$S(\omega) = \sum_\mu |\langle 0|F|\mu\rangle|^2 \delta(\omega - \Omega_\mu). \tag{3.39}$$

In DRPA calculations the transition matrix elements $\langle 0|F|\mu\rangle$ can be expressed by the transition density (3.16)

$$\langle 0|F|\mu\rangle = {\rm Tr}(f\rho^{(\mu)}) = \sum_{mi} f_{im}X^{(\mu)}_{mi} + f_{mi}Y^{(\mu)}_{mi}. \tag{3.40}$$

Expressing the δ-function by

$$-i\pi\delta(x) = \lim_{\eta\to 0} {\rm Im}\,\frac{1}{x+i\eta} \tag{3.41}$$

the strength function can be expressed in terms of the response function (3.28)

$$S(\omega) = -\frac{1}{\pi}\,{\rm Im}\sum_{\alpha\beta\alpha'\beta'} F^*_{\alpha\beta}R_{\alpha\beta\alpha'\beta'}(\omega)F_{\alpha'\beta'} = -\frac{1}{\pi}\,{\rm Im}\,R_{FF}(\omega),$$

where we have used the reduced response

$$R_{QF}(\omega) = \sum_{\alpha\beta\alpha'\beta'} Q^*_{\alpha\beta}R_{\alpha\beta\alpha'\beta'}(\omega)F_{\alpha'\beta'}, \tag{3.42}$$

describing the change of the expectation values of the operator Q in an external field F.

In DRPA calculations discussed above, the strength function vanishes everywhere except at the eigenfrequencies $\omega = \Omega_\mu$ of the system. In realistic systems we have discrete

states only below the neutron emission threshold. Because of the coupling to the continuum, above this value the strength function is a continuous function. In order to obtain continuous curve for $S(\omega)$ in DRPA calculations one usually introduces a smearing by a folding with a Lorentzian of width Γ finds:

$$S(\omega + i\frac{\Gamma}{2}) = -\frac{1}{\pi}\,\mathrm{Im}\,R_{FF}(\omega + i\frac{\Gamma}{2}) = \sum_{\nu}|\langle 0|F|\mu\rangle|^2 \frac{1}{2\pi}\frac{\Gamma}{(\omega-\Omega_\mu)^2 + \frac{1}{4}\Gamma^2}. \tag{3.43}$$

In this case the coupling to the continuum is introduced in a phenomenological way and the escape width Γ cannot be calculated in DRPA. On the other hand, in the response formalism the continuum can be taken into account fully by solving the linear Bethe Salpeter equation (3.36) in r-space (see Section 3.5).

3.2.2 Sum Rules

The number of collective and non collective states $|\mu\rangle$, obtained in the RPA diagonalization of the Hamiltonian is equal to the total number of the particle-hole components. Providing that the nuclear interaction is velocity independent, the product of the energy of these states times the square of the matrix elements of the external operator $\hat{F}$ is a model-independent quantity, known as energy-weighted sum rule m_1*:

$$m_1(\hat{F}) = \sum_n \Omega_n |\langle\nu|\hat{F}|0\rangle|^2 .\Omega) S(\omega) d(\hbar\omega) \tag{3.44}$$

One can prove that the above sum is equal to:

$$\sum_\nu \Omega_\nu |\langle\nu|\hat{F}|0\rangle|^2 = \frac{1}{2}\langle 0|[\hat{F},[H,\hat{F}]]|0\rangle. \tag{3.45}$$

The expectation value of the double commutator in Eq. (3.45) may be quite a simple operator, so that it can often be evaluated more easily than the left part. If, for instance, $\hat{F}$ is the electric dipole operator, the sum rule reflects simple properties of the system as a whole:

$$m_1 = \frac{NZe^2\hbar^2}{mA}, \tag{3.46}$$

where N and Z are the number of the neutrons and protons, A is the sum of them and m is the nucleon mass. It is often useful to consider other moments of the strength function, described in general by the equation:

$$m_k(\hat{F}) = \sum_\nu \Omega_\nu^k |\langle\nu|\hat{F}|0\rangle|^2, \tag{3.47}$$

*The presence of a velocity dependence in the nuclear mean field produces an extra contribution to the energy-weighted sum rule, usually written in the form $m_{1,D} = m_{1,TRK}(1+\kappa)$, where the enhancement factor κ is of the order of 0.1 to 0.3 in heavy nuclei, as obtained by the integration of the photoabsorption cross section up to about twice the peak energy of the GDR.

where interesting quantities can be deduced. For instance, the ratio m_1/m_0 is the quantity often compared with the experimental excitation energy of the corresponding resonance and is called the *centroid energy*. Of course, in most experiments, only a restricted range is accessible and therefore one also has to restrict the summation in Eq. (3.47) to the same energy window. One can also find the notation E_{-1} for $\sqrt{m_1/m_{-1}}$.

From the previous equations, we see that the sum rules depends crucially on the structure of the transition operator $\hat{F}$. This operator is determined by the requirement that *one* state exhausts a major part of the corresponding sum. As a consequence, we can write for isoscalar modes:

$$F(\mathbf{r}) = \sum_{i=1}^{A} r_i^{\lambda} Y_{\lambda 0} \qquad for\ \lambda > 0 \qquad and \qquad F(r) = \sum_{i=1}^{A} r_i^2 \qquad for\ \lambda = 0$$

where interesting quantities can be deduced [102]. For isovector modes, the isospin index τ_3 is also inserted in the above expression. In particular, the isovector dipole operator can be written as:

$$F(\mathbf{r}) = \frac{N}{A} \sum_{p=1}^{Z} r_p Y_{1M}(\hat{r}_p) - \frac{Z}{A} \sum_{n=1}^{N} r_n Y_{1M}(\hat{r}_p) \tag{3.48}$$

3.2.3 Separability and Channel Representation

The evaluation of the strength function (3.28) requires three main steps. As a starting point, one determines the interaction $V^{\mathrm{ph}}_{\alpha\beta\alpha'\beta'}$ of Eq. (3.36). In the second step, one calculates the free response function $R^0(\omega)$, while in the third step one solves the linear response equation (3.36).

Starting from the effective interaction, the numerical effort can be simplified considerably, if the interaction $V^{\mathrm{ph}}_{\alpha\beta\alpha'\beta'}$ is written as a sum of separable terms:

$$V^{\mathrm{ph}}_{\alpha\beta\alpha'\beta'} = \sum_{c} Q^{c}_{\alpha\beta} V^{\mathrm{ph}}_{c} Q^{\dagger\, c}_{\alpha'\beta'} \tag{3.49}$$

where Q^c are single particle operators characterized by the channel index c. From now on, we use this index to express all the possible degrees of freedom of the interaction. In the non-relativistic description, c includes the radial coordinate r and the discrete quantum numbers $\{J, S, T\}$. In relativistic description the nucleons are described by vector wavefunctions and thus c includes also the dirac quantum number D.

If we insert the effective interaction (3.49) into the generalized Bethe-Salpeter equation of Eq. (3.36) and introduce the reduced response function

$$R_{cc'}(\omega) = \sum_{\alpha\beta\alpha'\beta'} Q^{c\dagger}_{\alpha\beta} R_{\alpha\beta\alpha'\beta'}(\omega) Q^{c'}_{\alpha'\beta'}, \tag{3.50}$$

equation (3.36) turns into the reduced Bethe Salpeter equation:

$$R_{cc'}(\omega) = R^0_{cc'}(\omega) + \sum_{c''} R^0_{cc''}(\omega) V^{\rm ph}_{c''} R_{c''c'}(\omega). \tag{3.51}$$

The simplicity of this expression is obvious. Provided that the external operator $\hat{F}$ is expressed by the operators $\hat{Q}_c$ as:

$$\hat{F} = \sum_c f_c \hat{Q}_c. \tag{3.52}$$

we finally obtain the strength function as:

$$S(\omega) = -\frac{1}{\pi} \,\mathrm{Im}\, R_{FF} = -\frac{1}{\pi} \,\mathrm{Im} \sum_{cc'} f^*_c R_{cc'}(\omega) f_{c'}. \tag{3.53}$$

In the cases where the channel index c includes a continuous part, as for instance the radial coordinate r, this is an integral equation. In addition, in Eq. (3.51) the interaction $V^{\rm ph}_c$ is assumed to be diagonal with respect to the channel index c, although this assumption is not always valid, as we will stress later.

3.3 The Point coupling Effective Interaction

As we have discussed in the previous chapter, within a relativistic approach one is able to express the interaction between nucleons either by finite range meson fields, or by considering a contact interaction. In the second case, not only do we avoid the use of virtual mesons, but also we provide ourselves with a much simpler radial dependance for the interaction, which leads to the least numerical complexity. This simplicity is a strong statement not only for the static (RMF) but also for the present RPA calculations. Therefore, in this work, we concentrate in the latter option, where one uses a point coupling RMF approach for the ground state.

In order to derive the residual particle hole interaction, we start from the static case and the expression of the energy functional (2.42). Since the external field acts in such a way that small deviations from the equilibrium density matrix $\hat{\rho}_0$ are produced, i.e. $\hat{\rho} = \hat{\rho}_0 + \delta\hat{\rho}$, one can deduce the residual interaction by expanding the total energy up to second order in $\delta\hat{\rho}$. In particular, we have:

$$E(\hat{\rho}) = E(\hat{\rho}_0) + \sum_{\alpha\beta} \frac{\delta E}{\delta \hat{\rho}_{\alpha\beta}} + \frac{1}{2} \sum_{\alpha\beta\gamma\delta} \frac{\delta^2 E}{\delta\hat{\rho}_{\alpha\beta}\delta\hat{\rho}_{\gamma\delta}} \delta\hat{\rho}^*_{\alpha\beta}\delta\hat{\rho}_{\gamma\delta}. \tag{3.54}$$

The first derivative to be taken at the equilibrium density $(\delta E/\delta\hat{\rho}_{\alpha\beta})_0 = h^0_{\alpha\beta}$ is the stationary single-particle hamiltonian of Eq. (3.6) and eventually vanishes. The second derivative $(\delta^2 E/\delta\hat{\rho}_{\alpha\beta}\delta\hat{\rho}_{\gamma\delta})_0 = \delta h^0_{\alpha\beta}/\delta\hat{\rho}_{\gamma\delta}$ however describes how the single particle

Hamiltonian reacts to small changes in the density matrix and it can be identified as the particle-hole interaction:

$$\frac{\delta^2 E}{\delta\hat{\rho}_{\alpha\beta}\delta\hat{\rho}_{\gamma\delta}} = V^{ph}_{\alpha\delta\beta\gamma}. \tag{3.55}$$

The expansion of the second derivative (3.55) is carefully done in Appendix (A) and for the particular case of the PC-F1 parametrization of the point coupling energy functional, one gets:

$$\begin{aligned} V_c^{ph}(1,2) &= \Big\{\gamma_0^{(1)}[\alpha_S + 2\beta_S\rho_S + 3\gamma_S\rho_S^2 + \delta_S\Delta]\gamma_0^{(2)} \\ &\quad +\beta\gamma_0^{(1)}[\alpha_V + 3\gamma_V\rho_V^2 + \delta_V\Delta]\beta\gamma_0^{(2)} \\ &\quad +\beta\boldsymbol{\alpha}^{(1)}[\alpha_V + \gamma_V\rho_V^2 + \delta_V\Delta]\beta\boldsymbol{\alpha}^{(2)} \\ &\quad +\gamma_0\vec{\tau}^{(1)}[\alpha_{TS} + \delta_{TS}\Delta]\gamma_0\vec{\tau}^{(2)} \\ &\quad +\beta\gamma_0\vec{\tau}^{(1)}[\alpha_{TV} + \delta_{TV}\Delta]\beta\gamma_0\vec{\tau}^{(2)} \\ &\quad +\beta\boldsymbol{\alpha}\vec{\tau}^{(1)}[\alpha_{TV} + \delta_{TV}\Delta]\beta\boldsymbol{\alpha}\vec{\tau}^{(2)}\Big\}\cdot\delta(\mathbf{r}-\mathbf{r}') \\ &+ \gamma_0\frac{1+\tau_3}{2}^{(1)} v_C(\mathbf{r},\mathbf{r}')\gamma_0\frac{1+\tau_3}{2}^{(2)} \end{aligned} \tag{3.56}$$

Neglecting for the moment the Coulomb force, this can be written in a separable form as:

$$V^{\rm ph}(1,2) = \sum_c \Gamma_c^{(1)}\ \delta(\mathbf{r}_1-\mathbf{r}_2)v_c(\mathbf{r}_1)\Gamma_c^{\dagger(2)} \tag{3.57}$$

where the *vertices* Γ_c are 2×2 matrices acting on the indices (s,d,t) and reflect the different covariant structures of the fields including spin and isospin degrees of freedom. We express the 2×2 Dirac matrices as a direct product of spin matrices σ, where $\sigma_{S=0}=1$ and $\sigma_{S=1}=\sigma_\mu$, the Dirac matrices γ_D acting on large and small components:

$$\gamma_0 = \begin{pmatrix} 1 & 0 \\ 0 & -1 \end{pmatrix}, \quad 1 = \begin{pmatrix} 1 & 0 \\ 0 & 1 \end{pmatrix}, \quad \gamma_5 = \begin{pmatrix} 0 & 1 \\ 1 & 0 \end{pmatrix}. \tag{3.58}$$

and the isospin matrices τ_T, obtaining $\Gamma_c = \gamma_D \times \sigma_S \times \tau_T$ (see also the second column of Table 3.1).

For spherical nuclei, the densities and currents in the Lagrangian depend only on the radial coordinate r. Therefore we expand the δ-function in Eq. (3.57) in terms of spherical harmonics

$$\delta(\mathbf{r}_1-\mathbf{r}_2) = \frac{\delta(r_1-r_2)}{r_1 r_2}\sum_L Y_L(\Omega_1)\cdot Y_L(\Omega_2). \tag{3.59}$$

Combining spin (S) and orbital (L) degrees of freedom we find by re-coupling to total angular momentum J

$$(\sigma_S^{(1)}\cdot\sigma_S^{(2)})(Y_L(1)\cdot Y_L(2)) = \sum_J [\sigma_S Y_L]_J^{(1)}\cdot[\sigma_S Y_L]_J^{(2)} \tag{3.60}$$

Inserting this expression into Eq. (3.63) we obtain for the interaction a sum (or integral) of separable terms (channels)

$$V^{ph}(1,2) \;=\; \sum_c \int_0^\infty dr\; Q_c^{(1)}(r)\; v_{cc'}(r)\; Q_{c'}^{\dagger(2)}(r) \tag{3.61}$$

Each channel is characterized by a continuous parameter r and the discrete numbers $c = (D, S, L, J, T)$. The corresponding channel operators $Q_c^{(1)}(r)$ are local single particle operators

$$Q_c^{(1)}(r) \;=\; \frac{\delta(r-r_1)}{r r_1}\gamma_D^{(1)}\left[\sigma_S^{(1)} Y_L(\Omega_1)\right]_J \tau_T^{(1)} \tag{3.62}$$

and the upper indices (1) and (2) in Eq. (3.61) indicate that these operators act on the "coordinates" $1 = (r_1\Omega_1 s_1 d_1 t_1)$ and $2 = (r_2\Omega_2 s_2 d_2 t_2)$.

The total angular momentum is a good quantum number and for fixed J the sum over c in Eq. 3.61 runs only over specific numbers $c = (D, S, L, T)$ determined by the selection rules. We concentrate in this manuscript on states with natural parity, i.e. $\pi = (-)^L = (-)^J$. Considering that $S = 0$ for the scalar and the time-like vector and that $S = 1$ for the space-like vector we therefore have

$$L = \begin{cases} J & \text{for } S = 0 \\ J \pm 1 & \text{for } S = 1 \end{cases}$$

Finally we have eight discrete channels. Their quantum numbers are shown in Table 3.1. Of course, for $J = 0$ we have for $S = 1$ only $L = 1$, and therefore only six channels.

c	$\Gamma_c = \gamma_D \otimes \sigma_S \otimes \tau_T$	D	S	L	T
1	$\gamma_0 \otimes 1 \otimes 1$	S	0	J	0
2	$1 \otimes 1 \otimes 1$	V	0	J	0
3	$\gamma_5 \otimes \sigma \otimes 1$	V	1	$J-1$	0
4	$\gamma_5 \otimes \sigma \otimes 1$	V	1	$J+1$	0
5	$\gamma_0 \otimes 1 \otimes \tau_3$	S	0	J	1
6	$1 \otimes 1 \otimes \tau_3$	V	0	J	1
7	$\gamma_5 \otimes \sigma \otimes \tau_3$	V	1	$J-1$	1
8	$\gamma_5 \otimes \sigma \otimes \tau_3$	V	1	$J+1$	1

Table 3.1: Vertices and quantum numbers of the different channels in Eq. (3.57)

Finally, in Eq. (3.57) the effective interaction $v_c(\mathbf{r})$ describes the r-dependance and the strength of the different channels as it is derived in a consistent way from the

Lagrangian. In the PC-F1 parametrization, the terms derived from the four-fermion terms (2.38) are constants. Furthermore, due to a density dependence of the higher order terms (2.39) as well as the corresponding rearrangement terms, $\upsilon_c(\mathbf{r})$ depends on the static density and therefore on the coordinate $\mathbf{r}$. In addition, because of the derivative terms in (3.56), they also contain Laplace operators. Summarizing, we have:

$$\begin{array}{ll} c & \upsilon_c(\mathbf{r}) = \\ \text{scalar:} & \alpha_S + 2\beta_S\rho_S(r) + 3\gamma_S\rho_S^2(r) + \delta_S\Delta \\ \text{time-like vector:} & \alpha_V + 3\gamma_V\rho_V^2(r) + \delta_V\Delta \\ \text{space-like vector:} & \alpha_V + \gamma_V\rho_V^2(r) + \delta_V\Delta \end{array} \tag{3.63}$$

In the isovector case the constants α_S, α_V, δ_S and δ_V are replaced by α_{TS}, α_{TV}, δ_{TS} and δ_{TV}. As we see in Table 2.3 the corresponding values $\beta_{TS} = \gamma_{TS} = \gamma_{TV}$ vanish. So $\upsilon_c(\mathbf{r})$ will correspond to a matrix in channel space, where only the diagonal terms are non-zero, having $\hat{v}_{cc'}^{PC-F1} = \upsilon_c(\mathbf{r})\delta_{cc'}$.

However, the situation in the parameter set DD-PC1 of Niksic [98] is more complicated than that. The reason is that all the spin-isospin channels depend on the same baryon density. As we show in the Appendix (A), the second derivative of the energy functional leads to additional terms which are not diagonal in the channel space. The interaction $\upsilon_{cc'}^{DD-PC1}$ will be given here by the matrix (3.2)

DD-PC1	β	1	$\boldsymbol{\alpha}$	$\vec{\tau}$	$\boldsymbol{\alpha}\vec{\tau}$
β	$\alpha_S[\rho] + \delta_S\Delta$	$\alpha'_S[\rho]\rho_S$	0	0	0
1	$\alpha'_S[\rho]\rho_S$	$1/2\alpha''_S[\rho]\rho_S^2 + F_V[\rho]$ $+1/2\alpha''_{TV}\rho_{TV}^2$	0	$\alpha'_{TV}[\rho]\rho_{TV}$	0
$\boldsymbol{\alpha}$	0	0	-$\alpha_V[\rho]$	0	0
$\vec{\tau}$	0	$\alpha'_{TV}[\rho]\rho_{TV}$	0	$\alpha_{TV}[\rho]$	0
$\boldsymbol{\alpha}\vec{\tau}$	0	0	0	0	-$\alpha_{TV}[\rho]$

Table 3.2: The structure of the channel matrix $\upsilon_{cc'}(r, r')$ for the DD-PC1 parametrization. The functional $F_V[\rho] = \alpha_V[\rho] + 2\alpha'_V[\rho]\rho + 1/2\alpha''_V[\rho]\rho^2$

An essential feature of the effective interaction $\upsilon_{cc'}$ is that it contains derivative terms in the form of Laplacians Δ (retardation effects are neglected). As we show in the Appendix (B), in spherical coordinates this operator is expressed by:

$$\Delta = r^2 \overleftarrow{\partial}_r \frac{1}{r^2} \overrightarrow{\partial}_r + \frac{L(L+1) - 2}{r^2}. \tag{3.64}$$

Here the radial derivatives $\overleftarrow{\partial}_r$ and $\overrightarrow{\partial}_r$ act on the right and on the left side in Eq. (3.51), i.e. on $\mathcal{R}^0_{c'c}(r'r)$ and on $\mathcal{R}_{cc''}(r, r'')$. Since the integration is discretized $r \to r_n = nh$

the operator $\overrightarrow{\partial}_r$ is represented by a matrix in r-space as for instance by the tree-point formula:

$$\hat{\partial}_{nn'} = \frac{1}{2h}(\delta_{n',n+1} - \delta_{n',n-1}). \tag{3.65}$$

This means that the term $\upsilon_{cc'}(r)$ in Eq. (3.63) is no more diagonal in the coordinate r and it must be replaced by a more general expression $\upsilon_{cc'}(r, r')$.

The description of the residual interaction is completed by the inclusion of the Coulomb term. This term has been proven to be important and thus excluding it is not a good approximation. However, it needs special treatment because it brakes isospin symmetry. This problem is solved by expanding the Coulomb term in off-diagonal terms. This can be easily done, if we recall that V_C can be written as:

$$V_C(1,2) = (\frac{1}{2}(1+\tau_3))^{(1)} \frac{\alpha}{|\mathbf{r}_1 - \mathbf{r}_2|} (\frac{1}{2}(1+\tau_3))^{(2)} \tag{3.66}$$

where $\tau_3 = 1(-1)$ for protons (neutrons). After decomposing Eq. (3.66), we finally get:

$$V_{12}^C = \frac{1}{4}\frac{\alpha}{|\mathbf{r}_1 - \mathbf{r}_2|} \times (\mathbf{1}^{(1)}\mathbf{1}^{(2)} - \mathbf{1}^{(1)}\tau_3^{(2)} - \tau_3^{(1)}\mathbf{1}^{(2)} + \tau_3^{(1)}\tau_3^{(2)}).$$

That means that in isospin space, the Coulomb interaction can be split into four parts, two of which correspond to mixing (off-diagonal) terms. This leads to a Coulomb matrix $\upsilon_{cc'}^C(r, r')$ in Eq. (3.63) as shown in Table 3.3. The r dependance can be written as:

$$\frac{\alpha}{|\mathbf{r}_1 - \mathbf{r}_2|} = \sum_L \upsilon_{\mathrm{C}}(r, r') Y_L(\Omega) \cdot Y_L(\Omega') \tag{3.67}$$

with

$$\upsilon_{\mathrm{C}}(r, r') = \frac{4\pi\alpha}{2L+1} \cdot \frac{r_<^L}{r_>^{L+1}}, \tag{3.68}$$

and $r_<$ and $r_>$ are the smaller and the greater of r and r'.

	β	1	$\boldsymbol{\alpha}$	$\beta\vec{\tau}$	$\vec{\tau}$	$\boldsymbol{\alpha}\vec{\tau}$
β	0	0	0	0	0	0
1	0	$\frac{1}{4}\upsilon_C$	0	0	$\frac{1}{4}\upsilon_C$	0
$\boldsymbol{\alpha}$	0	0	$-\frac{1}{4}\upsilon_C$	0	0	$-\frac{1}{4}\upsilon_C$
$\beta\vec{\tau}$	0	0	0	0	0	0
$\vec{\tau}$	0	$\frac{1}{4}\upsilon_C$	0	0	$\frac{1}{4}\upsilon_C$	0
$\boldsymbol{\alpha}\vec{\tau}$	0	0	$-\frac{1}{4}\upsilon_C$	0	0	$-\frac{1}{4}\upsilon_C$

Table 3.3: The structure of the channel matrix $\upsilon_{cc'}^C(r, r')$ for the Coulomb interaction.

3.3.1 Relativistic Free Response Function

As we have discussed before, in most of the relativistic RPA approaches, one uses the same basis (harmonic oscillator or Woods-Saxon) for the entire single particle spectrum. We recall here that this spectrum has a discrete and a continuous part. Therefore the levels which lie in the positive energy continuum are fully discretized and obey the regular Dirac equation with fixed boundary conditions far outside the nucleus. The wavefunction of each state is characterized by the 2-spinors:

$$|\psi\rangle_{\kappa\, m} = \frac{1}{r}\begin{pmatrix} f_{n\kappa}(r)\mathcal{Y}_{\kappa\, m}(\Omega) \\ ig_{n\kappa}(r)\mathcal{Y}_{\bar{\kappa}\, m}(\Omega)\end{pmatrix}. \tag{3.69}$$

where the subscripts n, κ and m are principal and angular momentum quantum numbers; $\kappa = \mp(j+1/2)$ for $j = l \pm 1/2$, where j and l are the total and angular momenta of the nucleon. As usual, m is the z component of the total angular momentum. The spherical spinors $\mathcal{Y}_{\kappa\, m}(\Omega)$ are given in terms of spherical harmonics $Y_{lm_l}(\Omega)$ and Pauli spinors χ_λ as:

$$\mathcal{Y}_{\kappa\, m}(\Omega) = \sum_\lambda \langle lm-\lambda\tfrac{1}{2}\lambda|l\tfrac{1}{2}jm\rangle Y_{lm_l-\lambda}(\Omega)\chi_\lambda, \tag{3.70}$$

while the radial part of the functions $\mathcal{U}_h(\mathbf{r})$ satisfy the homogenous coupled Dirac equations:

$$\begin{aligned}\left(\frac{d}{dr}+\frac{\kappa}{r}\right) f(r) - [\varepsilon_h + M - (V+S)]g(r) &= 0 \\ \left(\frac{d}{dr}-\frac{\kappa}{r}\right) g(r) + [\varepsilon_h + M - (V+S)]f(r) &= 0,\end{aligned} \tag{3.71}$$

as it has been shown in the previous chapter.

Starting from Eq. (3.50) for the reduced response function, we derive the following expression for the corresponding reduced free response function, which depends only on the energy ω and the channel indices c, c':

$$\begin{aligned} R^0_{cc'}(\omega) &= \sum_{ph} \frac{\langle h|Q^+_c|p\rangle\langle p|Q_{c'}|h\rangle}{\omega-\varepsilon_p+\varepsilon_h+i\eta} - \frac{\langle p|Q^+_c|h\rangle\langle h|Q_{c'}|p\rangle}{\omega+\varepsilon_p-\varepsilon_h+i\eta} \\ &+ \sum_{\alpha\, h} \frac{\langle h|Q^+_c|\alpha\rangle\langle \alpha|Q_{c'}|h\rangle}{\omega-\varepsilon_\alpha+\varepsilon_h+i\eta} - \frac{\langle \alpha|Q^+_c|h\rangle\langle h|Q_{c'}|\alpha\rangle}{\omega+\varepsilon_\alpha-\varepsilon_h+i\eta} \end{aligned} \tag{3.72}$$

where h stands for occupied (hole), p for unoccupied (particle) states above the Fermi energy and α are the unoccupied states in the Dirac sea. This is a generalization of the free response function of Eq. (3.33) to include relativistic dynamics.

The operators Q_c given by Eq. (3.62) are characterized by the channel index which describe the residual interaction $V^{ph}_{cc'}$, namely $c = (r, DSLT)$. Each single particle

matrix element of the form $\langle p|Q_c|h\rangle$ in Eq. (3.72) separates into an angular, an isospin and a radial part.

$$\langle p|Q_c|h\rangle = \langle p|\tau_T|h\rangle\langle\kappa_p||\left[\sigma_S Y_L\right]_J||\kappa_h\rangle\langle p|\gamma_D|h\rangle_r. \tag{3.73}$$

Since we consider in this paper only *ph*-RPA in the same nucleus, the particle states have the same isospin as the hole states and thus the isospin matrix element $\langle p|\tau_T|h\rangle$ is simply a phase ± 1.

matrix elements $\langle p|\gamma_c|h\rangle_r = \langle p(r)|\gamma_D|h(r)\rangle$ then depend on a single r. They are found as sums over the large and small components in the radial spinors $|h(r)\rangle$ and $|p(r)\rangle$ for fixed values of r.

The angular matrix elements depend on the quantum numbers κ of particle and hole states, and, of course, on the channel quantum numbers S and L. In particular, we find for $S = 0$:

$$\langle lj||Y_J||l'j'\rangle = \frac{1+(-)^{l+l'+J}}{2}\frac{\hat{j}\hat{j}'\hat{J}}{\sqrt{4\pi}}(-)^{j-\frac{1}{2}}\begin{pmatrix} j & J & j' \\ -\frac{1}{2} & 0 & \frac{1}{2}\end{pmatrix} \tag{3.74}$$

while for $S = 1$, it is

$$\begin{aligned}\langle lj||\left[\sigma Y_L\right]_J||l'j'\rangle &= \frac{1+(-)^{l+l'+L}}{2}\frac{\hat{j}\hat{j}'\hat{L}\hat{J}}{\sqrt{4\pi}}\left[(-)^{j'+\frac{1}{2}}\begin{pmatrix} 1 & L & J \\ 0 & 0 & 0\end{pmatrix}\begin{pmatrix} j & J & j' \\ \frac{1}{2} & 0 & -\frac{1}{2}\end{pmatrix}\right. \\ &- \left.\sqrt{2}(-)^{l'}\begin{pmatrix} 1 & L & J \\ -1 & 0 & 1\end{pmatrix}\begin{pmatrix} j & J & j' \\ \frac{1}{2} & -1 & \frac{1}{2}\end{pmatrix}\right].\end{aligned} \tag{3.75}$$

Using for the angular and isospin part the abbreviation

$$Q^c_{ph} = \langle\kappa_p||\left[\sigma_S Y_L\right]_J||\kappa_h\rangle\langle p|\tau_T|h\rangle, \tag{3.76}$$

we finally obtain for the reduced response function of Eq. (3.72) in r-space:

$$\begin{aligned}\mathcal{R}^0_{cc'}(r,r';\omega) &= \sum_{ph}\left\{Q^{*c}_{ph}Q^{c'}_{ph}\frac{\langle h|\gamma^+_c|p\rangle_r\langle p|\gamma_{c'}|h\rangle_{r'}}{\omega-\varepsilon_p+\varepsilon_h+i\eta} - Q^{*c}_{hp}Q^{c'}_{hp}\frac{\langle h|\gamma_{c'}|p\rangle_{r'}\langle p|\gamma^+_c|h\rangle_r}{\omega+\varepsilon_p-\varepsilon_h+i\eta}\right\} \\ &+ \sum_{\alpha h}\left\{Q^{*c}_{\alpha h}Q^{c'}_{\alpha h}\frac{\langle h|\gamma^+_c|\alpha\rangle_r\langle\alpha|\gamma_{c'}|h\rangle_{r'}}{\omega-\varepsilon_\alpha+\varepsilon_h+i\eta} - Q^{*c}_{h\alpha}Q^{c'}_{h\alpha}\frac{\langle h|\gamma_{c'}|\alpha\rangle_{r'}\langle\alpha|\gamma^+_c|h\rangle_r}{\omega+\varepsilon_\alpha-\varepsilon_h+i\eta}\right\}\end{aligned} \tag{3.77}$$

Theoretically speaking, the set of unoccupied states (indices p and α) is infinite in length. In practical applications hoewever, one has to restrict this infinite set by a finite sum introducing an upper limit $\epsilon_p - \epsilon_h < E^{ph}_{cut}$ in energy for the particle states p and a lower limit $\epsilon_a - \epsilon_h > -E^{ah}_{cut}$ for the negative energy solutions a. These energy cut-offs are introduced in order to make the - otherwise infinite - sum, tractable, leading of course to a discretized spectrum.

$\mathcal{R}^0(\omega)$ has poles at the *ph*-energies $\omega = \pm(\varepsilon_p - \varepsilon_h)$.

3.3.2 Bethe-Salpeter Equation

Having defined the residual interaction V^{ph} and the free response function $R^0(\omega)$, we are now able to solve the reduced Bethe-Salpeter equation, which in the coordinate space is written by:

$$\begin{aligned}\mathcal{R}_{c,c'}(r,r';\omega) &= \mathcal{R}^0_{c,c'}(r,r';\omega) \\ &+ \sum_{c''}\int_0^\infty dr''\,\mathcal{R}^0_{c,c''}(r,r'';\omega)\upsilon_{c''}(r'')\frac{1}{r''^{\,2}}\mathcal{R}_{c'',c'}(r'',r';\omega).\end{aligned} \tag{3.78}$$

The numerical treatment of this equation requires a simple matrix representation, so that one can write:

$$\hat{\mathcal{R}}_{cc'}(\omega) = \hat{\mathcal{R}}^0_{cc'}(\omega) + \hat{\mathcal{R}}^0_{cc''}(\omega)\upsilon_{c''}\hat{\mathcal{R}}_{c''c'}(\omega), \tag{3.79}$$

or:

$$\hat{\mathcal{R}}_{cc'}(\omega) = \Big[1 - \hat{\mathcal{R}}^0(\omega)\upsilon\Big]^{-1}_{cc''}\hat{\mathcal{R}}^0_{c''c'}(\omega). \tag{3.80}$$

Numerically, the dimension of these matrices equals the interaction channels times the size of the r-mesh. Although the index c is fixed and well known from the previous analysis (eight channels for transitions of natural parity), the latter depends on the length of the coordinate space, i.e. the maximum value of r (typically $15 - 20\,fm$) as well as the step size $\Delta\, r$.

Proper investigations have shown that calculations involving isoscalar ($T = 0$) excitations are more sensitive to the choice of the r-mesh, that is, a finer mesh is required to reach a convergence, as compared to the isovector ($T = 1$) modes. Although this has not been fully understood yet, our experience let us assume that the main reason for that comes from the uncontrollable kink of the non-spectral Green's function at the point $r = r'$. Obviously, the finer the step size is, the better this king is evaluated and thus the more accurate the result is. But apparently, Isoscalar and Isovector modes do not give the same answer on how small the step size needs to be and there is unfortunately little room for improvement on this direction. As a result, the full dimension of the response matrix will vary between 400 and 800, which is already a factor ten smaller than the conventional RPA methods, which use a diagonalization routine in configuration space.

As we have seen, the evaluation of the strength function $S(\omega)$ is required in order to get an overview of how the nucleus responds to the external force. However, one should keep in mind that different external fields are sensitive to different pieces of the residual interaction. In other words, a multipole excitation of a given angular momentum J, parity π and isospin T, shortly described by the index c_F, will receive a direct contribution from those parts of the interaction which carry exactly the same quantum numbers. For instance isoscalar monopole excitations will be sensitive to the

isoscalar part of the interaction and so on. Therefore, we are only interested in one of the $\mathcal{R}_{cc'}$ terms, namely the one having:

$$c = c' = c_F$$

where c_F characterize the external probe. It is then more proper to rewrite the equation for the strength function as:

$$S(\omega) = \int\int d^3r\, d^3r' F^*(\mathbf{r})\mathcal{R}_{cc'}(\mathbf{r},\mathbf{r}';\omega)F(\mathbf{r}') \cdot \delta_{cc_F}\delta_{c'c_F} \tag{3.81}$$

By proper integration of the full response $\mathcal{R}_{c,c'}$ and keeping only terms that are "stimulated" by the external force, one is able to determine the strength distribution:

$$S(\omega) = \sum_{c\,c'} \delta_{cc_F}\delta_{c'c_F} \int\int d^3r d^3r'\, F(\mathbf{r})\mathcal{R}_{c\,c'}(\mathbf{r},\mathbf{r}')F(\mathbf{r}') \tag{3.82}$$

where c_F corresponds to the set of quantum numbers of the external field $\{J, T\}$.

A special attention must be paid in the case of the isovector dipole excitation ($J^\pi = 1^-, T = 1$). In such a case, more than one channel, i.e. the isoscalar and the isovector part are both contributing to the excitation probe and hence, the Kronecker delta is no more correct. In order to understand that, we recall that the dipole external field is:

$$D(r) = -\sum_{i=1}^{N} \frac{Z}{A}\mathbf{r}_i + \sum_{j=1}^{Z} \frac{N}{A}\mathbf{r}_j. \tag{3.83}$$

which can be rewritten using isospin operators as:

$$\begin{aligned} D &= \sum_{i=n,p} \left[-\frac{Z}{A}[\frac{1}{2}(1-\tau_3)] + \frac{N}{A}[\frac{1}{2}(1+\tau_3)] \right] \mathbf{r}_i \\ &= \sum_{i=n,p} \left[\frac{N-Z}{2A}\mathbf{1} + \frac{1}{2}\tau_3 \right] \mathbf{r}_i \end{aligned} \tag{3.84}$$

Obviously, both isoscalar and isovector terms take part in the summation (3.82), carrying the factors $\frac{N-Z}{2A}$ and $\frac{1}{2}$ respectively. We can easily generalize the idea of these *effective charges* in the equation (3.82), regardless the type of the excitation mode; one simply replaces the Kronecker deltas by the effective charges e_{cc_F}, (see table 3.3.2).

We remind that the full response function $\mathcal{R}_{cc'}(\omega)$ has poles at the eigen energies $E_\mu - E_0$ of the RPA-equation (3.28) in the same restricted space. For real frequencies ω it is purely real, and therefore the strength function vanishes everywhere apart from these poles. For complex energies $\omega + i\Delta/2$, however, these poles are shifted from the real axis and one obtains a continuous spectrum, with the phenomenological width Δ. This procedure yields identical results as the diagonalization of the RPA-matrix in (3.22) along with a subsequent folding with a Lorentzian as discussed in Eq. (3.43).

field	$T=0$	$T=1$	IVD
isoscalar scalar	0	0	0
isoscalar vector	1	0	$\frac{1}{2}\frac{N-Z}{A}$
isovector scalar	0	0	0
isovector vector	0	1	$\frac{1}{2}$

Table 3.4: *The effective charges of the different interaction channels with respect to the isospin of the excitation probe. These values stand for external fields of electric type including transitions of natural parity excitations.*

The sum rules (3.47) can be directly defined as moments of the strength function $S(\omega)$ [102]:

$$m_k = \int_0^\infty \omega^k S(\omega)\, d\omega. \tag{3.85}$$

They are helpful to characterize the spectral distribution of the oscillator strength. In particular they allow us to define the centroid energy by the ratio

$$E_c = \frac{m_1}{m_0}. \tag{3.86}$$

This quantity can be compared directly with experimental values. Of course, in most experiments only a restricted energy range is accessible and therefore one has to restrict the integration in Eq. (3.85) to the same energy window.

Other important quantities are transition densities in various channels c with respect to the operator F:

$$\delta\rho_c(r;\omega) = \sum_{c'} \int_o^\infty dr' \mathcal{R}_{cc'}(r,r';\omega) F_{c'}(r') \tag{3.87}$$

as for instance the neutron and proton transition densities:

$$\delta\rho(r)_{n,p} = \delta\rho_{T=0}(r;\omega) \pm \delta\rho_{T=1}(r;\omega) \tag{3.88}$$

3.4 Achievements and Limitations of Discretization Methods

Soon after the first application of the RPA approach in nuclear systems, it had been realized that excitation of nucleons between bound states is not enough to correctly describe the collective phenomena. Only when one included the transitions to the positive energy continuum, was the result successful.

Continuum has been always a not so easy task to handle with. For that reason it is taken into account approximately through the expansion of the s.p. wave function in the oscillation basis, or by means of its "discretization" [103].

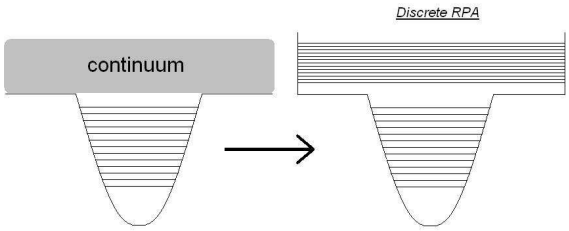

Figure 3.1: *In the discrete RPA, the continuum is approximated by a box which includes discrete levels, similar to the bound ones*

It is indeed convenient to introduce a potential "wall" around and in some distance from the nucleus, so that all the states which are embedded in this "box" will become discretized (Fig. 3.1). One then considers that transitions to continuum are treated like the usual single-particle excitations between bound states and thus, one can safely use either the interaction matrix element (3.35) using configuration space formalism or the single particle Green's function within the linear response formalism. The largest the wall is, the better the positive energy discrete states approximate the true continuum.

Under this approximation, the *discrete* Random Phase Approximation based on Point-Coupling RMF has been tested in the calculations of spherical double-closed nuclei and the results are on the level of the best meson-exchange approaches [104, 105]. In the case of nuclei with open-shell structure, additional effects, such as pairing correlation, must be included in the calculation and an extension of the present model, known as *Relativistic Quasiparticle Random Phase Approximation* (RQRPA) is performed.

In these calculations, the discretization of the continuum is indeed very successful in reproducing the position of the Giant Resonances, as well as the corresponding sum rules with great accuracy. This is basically the reason why people have trusted it for many years now. However, in all those discrete approaches, one virtually ignores the fact that the coupling between the hole levels ($\varepsilon < F$) to the actual continuum is necessary and eventually, important phenomena, such as the acquiring of the decay width by the discrete hole levels, are neglected.

That can be obvious, if one studies qualitatively the response function (3.28). Indeed, $R^0(\mathbf{r}, \mathbf{r}'; \omega)$ is a meromorphic function of ω, with simple poles at the exact excitation energies of the interacting system and thus, the strength function consists of sharp lines at these poles. Only after applying an artificial width via a proper Lorentzian fit, one gets the desirable smearing of the transition strength, as we nicely see in Fig. 3.2 [106].

We already know that the width of a resonance is directly connected to the exhaustion of the corresponding sum rules, but it also gives information about the half lives of the excited states. Therefore, it becomes obvious that the resonance width is a pure physical quantity and one cannot allow any arbitrariness imposed by the Lorentzian fitting.

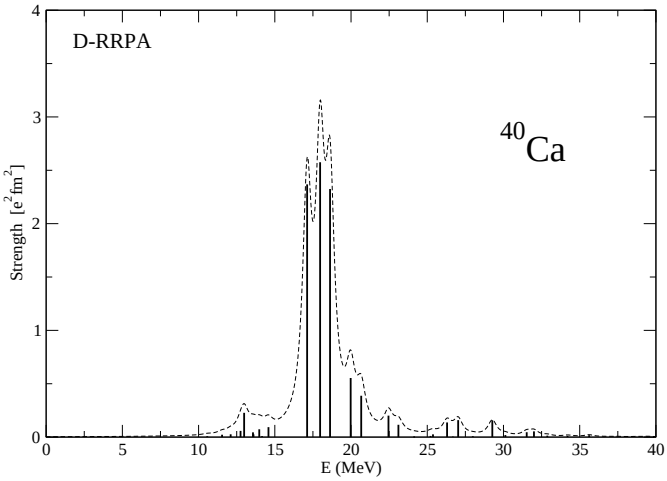

Figure 3.2: *Dipole strength distribution ($J^\pi = 1^-$) of the spherical nucleus ^{40}Ca. The sharp lines are the solutions of the discrete model (D-RRPA), while The dashed curve is the corresponding lorentzian with $\Gamma = 0.7MeV$.*

In the next section, we treat the continuum in the above RPA calculations in an explicit way. The approach we are going to use is called **Continuum Random Phase Approximation** (CRPA) and, although it has been used in the past for non-relativistic models [64, 107, 65], an attempt is being made here to connect it with the RPA based on the Relativistic Mean Field, and explore the new areas that this consideration opens.

3.5 Continuum RPA

As we have continuously and systematically underlined, the "standard" RPA scheme is based on the idea, under which a discrete single particle basis is used in the whole energy spectrum, including the positive energy continuum. The size of this spectrum is determined numerically by the energy cut-off E_{max} or in the case of expansion to harmonic oscillator basis, by the maximum value of the shell quantum number N_{max}. Keeping in mind that many p-h pairs contribute to the matrix elements of the external field, one can *a priori* expect that enlargement of the model space (increase of N_{max}) should lead to more accurate matrix elements. This of course means that any basis truncation leads always to some uncertainty. In that respect, it would be interesting to test the stability of the model, by letting $N \to \infty$, i.e. where one takes the full basis into account.

In terms of numerical effort, this looks impossible, not only for the present, but also for the future generations of computer power. In addition, the inclusion of major shells lying much higher than the Fermi level may be associated with the appearance of single-particle level crossings, which encounter principal limitations on the accuracy of the "discrete" approximation. Basically, only one major shell lying higher than the Fermi shell can be safely considered.

However, even without those two problems, the model faces a more important disadvantage, which is related to the unsatisfactory description of the finite structure of the strength distribution, namely the resonance width. The derivation of such a quantity is difficult and some times an unspeakable subject, which can be easily understood from the differences (sometime substantial) found among the related theoretical papers. It is however an important quantity, if one wants to explain the resonance's tails and the decay properties of the resonance. In this direction, the use of conventional RPA models, which simulate the width by applying a lorentzian curve upon the discrete transition strengths, cannot be the optimal choice.

Fortunately, over the years, people have come up with an alternative method to overpass these limitations, using the so called *Continuum RPA* [64]. By re-formulating the RPA response functions, one achieves a proper assessment of the entire positive energy continuum, where exact scattering wave-functions succeed the unsuitable discrete eigenstates. As a result, not only does the position and the sum rule of the giant resonances are better described, but also a continuous strength distribution is automatically derived.

The main goal of this chapter, is to construct a continuum RPA approach based on relativistic dynamics, in analogy to the existing non-relativistic continuum approaches.

3.5.1 Green's Function Formalism

It is relatively easy to show that solving the continuum RPA equations using the A-B formalism discussed in section (3.1) is practically impossible. At first, the use of exact scattering wave functions would cause a divergence in the interaction matrix element $\langle \alpha\beta \,|\hat{V}|\gamma\delta\rangle$, which is defined as an integral over particle and hole wavefunctions. Furthermore, the RPA amplitudes $X^{\nu}_{mi} = \langle\mu|\alpha^{\dagger}_{m}\alpha_{m}|0\rangle$ which correspond to overlap of the excited state $|\mu\rangle$ with a specific particle hole pair, would be inconsistent with this idea, since the existence of a scattering solution would not allow for a distinguishing between different particles having the same quantum numbers.

On the other side, the response function formalism appears to be more flexible in treating the scattering wave functions, since the different configuration terms appear only in a simple summation. The exact coupling to the continuum is taken care by the re-definition of the single-particle Green's function, needed to determine $R^{0}_{cc'}$. The rest of the linear response equations follow exactly the methodology of the previous chapter.

Using completeness, the reduced free response function of Eq. (3.77) can lead to an

expression including the Green's function:

$$\begin{aligned} R^0_{cc'}(\omega) &= \sum_h \langle\, h|Q^+_c \frac{1}{\omega+\varepsilon_h-\hat{h}} Q_{c'} - Q_{c'}\frac{1}{\omega-\varepsilon_h+\hat{h}} Q^+_c|h\rangle \\ &= \sum_h \langle h|Q^+_c G(\omega+\varepsilon_h)Q_{c'} + Q_{c'}G(-\omega+\varepsilon_h)Q^+_c|h\rangle. \end{aligned} \tag{3.89}$$

where $\langle h(r)| = (f^*_h(r)\ g^*_h(r))$ is the 2-dimensional radial Dirac spinor and $G(E)$ is the relativistic Green's function, which describes the propagation of a particle with energy E and quantum numbers κ from r to r'. It is also important to remember that the operator Q_c acts on the indices (s,d,t). From those quantum numbers, the Dirac index d corresponds to the large and small component of the wavefunction, and thus is connected to the radial dependance. Therefore, if one wants to obtain the reduced free response function in r space, the operator γ_D needs to be disentangled from the main body of the operator Q_c. One then can write:

$$\begin{aligned} \mathcal{R}^0_{cc'}(r,r';\omega) &= \sum_{h\kappa} \Big\{ Q^{*c}_{\kappa h} Q^{c'}_{\kappa h} \,\langle\, h(r)|\gamma^+_D G_\kappa(r,r';\omega+\varepsilon_h)\gamma_{D'}|h(r')\rangle \\ &+ \qquad Q^{*c}_{h\kappa} Q^{c'}_{h\kappa} \langle h(r')|\gamma_{D'} G_\kappa(r',r;-\omega+\varepsilon_h)\gamma^+_D|h(r)\rangle \Big\}. \end{aligned} \tag{3.90}$$

The sum runs over all the occupied states (hole) states h and over all the quantum numbers $\kappa = (lj)$ compatible with the selection rules in the reduced angular and isospin matrix elements:

$$Q^c_{h\kappa} :=\ e_{T_c}\langle \kappa_h||\,[\sigma_{S_c}Y_{L_c}]_J\,||\kappa\rangle, \tag{3.91}$$

where $e_{T_c} = 1$ in the isoscalar channel ($T_c = 0$) and $e_{T_c} = \pm 1$ (for protons or neutrons) in the isovector channel ($T_c = 1$). The reduced matrix elements of the operator $[\sigma_{S_c}Y_{L_c}]_J$ contain integrations over the orientation angles Ω and sums over the spin indices. The matrix elements of the form $\langle h|\gamma_D G(E)\gamma_{D'}|h\rangle$ thus depend on r and r' and are obtained by summing over the Dirac indices $d = 1,2$ for large and small components.

We have already seen in the previous chapter that the Green's function $G_\kappa(r,r',E)$ can be calculated by spectral representation, i.e. as a discrete sum:

$$G_\kappa(r,r';E) = \sum_n \frac{|n(r)\rangle\langle n(r')|}{E-\varepsilon_n}. \tag{3.92}$$

over a complete set of eigenstates $|n(r)\rangle$ of the radial Dirac equation (2.53) with the quantum number κ using box boundary conditions (or an oscillator expansion). Therefore $|n(r)\rangle$ contains both hole $|h(r)\rangle$ and particle $|p(r)\rangle$ states, although only the latter survive in Eq. (3.90)

In the present problem, however, the exact treatment of the continuum requires that exact scattering wave functions are used instead of the discrete p states and thus,

another representation is needed For this reason, we use the so called non-spectral representation, firstly described in the work of Schlomo and Bertsch [64]. In this pioneering work, the non-relativistic Green's function was constructed at each energy from two linearly independent solutions of the Schroedinger equation with different boundary conditions at $r = 0$ and at $r \to \infty$. In the relativistic case, the situation is similar; however, the Dirac-equation in r-space is a two-dimensional equation and therefore the corresponding single particle Green's function is a 2×2 matrix. As in the non-relativistic case, $G(E)$ obeys the inhomogeneous equation:

$$\Big(E - \hat{h}_\kappa(r)\Big)\, G_\kappa(r, r'; E) = \delta(r - r'), \tag{3.93}$$

where $\hat{h}_\kappa(r)$ is the radial Dirac hamiltonian of Eq. (2.53) depending on the quantum number $\kappa = (lj)$. This Green's function can be constructed at each energy E from two linearly independent solutions

$$|u(r)\rangle = \begin{pmatrix} f_u(r) \\ g_u(r) \end{pmatrix}, \qquad |w(r)\rangle = \begin{pmatrix} f_w(r) \\ g_w(r) \end{pmatrix} \tag{3.94}$$

$$\langle u^*(r)| = (f_u(r)\, g_u(r)), \langle w^*(r)| = (f_w(r)\, g_w(r)) \tag{3.95}$$

of the homogenous (Dirac) equation with the same energy E

$$\Big(E - \hat{h}_\kappa(r)\Big)\, |u(r)\rangle = 0, \qquad \Big(E - \hat{h}_\kappa(r)\Big)\, |w(r)\rangle = 0, \tag{3.96}$$

but with different boundary conditions. The functions $u(r)$ and $w(r)$ are normalized in such a way that the Wronskian is equal to:

$$W = \begin{vmatrix} f_w(r) & f_u(r) \\ g_w(r) & g_u(r) \end{vmatrix} = f_w(r) g_u(r) - g_w(r) f_u(r) = 1. \tag{3.97}$$

Of course these scattering solutions depend on the energy E and on the quantum number κ, i.e. we have $|u_\kappa(r; E)\rangle$ and $|w_\kappa(r; E)\rangle$. Using the bracket notation of Dirac for the 2-dimensional spinors and following Ref. [108] we can express this Greens's function as:

$$G_\kappa(r, r'; E) = \begin{cases} |w_\kappa(r; E)\rangle\langle u^*_\kappa(r'; E)| & \text{for } r > r' \\ |u_\kappa(r; E)\rangle\langle w^*_\kappa(r'; E)| & \text{for } r < r' \end{cases} \tag{3.98}$$

with the general property:

$$G_\kappa(r', r; E) = G^\top_\kappa(r, r'; E) \tag{3.99}$$

The solution $u_\kappa(r)$ is regular at the origin, i.e. following Ref. [109] we have for $E > V+S$ in the limit $r \to 0$:

$$u(r) = r \begin{pmatrix} j_l(kr) \\ \frac{\kappa}{|\kappa|} \frac{E-V-S}{k} j_{\tilde{l}}(kr) \end{pmatrix} \overset{r=0}{\to} \begin{pmatrix} \frac{r}{(2l+1)!!}(kr)^l \\ \frac{\kappa}{|\kappa|} \frac{r(E-V-S)}{k(2\tilde{l}+1)!!}(kr)^{\tilde{l}} \end{pmatrix}, \tag{3.100}$$

with $k^2 = (E-V-S)(E-V+S+2m) > 0$ and $j_l(z)$ is a spherical Bessel function of the first kind. The wave function $w_\kappa(r)$ is irregular and represents at large distances for $E > 0$ an outgoing wave, i.e. we have for $r \to \infty$

$$w(r) \overset{E>0}{=} \begin{pmatrix} r h^{(1)}_l(kr) \\ \frac{\kappa}{|\kappa|} \frac{ikr}{E+2m} h^{(1)}_{\tilde{l}}(kr) \end{pmatrix} \overset{r\to\infty}{\to} \begin{pmatrix} 1 \\ \frac{\kappa}{|\kappa|} \frac{ik}{E+2m} \end{pmatrix} e^{ikr}, \tag{3.101}$$

where $h_l^{(1)}(z)$ is the spherical Hankel function of the first kind and for $E < 0$ an exponentially decaying state, i.e. we have for $r \to \infty$

$$w(r) \overset{E\leq 0}{=} \begin{pmatrix} r\sqrt{\frac{2Kr}{\pi}}K_{l+\frac{1}{2}}(Kr) \\ \frac{-Kr}{E+2m}\sqrt{\frac{2Kr}{\pi}}K_{\tilde{l}+\frac{1}{2}}(Kr) \end{pmatrix} \overset{r\to\infty}{\to} \begin{pmatrix} 1 \\ \frac{-K}{E+2m} \end{pmatrix} e^{-Kr}, \tag{3.102}$$

where $K^2 = (V - S - E)(E - V + S + 2m) > 0$ and $j_l(z)$ and $K_{l+1/2}(z)$ are modified spherical Bessel functions [110]. For $E < 0$ the two scattering solutions are both real. This absence of any imaginary term will eventually give no contribution to the strength function of Eq. (3.39). We have to keep in mind, however, that at energies that correspond to eigen energies of a bound state, the solutions $u_\kappa(r, E)$ and $w_\kappa(r, E)$ coincide up to a factor, which means that the Wronskian vanishes at this energy. This corresponds to a pole in the response function on the real energy axis. By adding a small imaginary part to the energy $E \to E + i\eta$ we obtain a sharp peak in the strength distribution.

Having the exact form of the Green's function for the static radial Dirac equation (2.53), one can finally construct the non-spectral or continuum reduced response function (3.90):

$$\begin{aligned} \mathcal{R}^0_{cc'}(rr';\omega) &= \sum_{h\kappa} \Big\{ Q^{*c}_{\kappa h} Q^{c'}_{\kappa h} \gamma^c_{hw}(r;\omega+\varepsilon_h)\gamma^{c'}_{uh}(r';\omega+\varepsilon_h) \\ &- Q^{*c}_{h\kappa} Q^{c'}_{h\kappa} \gamma^c_{hw}(r;\omega-\varepsilon_h)\gamma^{c'}_{uh}(r';\omega-\varepsilon_h) \Big\} \Theta(r-r') \\ &+ \sum_{h\kappa} \Big\{ Q^{*c}_{\kappa h} Q^{c'}_{\kappa h} \gamma^c_{hu}(r;\omega+\varepsilon_h)\gamma^{c'}_{wh}(r;\omega+\varepsilon_h) \\ &- Q^{*c}_{h\kappa} Q^{c'}_{h\kappa} \gamma^c_{hu}(r;\omega-\varepsilon_h)\gamma^{c'}_{wh}(r';\omega-\varepsilon_h) \Big\} \Theta(r'-r) \end{aligned} \tag{3.103}$$

where the Dirac matrix elements depend on the coordinate r:

$$\gamma^c_{hw}(r;E) = \langle h|\gamma_c|w(E)\rangle_r, \tag{3.104}$$
$$\gamma^c_{hu}(r;E) = \langle h|\gamma_c|u(E)\rangle_r, \tag{3.105}$$
$$\gamma^c_{uh}(r;E) = \langle u^*(E)|\gamma_c|h\rangle_r, \tag{3.106}$$
$$\gamma^c_{wh}(r;E) = \langle w^*(E)|\gamma_c|h\rangle_r. \tag{3.107}$$

We have discussed earlier, that the Continuum RPA, is capable of reproducing a finite structure of the strength distribution, and eventually a resonance width. This is easily realized after looking at the definition of the irregular function (3.101). Whenever this wave function is a complex function, it is reasonable for the imaginary part of the response function and thus it offers a nonzero strength function $S(\omega) \propto Im[R(\omega)]$

without the need of any auxiliary parameter $i\eta$. Of course this is true only for energies above the neutron emission threshold.

A question then emerges on how satisfactory this resonance width is, as compared to the one deduced from experimental data. To answer this, we need to understand better the nature of the width which is derived from our method. Since it is connected to nucleon transitions to unbound levels, there is a certain probability that the nucleon will escape the nucleus. This probability mostly depends on the height of the centrifugal barrier and of the Coulomb barrier, if the excited particle is a proton. The higher the barrier is, the longer the particle stays in the excited state and hence, the probability of particle decay is connected to the width of this particular level. Therefore, the resonance width that is deduced by the continuum calculations is called decay or escape width $\Gamma^{\uparrow}$.

Unfortunately, $\Gamma^{\uparrow}$ is only a part of the total width that corresponds to the experimental outcome. From a microscopic point of view, the total width of a giant resonance has three sources. A second part would correspond to the Landau damping in the finite nucleus which is regarded as the fragmentation of the resonance over the particle-hole configurations.

A third part would originate from a coupling of the simple RPA excitations to more complex configurations, such as 2p2h and so on. This gives the so called spreading width ($\Gamma^{\downarrow}$). It has been shown in recent investigations of the coupling to these configurations within the framework of the relativistic time-blocking approximation (RTBA) [111] or the relativistic quasiparticle-time-blocking approximation (RQTBA) [112] that such couplings can be taken into account successfully in a fully consistent way starting from one density functional $E[\rho]$. So far, relativistic investigations of this type have been carried out with discrete methods. At present, investigations in this direction including the continuum properly go beyond the scope of this work.

Through the following calculations, we will address the influence of $\Gamma^{\uparrow}$ in the total width, and thus get an overview of the contribution of the continuum representation in the overall strength contribution.

Chapter 4

Results

Electric and magnetic giant resonances in the atomic nucleus represent a spectacular example of the complexity of collective phenomena that take place in many-body fermionic quantum systems. In atomic nuclei these collective excitations are usually classified according to their multipolarity ΔL, spin ΔS and isospin ΔT quantum numbers [113, 114]. The first experimental observation of the phenomenon of increased absorption cross section of photons from some target nuclei was made by Bothe and Gentner [115] and was later confirmed by Baldwin and Klaiber [116]. An interpretation was given by Goldhaber and Teller [117] within the macroscopic hydrodynamical model, which treated protons and neutrons as rigid fluids, oscillating relative to each other. This mode was identified as an isovector giant dipole resonance (IVGDR) characterized by the multipolarity, spin and isospin transfers $\Delta L = 1$, $\Delta S = 0$ and $\Delta T = 1$ respectively. Then followed the observation of other collective modes, such as the isoscalar giant monopole resonance (ISGMR) and the isoscalar quadrupole resonance (ISGQR). In addition we have the Isoscalar Dipole Resonance (ISGDR) revealing the spurious state corresponding to a translational motion of the nucleus. These modes show up in an energy range of $10-30$ MeV and they exhaust a major portion of the corresponding sum rules [55, 54].

From a microscopic point of view, these vibrations are described via coherent overlap of many one-particle-one-hole (1p-1h) excitations. A schematic representation of such a description can be seen in Fig. 4.1 where 1p-1h transitions contribute coherently to a quadrupole ($\Delta = 2$) mode. As we have already discussed, the key method to study this collective modes is via the random phase approximation.

In the previous section we briefly described how conventional RPA methods treat the continuum part of the spectrum through the introduction of a potential "wall" far from the nucleus. In the credit side of this approach, general properties of collective excitations can be very well reproduced, either by using finite range or point coupling interactions in the mean field level. Since CRPA can treat the coupling to the con-

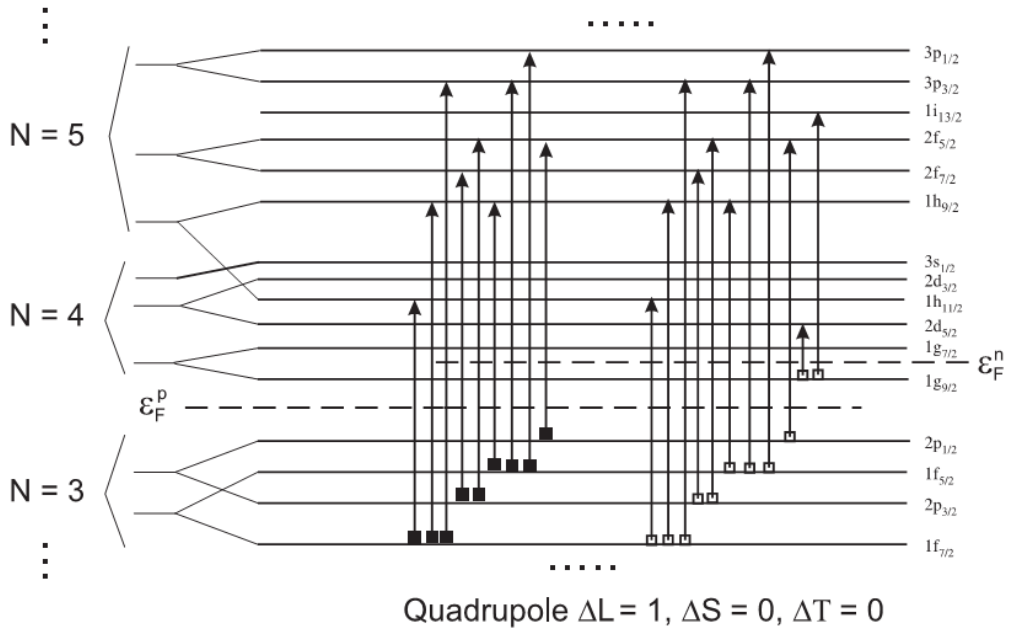

Figure 4.1: An example of microscopic representation of giant resonances as a coherent superposition of many particle-hole transitions. Shown in the case for electric quadrupole ($\Delta = 2$) excitation in the ^{90}Zr nucleus. Protons (arrows with solid squares) and neutrons (arrows with open squares) 1p-1h transitions from levels below to levels above the Fermi level ε_F are shown.

tinuum exactly, it is of interest to see how well this model does in reproducing the properties of excited state in finite nuclei, in particular the giant resonances.

4.1 Numerical Details

In the following, we perform several calculations using the relativistic continuum RPA approach in r-space with Point Coupling forces [46] and try to investigate how the collective excitation phenomena depend on an exact coupling to the continuum. In a first attempt, we select the doubly magic nuclei ^{16}O, ^{40}Ca, ^{132}Sn and ^{208}Pb.

The ground state of the nucleus under consideration is determined by solving the self-consistent RMF equations (2.53) for the parameter set PC-F1 given in Table 2.3. The method we are using is a fourth order Runge-Kutta in r-space (Dirac-mesh) where nucleons move in a spherical box with radius $R_D = 15$ fm and with a mesh size $d_D = 0.05$ fm.

Using the single particle wave functions and the corresponding energies of this static solution, we determine the free response $\mathcal{R}^0$ of Eq. (3.90) in the same box radius but using a wider mesh in r-space (response-mesh). The size d_R of this mesh depends on

the excitation mode; for the monopole modes we use $d_R = 0.15$ fm, while for the dipole a larger interval $d_R = 0.30$ fm is sufficient. Then we solve the Bethe salpeter equation (3.78) to get the strength distribution $S(\omega)$.

At the same time, we perform similar calculations using the discrete RPA approach, where the continuum is not treated exactly, aiming of course to a more precise comparison with the CRPA results. For those calculations, an energy cut-off is necessary, so that a feasible diagonalization is achieved. In particular, we have used an energy cut-off $|\epsilon_p - \epsilon_h| < E^{ph}_{cut} = 300$ MeV for the configurations with particles above the Fermi sea and $|\epsilon_a - \epsilon_h| < E^{ah}_{cut} = 1500$ MeV for configurations with anti-particles in the Dirac sea.

4.2 Multipole Resonances

4.2.1 Isoscalar Giant Monopole Resonances

Results for the isoscalar monopole strength distribution are attainable, once the corresponding external field

$$F^{T=0}_{L=0} = \sum_i^A r_i^2 \tag{4.1}$$

is used. In this case, the classical energy weighted sum rule $m_1(E0)$ becomes:

$$m_1(E0) = \frac{1}{2}\langle [F,[T,F]]\rangle = \frac{\hbar^2}{2m}\langle \nabla^2 F\rangle = \frac{2\hbar^2}{m}\langle r^2\rangle. \tag{4.2}$$

The doubly magic spherical nucleus ^{208}Pb is a particularly good case of nuclear system to begin with, since it has been used in the literature to test numerous nuclear structure models in the past, in particular applications of the random phase approximation [118, 119, 120, 121, 122, 123, 124].

In Fig. 4.2 we show the ISGMR strength distribution obtained by continuum RPA (full red line) and compare it with the discrete B(E0) values (blue) obtained by the spectral representation of the response function for the same parameter set PC-F1 [46].

Using the CRPA approach, we find for the calculated centroid energy defined in Eq. (4.2) that $m_1/m_0 = 14.40$ MeV, which is rather close to the result $m_1/m_0 = 14.17$ MeV deduced from discrete RPA calculations as well as to the experimental value $m_1/m_0 = 13.96 \pm 0.2$ MeV [125].

In those two methods, no additional smearing $\Delta = 0$ has been used. This means that the observed width of the continuum RPA strength corresponds entirely to the escape

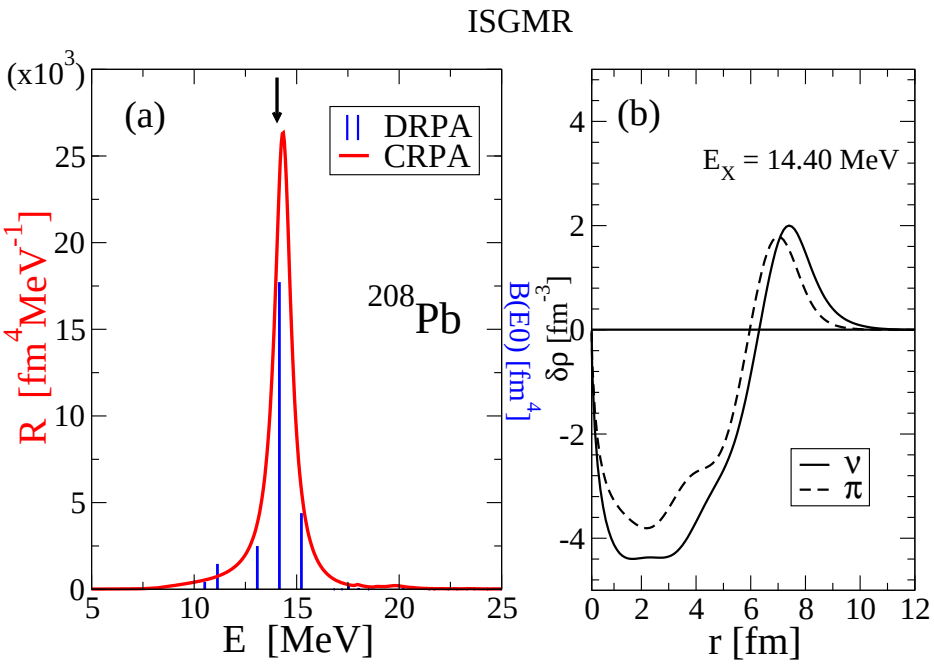

Figure 4.2: Left panel: The isoscalar monopole spectrum in ^{208}Pb, calculated with the parameter set PC-F1. The red curve corresponds to the strength distribution (units on the l.h.s.) obtained by CRPA with $\Delta = 0$, the blue lines give the discrete B(E0)-values (units on the r.h.s.) obtained by the spectral representation with the same force. The black arrow indicates the experimental centroid energy of the resonance [125]. Right panel: the neutron and proton transition densities at the peak with the energy $E = 14.40$ MeV.

with which in the Pb region is very small, due to the relatively high Coulomb and centrifugal barriers in this heavy nucleus. In contrast, discrete RPA provides no width at all. Otherwise, the agreement of these two methods in this nucleus is excellent.

In the second panel of Fig. 4.2, we give the neutron and proton transition densities at the peak energy, as it is calculated in Eq. (3.88). They emphasize the collective character of the isoscalar breathing mode extended over the entire interior of the nucleus with neutrons and protons always in phase.

In addition, the energy weighted sum rule obtained in CRPA using Eq. (3.85) is $m_1(E0) = 5.448 \cdot 10^5$ [MeV·fm^4]. This result is in excellent agreement with the DRPA calculation $m_1(E0) = 5.446 \cdot 10^5$ [MeV·fm^4] as well as the classical value $m_1(E0) = 4A\hbar/2m\langle r^2\rangle = 5.453 \cdot 10^5$ [MeV·fm^4]. This shows that the results obtained in the literature by relativistic RPA calculations using the spectral method are very reliable for such heavy nuclei [126, 53, 56, 54].

In Fig. 4.3 we show the E0 strength distributions for the lighter doubly magic nuclei ^{16}O, ^{40}Ca, and ^{132}Sn. As in Fig. 4.2, the smearing parameter Δ is zero, but now the escape width is considerably larger for these nuclei. Fig. 4.4 summarizes the results for the isoscalar monopole strength distributions as a function of the mass number A.

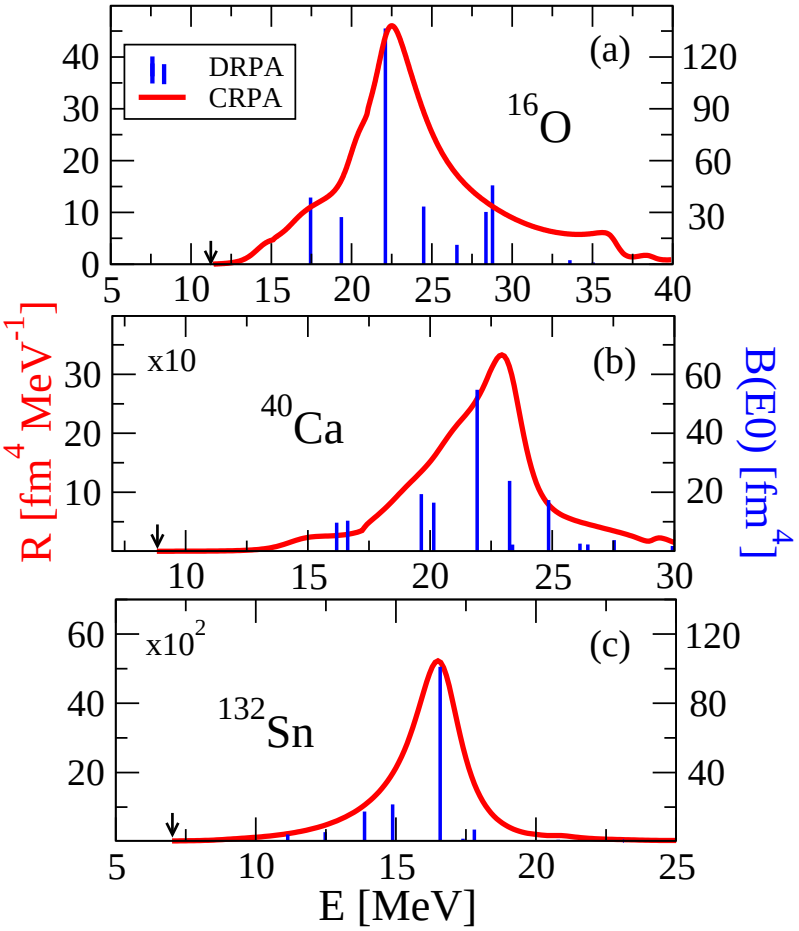

Figure 4.3: The isoscalar monopole strength distribution in the doubly magic nuclei ^{16}O, ^{40}Ca, and ^{132}Sn. Details are the same as in the left panel of Fig. 4.2.

In the upper panel, we plot the centroid energies of both continuum RPA (red dots) and discrete RPA (blue dots), together with the experimental centroid energies taken from Ref. [125]. We also show the phenomenological A-dependence $\bar{E}_{0^+} \approx 80\, A^{-1/3}$ by the dashed line. It becomes clear that CRPA can successfully reproduce collective excitations over the known range of nuclei.

In the lower panel of Fig. 4.4 we show the escape width $\Gamma^{\uparrow}$ of E0 resonances. The red values correspond to the full width half maximum (FWHM) of the peak, using continuum RPA , while the experimental values are indicated in black. The evident disagreement is not surprising, if we consider that only $1p1h$-configurations are taken into account, i.e. the major part of the width resulting from the coupling to more complicated configurations such as $2p2h$ etc. is not described well in this simple RPA approach. It has been shown in recent investigations of the coupling to complex configurations within the framework of the relativistic time-blocking approximation (RTBA) [111] or the relativistic quasiparticle-time-blocking approximation (RQTBA) [112] that such couplings can be taken into account successfully in a fully consistent way starting from one density functional $E[\rho]$. So far, relativistic investigations of this type have been carried

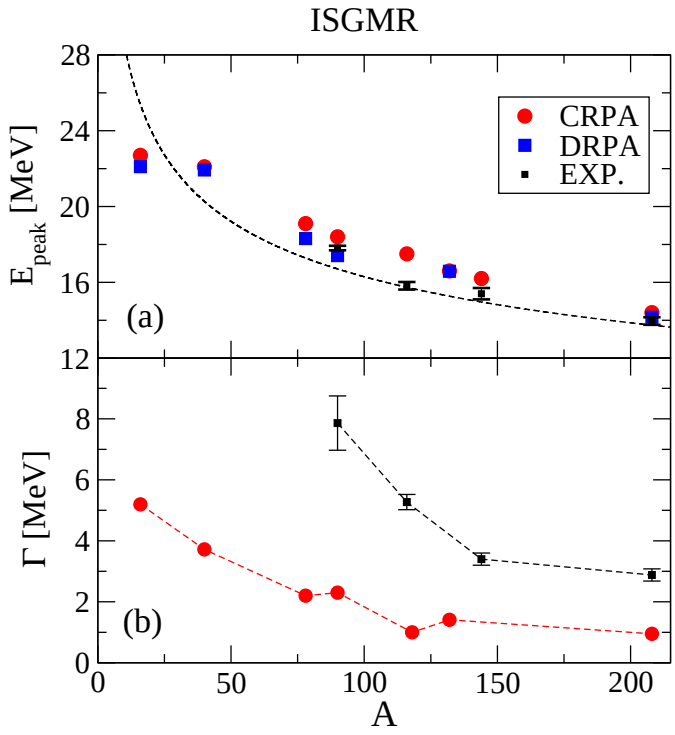

Figure 4.4: Upper panel: The ISGMR centroid energies as a function of the mass number. Lower panel: The experimental and theoretical width of the ISGMR as a function of the mass number. Details are given in the text

out with discrete methods. At present, investigations in this direction including the continuum properly go beyond the scope of this paper.

As we have mentioned in Chapter 2, a new parameter set based on Point Coupling Lagrangian has been recently introduced to describe static and collective phenomena. Known as DD-PC1 [98], this set has been adjusted to spherical open-shell as well as to axially deformed nuclei and hence, it is expected have a better predicting power in the nuclei which require the inclusion of pairing correlations.

On the other hand, the parameter set PC-F1 has been adjusted to spherical double-closed nuclei. It is thus of great interest to study and compare these two available parameter sets PC-F1 and DD-PC1 in view of their ability to reproduce the giant multipole resonances for various group of nuclei. In Fig 4.5 the monopole strength distribution for the group of the double closed-shell nuclei ^{16}O, ^{40}Ca, ^{90}Zr and ^{132}Sn is shown. One can clearly see that, in the case of medium and heavy nuclei, the two sets give almost similar excitation energies and escape widths while a small dissgreement appears in the light nuclei. In both cases however, the energy weighted sum rules are equally exhausted.

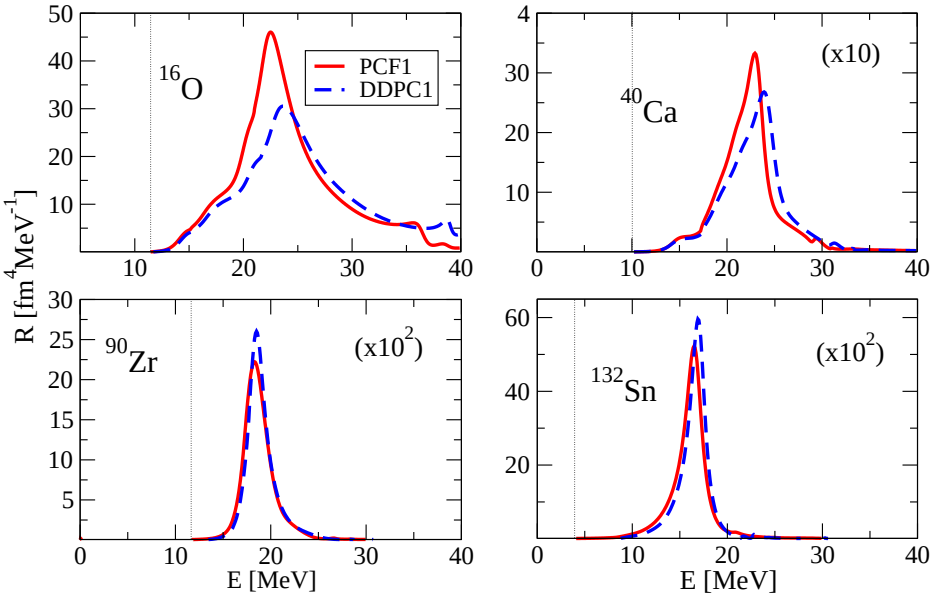

Figure 4.5: The isoscalar monopole strength distribution for the doubly magic nuclei ^{16}O, ^{40}Ca, ^{90}Zr and ^{132}Sn. Calculations using PC-F1 are represented by solid curves, while dashed curves correspond to DD-PC1 calculations [98].The vertical dotted line indicates the neutron emission threshold.

4.2.2 Isovector Giant Dipole Resonances

Isovector Giant Dipole resonance is the most well studied collective excitation and the first to be observed experimentally [116]. An external electromagnetic field of the form:

$$F_{L=1}^{T=1} = \frac{N}{A}\sum_{p=1}^{Z} r_p Y_{1M}(\Omega_p) - \frac{Z}{A}\sum_{n=1}^{N} r_n Y_{1M}(\Omega_p) \tag{4.3}$$

causes protons and neutrons to oscillate in opposite phases to each other and this leads to a pronounced peak in the photoabsorption cross section. This mode has been well studied in many nuclei [113].

With the increasing number of experiments in systems far from stability and systems with large neutron excess, one has been able to observe also low-lying E1 strength in the area of the neutron emission threshold. It is called Pygmy Dipole Resonance PDR and can be interpreted as a collective mode with dipole character where the neutron skin oscillates against an isospin saturated proton-neutron core. This mode has first been predicted in phenomenological models [127, 128] exhausting several percent of the electric dipole sum rule. In recent years, it has been intensively investigated both on the experimental side by the Darmstadt group [129, 130] as well as on the theoretical side, using discrete relativistic RPA calculations based on NL3 [131, 132].

In Fig. 4.6 we show in the upper panel the results of the isovector dipole strength E1 in the nucleus ^{208}Pb using the CRPA approach. The centroid energy at 13.32 MeV is in

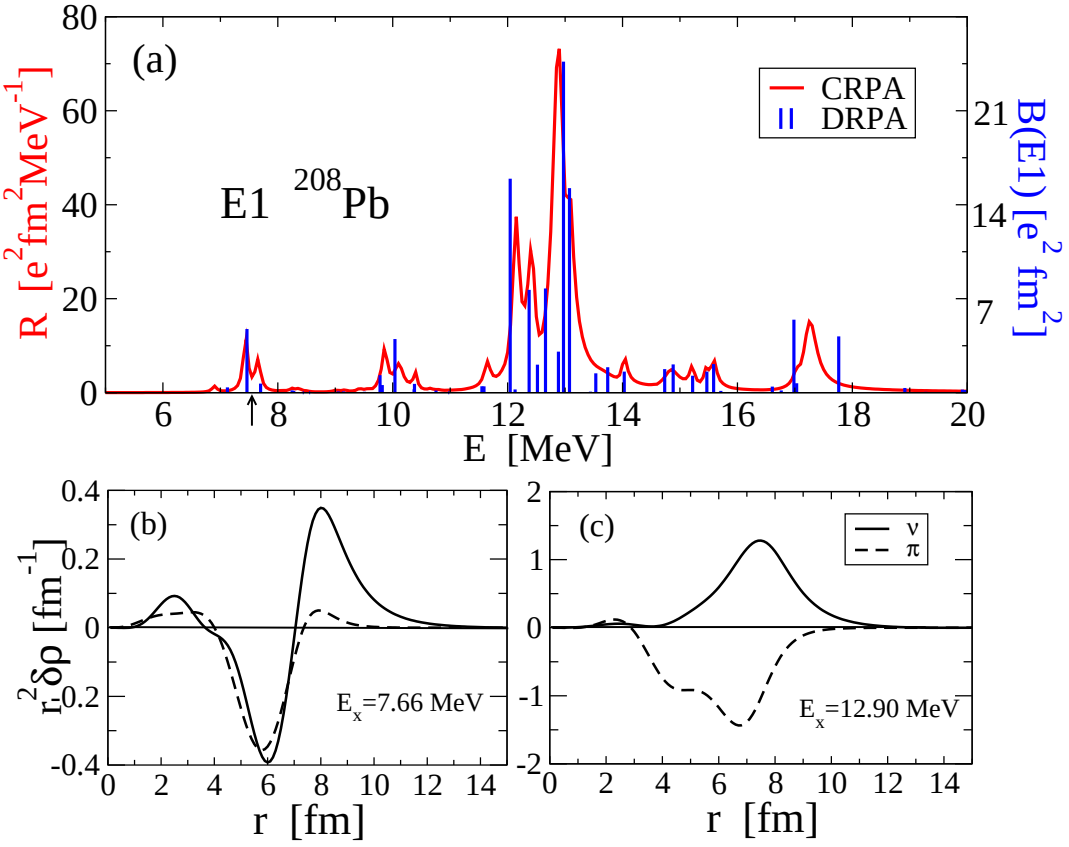

Figure 4.6: Upper panel: The isovector dipole strength distribution in ^{208}Pb. Details are essentially the same as in the left panel of Fig. 4.2. However, in order to distinguish the continuum (red curve) and the discrete (blue lines) calculations we have used here a small smearing parameter $\Delta = 10$ keV in the continuum calculation. The black arrow indicates the theoretical neutron emission threshold. Lower panel: transition densities for neutrons and protons at the energy of the PDR (left) and at the GDR (right).

excellent agreement with the experimental excitation energy $E = 13.3$ MeV [133]. The energy weighted sum rule (3.85) is found as $m_1(E1) = 916.28$ [MeV·fm^2]. This result is in agreement with the DRPA calculation, where we obtain $m_1(E1) = 943.32$ [MeV·fm^2] and as usual somewhat (23.8 %) larger than the classical Thomas-Reiche-Kuhn sum rule

$$m_{\mathrm{TRK}} = \frac{9}{4\pi}\frac{\hbar^2}{2m}\frac{NZ}{A} = 740.13\ [\mathrm{MeV}\cdot\mathrm{fm}^2]. \tag{4.4}$$

In addition to the giant dipole resonance a smaller peak appears at the energy region of the neutron emission threshold around $E \sim 7.5$ MeV, that corresponds to the pygmy resonance.

In the lower panel of Fig. 4.6 we give the transition densities associated the low-lying peak at $E = 7.66$ MeV and the GDR peak at $E = 12.9$ MeV. The higher peak has clearly an isovector character, since the neutrons are oscillating against the protons

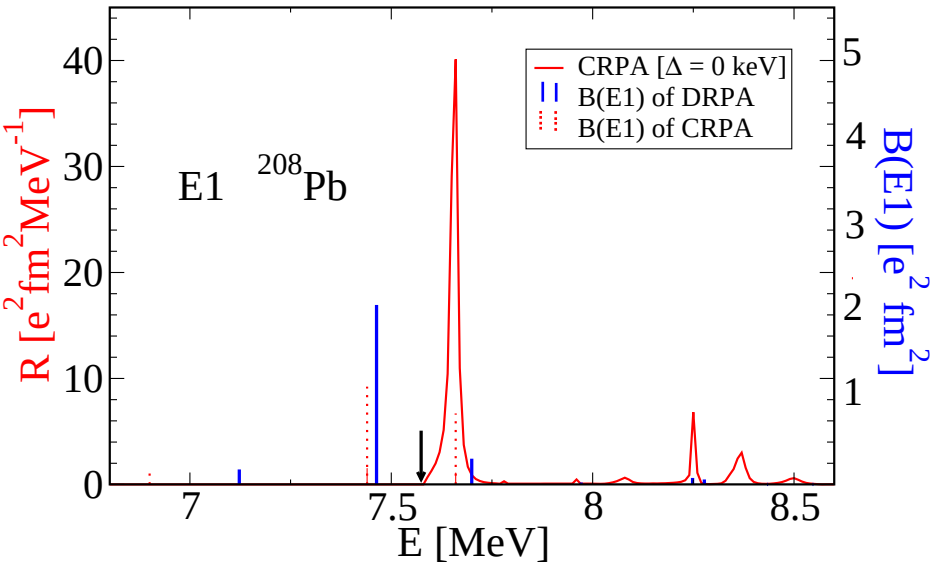

Figure 4.7: The E1 pygmy resonance (PDR) in the nucleus ^{208}Pb. The black arrow indicates the theoretical neutron emission threshold at $E_{\rm th}$ = 7.58 MeV. The units on the l.h.s. characterize the dipole strength given by a red continuous curve of CRPA calculations above the neutron threshold. The units on the r.h.s characterize the discrete B(E1)-values given by the length of the blue vertical lines resulting from DRPA and the red dashed lines obtained by CRPA calculations below the threshold.

over a large radial range centered at the surface. The lower peak shows an isoscalar core, where neutrons and protons oscillate in phase and a pure neutron skin moving against the $T = 0$ core. This is the typical behavior of the pygmy mode.

Closer investigation of pygmy resonances have shown that this mode is in the neighborhood of the neutron separation threshold, slightly below for small and slightly above for large neutron excess (see for instance Ref. [134]). It is therefore of particular importance to study this mode with a proper treatment of the continuum, since in most of the previous investigations this has not been possible [135]. We show in Fig. 4.7 the details of the PDR in the nucleus ^{208}Pb. Above the theoretical neutron separation threshold which is found at $E_{\rm th}$ = 7.58 MeV (black arrow) we have a continuous red curve showing the E1 strength distribution calculated with CRPA (units at the l.h.s) and also few full blue vertical lines that correspond to the discrete poles of the DRPA equations (3.92) (units at the r.h.s.) and with length equal to the corresponding B(E1) values.

In the same figure and below the threshold we have in both cases discrete lines. The solid blue ones are again the eigen-solutions of the DRPA-equation (3). The solutions of the CRPA equations lead in this region also to discrete poles. We show them by dashed red lines at the pole of the full response function. Numerically, the only way to determine the B(E1) values of these poles in CRPA is by using very small imaginary parts $\Delta \to 0$ in the frequency $\omega + i\frac{1}{2}\Delta$ and then determining the B(E1) values by

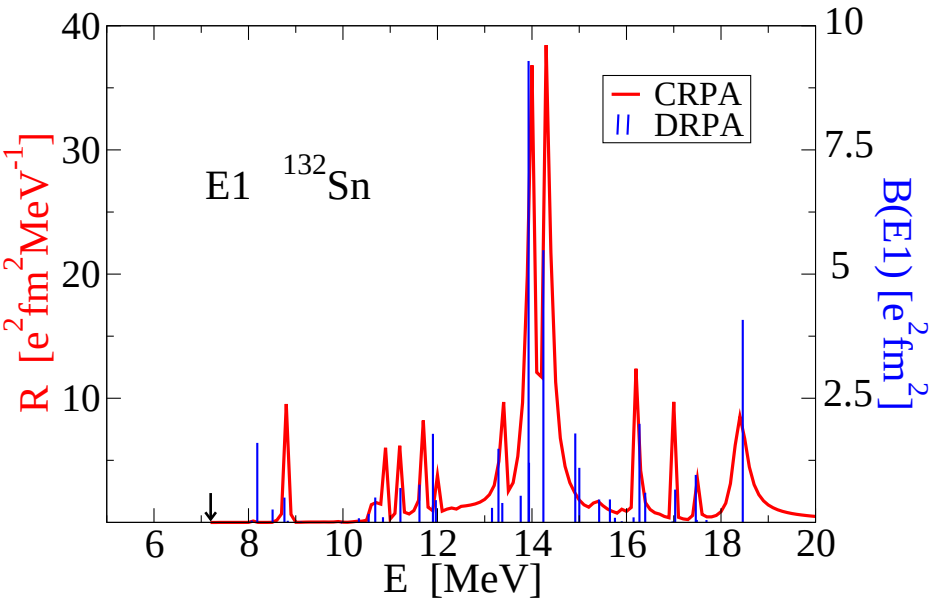

Figure 4.8: The isovector dipole strength distribution in ^{132}Sn. Details are the same as in the upper panel of Fig. 4.6.

	CRPA		DRPA	
No.	E	B(E1)	E	B(E1)
1	6.90	0.19	7.12	0.23
2	7.44	1.45	7.46	2.82
3	*7.66*	*1.11*	7.69	0.40
Σ		2.75		3.45

Table 4.1: Energies and B(E1) values for the three most dominant peaks in the PDR area around the neutron threshold for the nucleus ^{208}Pb for continuum (CRPA) and discrete (DRPA) calculations. The numbers given in italic correspond to resonances in the CRPA calculations. The units are MeV for the energies and [e^{2}fm^2] for the B(E1) values. More details are given in the text

simple integration over a small interval around this pole.

By doing that, we finally observe that there are differences in the details between the continuum and the discrete RPA calculations close to the neutron separation threshold. In Table 4.1 we show for both calculations the three most dominant peaks in the area of the PDR around 7.5 MeV. In the discrete calculations (DRPA) the strength is concentrated in one peak at $E = 7.46$ MeV, whereas in the continuum calculations (CRPA) most of the strength in this region is distributed over two peaks, one below the neutron threshold at $E = 7.44$ MeV and a sharp resonance slightly above the threshold at $E = 7.66$ MeV. The energy weighted strength in this area is 17.09 [e^{2}fm^2]

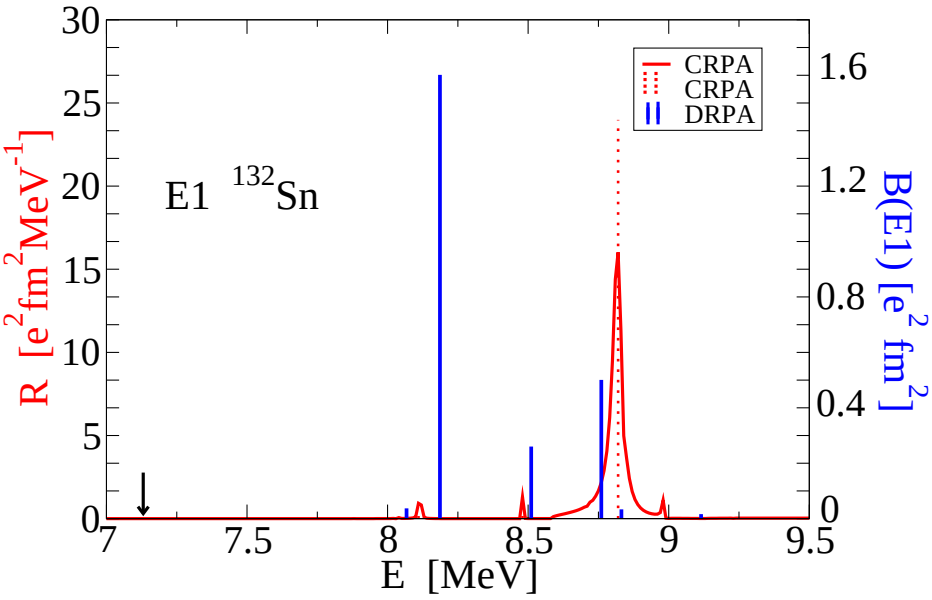

Figure 4.9: The E1 pygmy resonance (PDR) in the nucleus ^{132}Sn. Details are the same as in Fig. 4.7. The arrow indicates the theoretical neutron emission threshold at $E_{\rm th} = 7.13$ MeV.

(i.e. 1.86 % of the total sum rule) for CRPA and 26.95 [e^{2}fm^2] (i.e. 2.85 % of the total sum rule) for DRPA.

	CRPA		DRPA	
No	E	B(E1)	E	B(E1)
1	8.11	0.03	8.067	0.037
2	8.48	0.02	8.186	1.601
3	8.82	1.44	8.511	0.260
Σ		1.490		1.898

Table 4.2: Energies and B(E1) values for the three most dominant peaks in the PDR area above the neutron threshold for the nucleus ^{132}Sn for continuum (CRPA) and discrete (DRPA) calculations. The units are MeV for the energies and [e^{2}fm^2] for the B(E1) values. More details are given in the text

In Fig. 4.8 we show the distribution of the isovector dipole strength in the doubly magic nucleus ^{132}Sn. Again, results using continuum RPA equations (red curve) are compared with the solutions obtained from the spectral representation (blue lines). As one can see, there is excellent agreement between the two methods, as far as the resonance position and the overall distribution is concerned. Moreover, the energy weighted sum rule obtained in CRPA is given by $m_1(E1) = 563.60$ [MeV·fm^2], which is in very good agreement with the DRPA calculation $m_1(E1) = 591.02$ [MeV·fm^4] and 22,9 % larger than the Thomas-Reiche-Kuhn sum rule in Eq. (4.4)

In addition, we find that the escape width in this nucleus is considerably smaller in the E1 channel as compared to the E0 channel in Fig. 4.3. This has the following explanation: The selection rules for *ph*-excitations with E0 character is $\Delta j = 0$ and no change in parity. It turns out that most of the *ph*-excitations contributing to the strong peak in the resonance region have rather small ℓ values for the particle configurations and therefore a very low or no centrifugal barrier. This is different for the E1 resonance. Here we have a change in parity and in addition changes of $\Delta j = 0, \pm 1$ and here a large part of the contributing *ph*-pairs have particles with larger ℓ-values and a strong centrifugal barrier and hence the width becomes smaller.

	CRPA	DRPA	Exp.
^{16}O	20.6279	21.623	23.35±0.12 [136]
^{40}Ca	18.367	19.32	21.76±0.11 [137]
^{132}Sn	14.503	14.78	
^{208}Pb	13.32	13.23	13.3±0.10 [133]

Table 4.3: Isovector dipole (IVGDR) excitation energies in [MeV] for several spherical nuclei, calculated with both continuum and discrete relativistic RPA based on the point coupling force PC-F1.

In Fig. 4.9 we show the region of the PDR in the doubly magic nucleus ^{132}Sn. As already found in Ref. [134], the theoretical neutron emission threshold at $E = 7.13$ MeV lies much below the area of interest. As before, we calculate the B(E1) values of the prominent peaks, for both discrete and continuum calculations with the total strength to be in nice agreement. In Table 4.2 we show in what extent each level contributes to the total pygmy collective state. Finally, the energy weighted strength m_1 in this area is 13.24 [e^{2}fm^2] (i.e. 2.35 % of the total sum rule) for CRPA and 20.45 [e^{2}fm^2] (i.e. 3.46 % of the total sum rule) for DRPA.

In the left panels of Fig. 4.10 we show the electric dipole strength distribution of the lighter nuclei ^{16}O, ^{40}Ca, ^{58}Ni and ^{90}Zr. At first we observe that the systematic rule of $\bar{E}_{1^-} \approx 31.2\, A^{-1/3} + 20.6\, A^{-1/6}$ is nicely reproduced in our calculations. The position of the corresponding peaks and poles with large strength are in rather good agreement, as one can also see in Table 4.3. We find, however, that in the continuum calculations a much larger escape width emerges, in particular for the nucleus ^{16}O, due of course to the very low coulomb and centrifugal barriers. In the right panels of Fig. 4.10 the neutron and proton transition densities for the corresponding excitation energy for the four nuclei are given. It is very clear that all cases, this high concentration of excitation strength corresponds to a pure oscillation of the neutrons against protons.

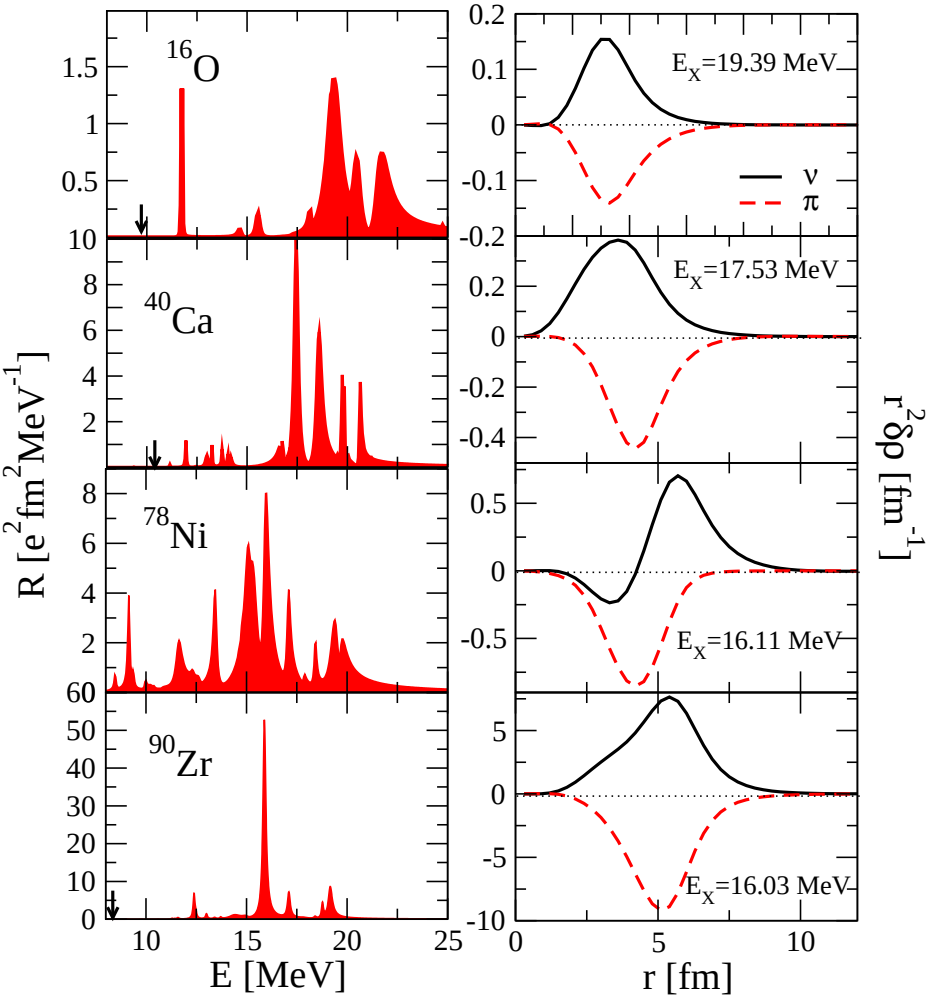

Figure 4.10: Left panels: The isovector dipole strength distribution for the nuclei ^{16}O, ^{40}Ca, ^{58}Ni and ^{90}Zr. The theoretical neutron separation energies are indicated by black arrows. The comparison of the excitation energies with the DRPA calculations as well as the experimental values are given in Table 4.3. Right panels: The corresponding neutron and proton transition densities for the peak energies of the four nuclei.

4.2.3 Isoscalar Giant Dipole Resonances

Besides the distribution of the isovector dipole strength which is dominated by the IVGDR in many experimental spectra, in recent years there has also been considerable interest in measuring the isoscalar dipole strength distribution [138, 139, 140]. In a similar way, one expects to find the ISGDR, which corresponds to a compression wave going through the nucleus along a definite direction and to learn from such experiments more about the nuclear incompressibility. Relativistic calculations based on discrete RPA [126, 56, 122] have shown that the resonance energy of this mode is indeed closely connected to the incompressibility of nuclear matter.

Along with this ISGDR resonance built on $3\hbar\omega$-excitations above 20 MeV, calculations based on both relativistic [126] and non-relativistic [141] RPA approaches have revealed a low-lying isoscalar dipole strength in the region below and around 10 MeV. Experimental investigations with inelastic scattering of α-particles at small angles [142, 140] have also found isoscalar dipole strength in this region. This strength has been attributed in Ref. [143] to an exotic mode of a toroidal motion predicted already in early theoretical investigations on multipole expansions of systems with currents [144, 145] and investigated also by semiclassical methods [146, 147]

On the theoretical point of view, there is further interest in the isoscalar dipole mode, characterized by the quantum numbers ($J^\pi = 1^-, T = 0$), because it contains the Goldstone mode connected with the violation of translational symmetry in the mean field solutions. This mode corresponds to the center of mass motion of the entire nucleus. Because of the missing restoring force, this mode has vanishing excitation energy. It is one of the essential advantages of the RPA approximation, that it preserves translational symmetry and therefore it has an eigenvalue at zero energy with the eigenfunction given by the *ph*-matrix elements of the linear momentum operator.

Since the ISGDR is expected to be a $3\hbar\omega$-excitation it is usually associated with the external field derived in Ref. [148]

$$F^{T=0}_{L=1} \;=\; \sum_{i}^{A}(r_i^3 - \eta r_i)Y_{1\mu}(\Omega_i) \tag{4.5}$$

where $\eta = \frac{5}{3}\langle r^2\rangle$.

In the upper panel of Figs. 4.11 we display the distribution of the isoscalar dipole strength in ^{208}Pb, calculated with the operator (4.5) for $\eta = 0$, that is, we take no action for the spurious state. We therefore observe a huge peak close to zero energy, which dominates the spectrum and corresponds to the spurious translational mode.

It turns out that the position of this spurious state is an extremely sensitive object which strongly depends on the numerics of the model. Of course the optimal would be to calculate the spurious state at exactly zero energy. Therefore this excitation mode presents an ideal benchmark for numerical efficiency of the RPA or the linear response equations. Detailed studies have shown that the exact separation of the spurious state requires a fully self-consistent solution [121]; a fact which was not given in most of the older applications with Skyrme or Gogny forces. In many cases, only few of the different terms in the residual interaction had been taken into account in RPA calculations.

In addition, the configuration space must be full. Indeed, the discussed drawback of the conventional spectral representation in a truncated *ph*-configuration space affects the position of the spurious state. Therefore, the convergence to zero eigenvalue of the spurious translational mode occurs very slowly and only in extremely large configuration space. In relativistic applications this is translated to including also large spectrum in the Dirac sea [149, 53]. As a consequence, in the spectral representation, one has

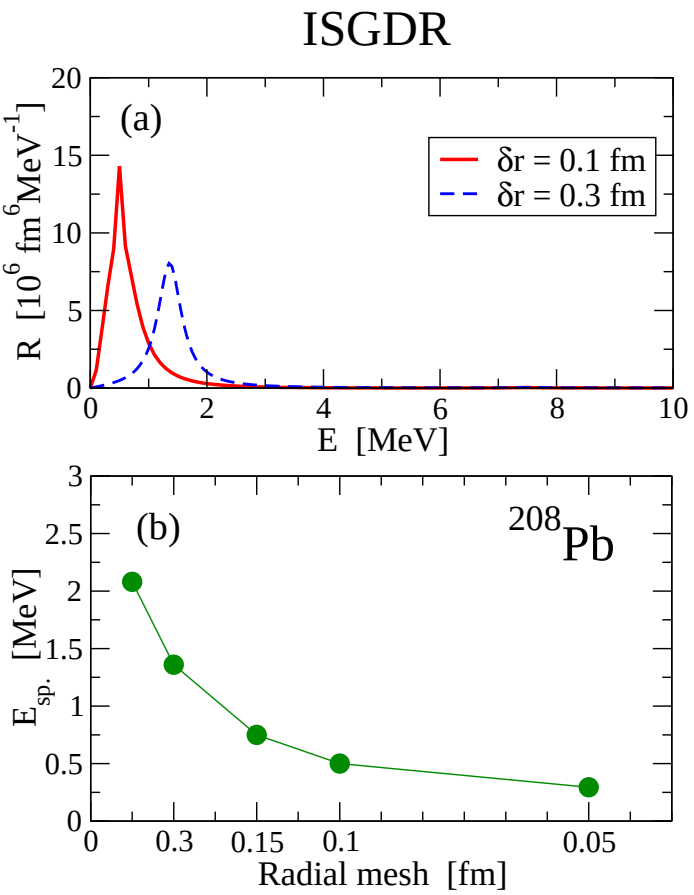

Figure 4.11: Upper panel: Spurious E1 isovector strength distribution in ^{208}Pb obtained by CRPA calculations with two different values of the radial mesh size δr. Lower panel: the position of the spurious E1-state as a function of the radial mesh size

to take into account many configuration with particles in the Dirac and holes in the Fermi sea, which complicates the numerical applications considerably and inevitably decreases the efficiency of the method.

Fortunately, using the continuum RPA approach, one is free from such constraints and limitations, since the entire configuration space is automatically included. In Fig. 4.11 we show that the spurious state depends only on the mesh size used for the solution of the continuum response equation (the response mesh). In the upper panel of Fig. 4.11 we present two calculations with different mesh-sizes, where in the lower panel we show how the spurious state moves to zero energy as we use a finer radial interval. For the ideal case of an infinitesimal mesh, the strength connected with the spurious state would be completely separated from the rest of the spectrum.

If we properly subtract the spurious state in the upper part of Fig. 4.11 and focus on the high-energy region, some small but finite fragments of the remaining strength are revealed. They are shown in Fig. 4.12 in a scale increased by three orders of magnitude. The main part of the remaining spectrum is located at $E \approx 25$ MeV. This "exotic"

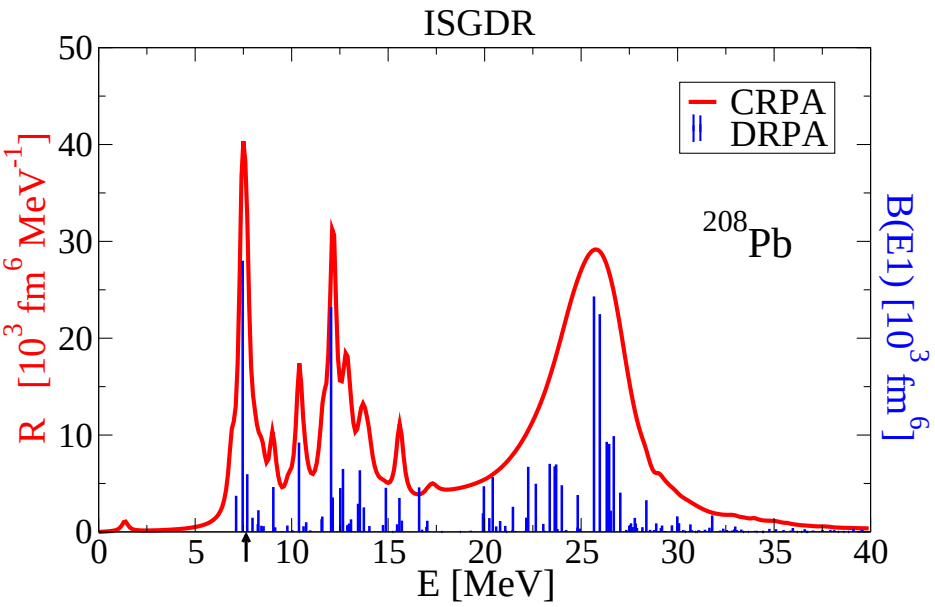

Figure 4.12: The isoscalar dipole strength distribution in ^{208}Pb. Details are the same as in the upper panel of Fig. 4.6.

mode is best described as a "hydrodynamical density oscillation", in which the volume of the nucleus remains constant and the state can be visualized as a compression wave oscillating back and forth through the nucleus [143].

	Low[MeV]	High[MeV]
CRPA	10.97	25.05
Hamamoto *et al* [150]	~ 14	23.4
Coló *et al* [151]	10.9	23.9
Vretenar *et al.* [126]	10.4	26.
Piekarewicz [122]	$\sim$ 8	24.4
Shlomo, Sanzhur [152]	~ 15	~ 25
Uchida *et al.* [140]	12.7 ± 0.2	22.4 ± 0.5

Table 4.4: Self-consistent (relativistic and non-relativistic) RPA calculations performed for the ISGDR in ^{208}Pb, compared with the most recent experimental data. The two columns refer to the centroid energies of both the low- and high-energy sides of the ISGDR mode.

Moreover, Fig. 4.12 shows an additional mode in the region of $10 - 15$ MeV that exhausts roughly 20% of the total sum rule. This peak does not correspond to a compression mode, but rather to a kind of toroidal motion discussed in [143, 153]. The toroidal dipole mode is understood as a transverse zero-sound wave and its experimental observation would invalidate the hydrodynamical picture of the nuclear medium, since there is no restoring force for such modes in an ideal fluid.

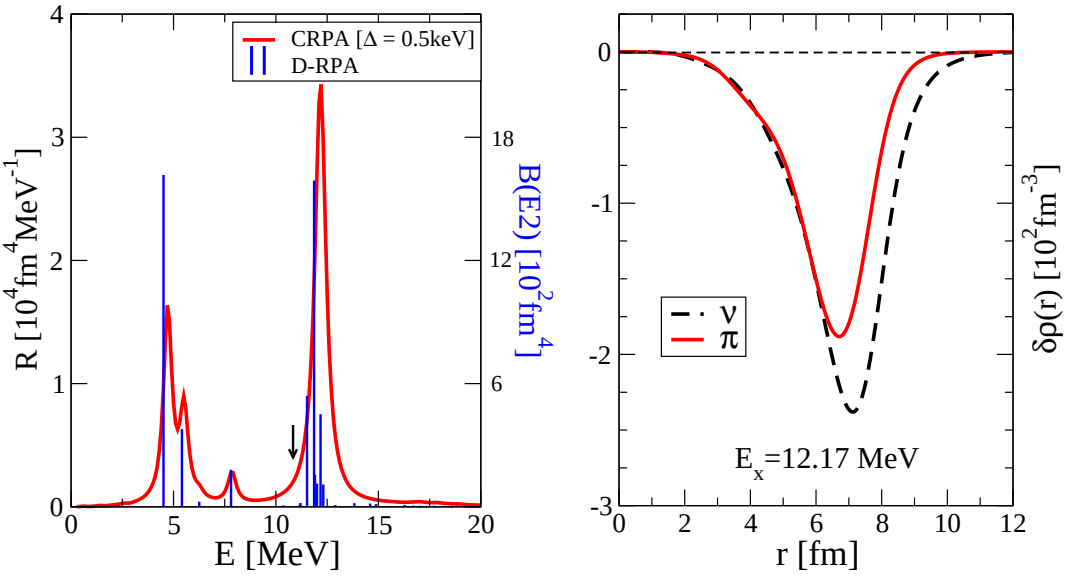

Figure 4.13: Left: The isoscalar giant quadrupole strength distribution in ^{208}Pb. Details are the same as in the left panel of Fig. 4.2. The experimental peak energy is indicated by the arrow. Right: Proton and neutron transition densities at the peak energy of the ISGQR for the same nucleus.

In conclusion, continuum RPA calculations manages not only to predict the existence of the toroidal and the compression mode, but also to achieve a reasonable agreement of the corresponding centroid energies to other models which focus on the same problem, as well as to recent experimental data [140, 138]. In Table 4.4, these results are presented for the case of the well studied ^{208}Pb.

4.2.4 Isoscalar Giant Quadrupole Resonances

Since its discovery [154], the ISGQR has been extensively studied in several nuclei and within various reactions [155, 156], so that nowadays systematic experimental data exist on its energy centroid, resonance width, and the exhausted strength in terms of the energy-weighted sum rule (EWSR) [156]. Macroscopically the ISGQR can be described as a quadrupole ($L = 2$) shape vibration of a nucleus, the protons and neutrons oscillating in phase, thereby defining the isoscalar ($\Delta T = 0$) nature of this resonance. The microscopic structure is given in Fig. 4.1 describing the p-h configurations coupled by the residual interaction.

In the left panel of Fig. 4.13 we show the continuum RPA calculations for the ISGQR of the nucleus ^{208}Pb. The excitation energy is slightly overestimated, as compared to the experimental resonance energy $E_x = 10.89 \pm 0.30$ MeV [125]. However, this is a systematic deviation that torments all the relativistic RPA approaches, as one can see also from the results of the discrete RPA, given in the same figure by blue sharp lines [103].

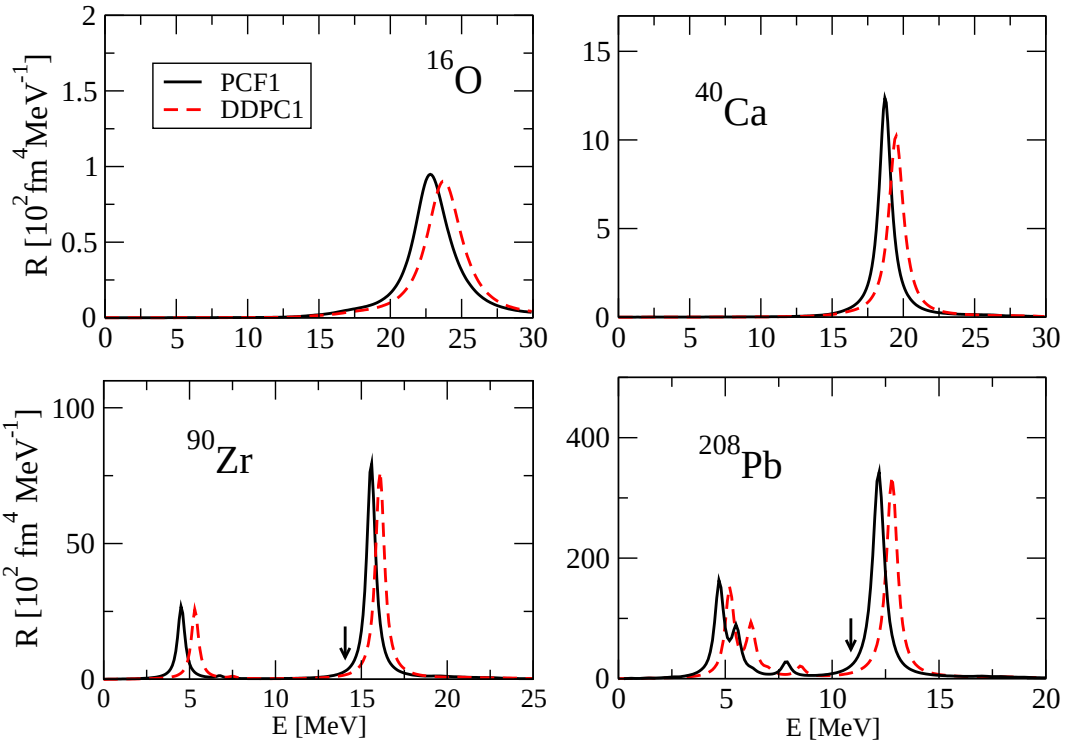

Figure 4.14: The isoscalar giant quadrupole strength distribution for four double magic nuclei, using the point coupling parametrizations PC-F1 (solid curves) and DD-PC1 (dashed curves).

Another characteristic of this excitation mode, is the appearance of a sharp low-lying state, which is very collective. As we can see, this state lies in an energy area much below the particle emission threshold. Hence, in order to produce it within the continuum RPA, one needs to introduce a small smearing parameter (in Fig. 4.13 it is $\Delta = 0.5$ MeV). In the right panel of the same figure, the proton and neutron transition probabilities at the peak energy show explicitly the isoscalar nature of the mode.

Further calculations in the quadrupole excitations have been performed, concerning comparison between different parameter sets on several double-magic nuclei. In Fig. 4.14, we deploy the ISGQR for the nuclei ^{16}O, ^{40}Ca, ^{90}Zr and ^{132}Pb. We see that the low-lying state appears only in heavy nuclei. That is an indication that it is constructed exclusivly by the transition of a high-l single-particle state, which does not exist in light nuclei. In addition, one clearly observes that the two parameter sets PC-F1 and DD-PC1 are overall in very nice agreement to each other but with the PC-F1 to be overall closer to the experimental values.

Chapter 5

Quasiparticle continuum RPA

Until now we have been considering only spherical nuclei with doubly closed shells for the application of the CRPA approach. In the framework of the shell model, nucleons were assumed to move in the ground states independently in a self-consistent field, without the account of any correlations. In a time-dependent description of excited states this has lead to the well known particle-hole structure of the random phase approximation.

However, closed shell nuclei represent only a very small portion of the entire nuclear chart and thus, the CRPA which was defined in the previous chapter meets obvious limitations in the direction towards describing properties of the majority of nuclei. As a next step, we consider semi-magic nuclei and go farther away from a closed major shell. In this case one type of nucleons (protons or neutrons) move in degenerate orbits and the residual interaction cannot be neglected. Particle-particle (pp) correlation lead to a phase-transition to superfluid systems. In the case of open shells for protons and neutrons we have in addition strong particle-hole correlations leading to deformed shapes.

Deformed nuclei will not be considered in this study. Nevertheless, the description of semi-magic open-shell nuclei requires an extension of the concept of particles and holes, regardless the fact that the spherical symmetry is still preserved. It is thus helpful to introduce Bogoliubov quasi-particles, which in the framework of second quantization can be understood as a superposition of creation and annihilation operators. The essence of the quasiparticle method is contained in the simple picture of a quasiparticle shell model, which consists of a quasiparticle vacuum and non-interacting quasiparticles.

In this section, the nuclear model enhanced by the pairing interaction will be used in order to give the appropriate wave functions and energy spectrum for the calculation of both ground and excited states of open-shell nuclei.

This approximation is properly studied in the framework of the BCS-model. In the next section we discuss the basic principles of this model and the way it is adjusted in our continuum RPA method to describe collective phenomena of single-magic open shell nuclei. Since nuclei with open shells for protons and for neutrons are usually deformed we concentrate here on single magic nuclei, where only one type of particles are in open shells and therefore one type of nucleons are participating in pairing.

5.1 The RMF plus BCS Model

At the basis of the BCS method lies the formalism of second quantization. The nuclear system is described by a spherical shell model with the appropriate single particle energies ε_k and a residual two-body interaction

$$\hat{H} = \sum_k \varepsilon_k a_k^\dagger a_k + \frac{1}{2} \sum_{klmn} V_{klmn} a_k^\dagger a_l^\dagger a_m a_n. \tag{5.1}$$

where $a_k^\dagger$ creates a particle in state $|k\rangle$ and a_k annihilates a particle in the same state. As a consequence the bar vacuum $|-\rangle$ is defined as:

$$a_k|-\rangle = 0. \tag{5.2}$$

Within the shell model the ground state $|0\rangle$ is understood as a state where all levels $|i\rangle$ below Fermi energy are occupied and all levels $|m\rangle$ above the Fermi energy are empty. As a consequence the shell model ground state $|0\rangle$ has the property

$$a_i^\dagger|0\rangle = 0, \qquad a_m|0\rangle = 0. \tag{5.3}$$

The pairing interaction leads to the fact that the levels are only partially occupied. Within the BCS-model for pairing only matrix elements V_{klmn} of the type $V_{k\bar{k}l\bar{l}}$ are considered, where $|\bar{k}\rangle$ is the time-reversed state of $|k\rangle$. A very simple and powerful model of this type is the seniority model with a simple attractive monopole force. The pairing matrix elements in this case are constant within a certain pairing window around the Fermi surface and zero elsewhere. The Hamiltonian is then given by:

$$\hat{H} = \sum_k \varepsilon_k a_k^\dagger a_k + \hat{V}_{pair}. \tag{5.4}$$

where the first term represents the sum of the spherical single-particle energies ε_j while the second term represents the pairing interactions between nucleons in the unfilled shell. Introducing the creation and annihilation operators for Cooper pairs

$$\begin{aligned} S^\dagger &= \sum_{jm>0} a_{jm}^\dagger \tilde{a}_{jm}^\dagger \\ S &= \sum_{jm>0} \tilde{a}_{jm} a_{jm} \end{aligned} \tag{5.5}$$

with $\tilde{a}_{jm} = (-)^{j-m} a_{j-m}$, the pairing interaction $\hat{V}_{pair}$ is written as:

$$\hat{V}_{pair} = -\frac{G}{2}(S^\dagger S + S S^\dagger). \tag{5.6}$$

where the parameter G determines the strength.

The ground state in the BCS-model is given by:

$$|\mathrm{BCS}\rangle = \prod_{k>0}(u_k + v_k a_k^\dagger \tilde{a}_k^\dagger)|-\rangle, \qquad u_k^2 + v_k^2 = 1. \tag{5.7}$$

In this model the orbits are only partially occupied and v_k^2 corresponds to the probability that the orbit k is occupied. The nuclear ground state can be represented as the quasiparticle vacuum:

$$\alpha_k|\mathrm{BCS}\rangle = 0, \tag{5.8}$$

where the operators $\alpha_k^\dagger$, α_k refer to a new set of quasiparticle creation and annihilation operators obeying the Bogoliubov-Valatin transformation:

$$\alpha_k^\dagger = u_k a_k^\dagger + v_k \tilde{a}_k, \tag{5.9}$$

$$\tilde{\alpha}_k^\dagger = u_k \tilde{a}_k^\dagger - v_k a_k. \tag{5.10}$$

As this transformation mixes states with different particle number, the particle number symmetry is broken spontaneously. In other words, the new mean field Hamiltonian does not commute with the particle number operator $\hat{N} = \sum_k a_k^\dagger a_k$. For that reason it is necessary to introduce a constraint in the Hamiltonian (5.4):

$$\hat{H}' = \hat{H} - \lambda \hat{N}, \tag{5.11}$$

The parameter λ is the chemical potential that serves as a Lagrange multiplier and takes care of the fact that the particle number is preserved on the average.

Using the above Hamiltonian one can write

$$\langle \mathrm{BCS}|\hat{H} - \lambda \hat{N}|\mathrm{BCS}\rangle = \sum_k (\varepsilon_k - \lambda) v_k^2 - G\left(\sum_{k>0} u_k v_k\right)^2 \tag{5.12}$$

The amplitudes u_k and v_k are derived from the variational equation

$$\delta\langle \mathrm{BCS}|\hat{H} - \lambda \hat{N}|\mathrm{BCS}\rangle = 0 \tag{5.13}$$

and one finds

$$u_k^2 = \frac{1}{2}\left(1 + \frac{\varepsilon_k - \lambda}{E_k}\right), \qquad v_k^2 = \frac{1}{2}\left(1 - \frac{\varepsilon_k - \lambda}{E_k}\right), \tag{5.14}$$

where E_k are the quasiparticle energies

$$E_k = \sqrt{(\varepsilon_k - \lambda)^2 + \Delta^2} > 0. \tag{5.15}$$

The chemical potential λ is defined in such a way as to satisfy the particle number:

$$N = \sum_{k>0} v_k^2, \tag{5.16}$$

Finally, the quantity

$$\Delta = G \sum_{k>0} u_k v_k \tag{5.17}$$

is called the pairing gap, since it causes a gap in the spectrum. It is determined by the so called *gap equation*:

$$\frac{1}{G} = \sum_{k>0} \frac{1}{2E_k}. \tag{5.18}$$

In practical calculations, the equation (5.17) goes to zero for high energy states but not with a safficient speed, so that the pairing energy of the system eventually diverges. It is therefore necessary to prevent the anyhow unrealistic pairing of these states and to confine the region of influence of the pairing force to the vicinity of the Fermi surface. This is done by introducing a pairing window at some energy E_p, meaning that any state with energy higher than E_p has exactly zero occupation probability.

Further study have shown that a sharp pairing window, similar to a step function, can lead to the failure of the convergence for some nuclei. In contrast, this problem is overpassed if we allow for a soft pairing window. This is accomplished by defining the pairing cut-off factor:

$$f_k = \frac{1}{1 + e^{\frac{\varepsilon_k - \lambda - E_p}{\mu}}} \tag{5.19}$$

which contributes to the total energy and thus to the gap equation as an artificial pairing range. In Eq. (5.19), E_p is the pairing window, λ is the chemical potential and μ defines how smoothly this range is reached.

With this definition of the pairing cut-off, the gap equation (5.18) becomes:

$$\frac{1}{G} = \sum_{k>0} f_k \frac{1}{2E_k}. \tag{5.20}$$

In Fig. 5.2 the pairing cut-off is given as a function of the single particle energies. The two plots correspond to two different pairing windows, while the drop lines indicate the occupation numbers of the single particle states which participate in the pairing interaction. We have to keep in mind that the entire idea of a pairing cut-off is a purely technical method and it is used only to ensure a successful convergence of the RMF equations. More about this figure will be discussed in the following section , where we investigate the influence of superfluidity on the response theory, i.e. the quasiparticle RPA.

There are essentially two points, which have to be considered: (i) BCS theory causes partial occupation. As compared to normal response theory we can no longer distinguish particles and holes. Instead of *ph* - pairs we have two-quasiparticle pairs and this leads to certain occupation numbers in the linear response equations. (ii) the pairing interaction in the Hamiltonian or the corresponding pairing energy in the density functional causes an effective pairing interaction between the two-quasiparticle components. This effect is usually called *dynamical pairing* and is often neglected in practical applications. In fact, in the conventional applications of continuum RPA based on BCS (Refs. [157, 107]), dynamical pairing has not been taken into account. We will discuss it in the Section 5.3.

5.2 Linear Response Theory with Pairing

Following the conventional formulation of the linear response equations and neglecting in this section the *pp*-interaction in the response equation, we start with the residual *ph*-interaction given as a sum of separable terms (Chapt. 3) :

$$V^{\rm ph}_{\alpha\beta\alpha'\beta'} = \sum_c Q^c_{\alpha\beta} V^{\rm ph}_c Q^{\dagger\, c}_{\alpha'\beta'}, \tag{5.21}$$

where the one-body operator $\hat{Q}$, is of the type $a^\dagger a$, similar to the external field $\hat{F}$. The response functions are now written in terms of quasi-particles. For instance, we obtain for the free reduced response function $\mathcal{R}^0_{cc'}(\omega) = Q_c R^0(\omega) Q^+_{c'}$ by summing over two-quasiparticle configurations $|kk'\rangle = \alpha^\dagger_k \alpha^\dagger_{k'} |{\rm BCS}\rangle$:

$$\mathcal{R}^0_{cc'}(\omega) = \sum_{k<k'} \left\{ \frac{\langle\, {\rm BCS}|\hat{Q}^\dagger_c|kk'\rangle\langle kk'|\hat{Q}_c|{\rm BCS}\rangle}{\omega - E_k - E_{k'} + i\eta} - \frac{\langle kk'|\hat{Q}^\dagger_c|{\rm BCS}\rangle\langle\, {\rm BCS}|\hat{Q}_c|kk'\rangle}{\omega + E_k + E_{k'} + i\eta} \right\}. \tag{5.22}$$

Since $|{\rm BCS}\rangle$ represents the quasiparticle vacuum, it is useful to evaluate the matrix elements $\langle kk'|\hat{Q}_c|{\rm BCS}\rangle$ in the quasiparticle representation. In this representation we have

$$\hat{Q} = Q^0 + \sum_{kk'} Q^{11}_{kk'} \alpha^\dagger_k \alpha_{k'} + \frac{1}{2} \sum_{kk'} (Q^{20}_{kk'} \alpha^\dagger_k \alpha^\dagger_{k'} + Q^{02}_{kk'} \alpha_k \alpha_{k'}) \tag{5.23}$$

with:

$$Q^{11}_{kk'} = (u_k u_{k'} + (-)^S v_k v_{k'}) \langle k|\hat{Q}|k'\rangle = \xi^S_{kk'} \langle k|\hat{Q}|k'\rangle \tag{5.24}$$

$$Q^{20}_{kk'} = (u_k v_{k'} + (-)^S v_k u_{k'}) \langle k|\hat{Q}|k'\rangle = \eta^S_{kk'} \langle k|\hat{Q}|k'\rangle = Q^{02*}_{kk'} \quad , \tag{5.25}$$

where $\langle k|\hat{Q}|k'\rangle$ are the matrix elements of the operator $\hat{Q}$ for the particle states k and k'. The phase $(-)^S = \pm 1$ depends on the time-reversal properties of the operator, i.e. it is plus for scalar and time-like parts of vectors ($S = 0$), while minus stands for space-like components of the vector fields ($S = 1$).

After some algebraic calculations we find

$$\langle kk'|\hat{Q}|\mathrm{BCS}\rangle = Q^{20}_{kk'} = \eta^{S}_{kk'}\langle k|\hat{Q}|k'\rangle \tag{5.26}$$

Now, within the BCS-model, the sum in the free response runs not over the ph-pairs but over all quasi-particle pairs kk' with the corresponding occupation factors $\eta^{S}_{kk'}$. After coupling to good angular momentum we obtain

$$\begin{aligned}\mathcal{R}^{0}_{cc'}(r,r';\omega) &= \sum_{k\le k'}\frac{1}{1+\delta_{kk'}}\eta^{S}_{kk'}\langle k||Q_c||k'\rangle_r\eta^{S'}_{kk'}\langle k||Q_{c'}||k\rangle_{r'} \\ &\times \left(\frac{1}{\omega - E_k - E_{k'} + i\eta} - \frac{(-)^{S+S'}}{\omega + E_k + E_{k'} + i\eta}\right)\end{aligned} \tag{5.27}$$

where k and k' run over all the quasiparticle levels with energy $\varepsilon_k < \varepsilon_{k'}$. The factor $1/\sqrt{1+\delta_{kk'}}$ which is counted twice in the above equation, is used in order to eliminate a double counting in the case where $k = k'$.

It is well known that BCS-theory leads to stable bound systems only in the case where the levels in the continuum stay empty. For all other cases one needs non-relativistic HFB or relativistic Hartree-Bogoliubov (RHB) theory (see Refs. [158, 49]. We therefore restrict ourselves in the following to nuclei with a Fermi level far enough from the continuum limit, such that the pairing window does not allow occupation in the continuum, i.e. all levels with quasiparticle energies $\varepsilon_k > 0$ have vanishing occupation probabilities $v^2_k = 0$.

We have seen in previous chapters that the non-spectral representation includes automatically the transition to bound and unbound states. On one hand, levels in the continuum ($\varepsilon > 0$) should be described by scattering wave functions and hence have occupation numbers $v^2_k = 0$. In contrast, the bound states ($\varepsilon_k < 0$) can have arbitrary occupation probability, and therefore they have to be treated as quasiparticles. This immediately implies that the transitions to bound and unbound states have to be distinguished when we treat quasiparticle RPA in the continuum.

Therefore, in order to treat the continuum properly, the model has inevitably to mix spectral and non-spectral representations. As discussed in the non-relativistic and non-self-consistent case by Kamerdziev et al [157] and by Hagino and Sagawa [159], and shown schematically in Fig. 5.1, one separates $R^0(\omega)$ in a non-spectral part $\mathcal{R}^0_{\mathrm{cont}}$, where a quasiparticle with occupation probability v^2_k and $\varepsilon_k < 0$ is promoted to a pure particle (not necessarily in the continuum) and in a spectral part $\mathcal{R}^0_{\mathrm{2qp}}$ where a quasiparticle k with $\varepsilon_k < 0$ is promoted to another quasiparticle k' with $\varepsilon'_k < 0$ inside the nuclear potential. However, as clearly seen from Fig. 5.1 we find in this case a double counting of transitions between bound states. This has to be corrected by subtracting the term $\mathcal{R}^0_{\mathrm{corr}}$.

This picture of continuum Quasiparticle-RPA (CQRPA) can be formally given by a sum of the three terms shown in Fig. 5.1 (for simplicity we neglect the arguments

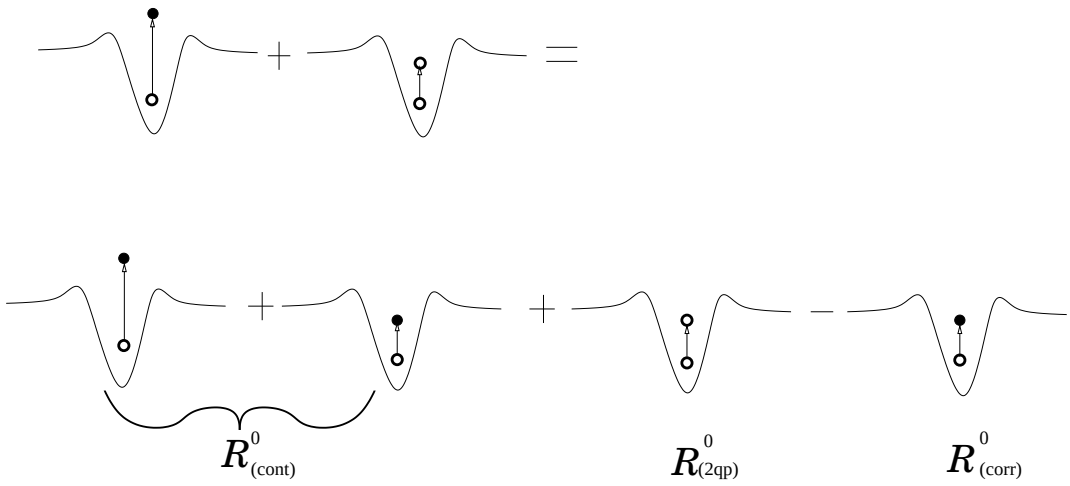

Figure 5.1: Various configurations used for the calculation of the free quasiparticle response. Filled circles (•) refer to a pure particle ($v_k^2 = 0$), while empty circles (∘) indicates ($v_k^2 > 0$) or quasiparticles. Details are given in the text.

$(rc, r'c'; \omega)$ and use $E_{kk'} = E_k + E_{k'}$ here:

$$\begin{aligned}
\mathcal{R}^0_{\rm cont} &= \sum_k v_k^2 \langle k(r)|Q_c G(r,r';\omega - E_k + \lambda) && (5.28)\\
&+ (-)^{S+S'} G(r',r;-\omega - E_k + \lambda) Q^\dagger_{c'}|k(r')\rangle,\\
\mathcal{R}^0_{\rm 2qp} &= \sum_{k\le k'} \frac{1}{1+\delta_{kk'}} \eta^S_{kk'} \langle k||Q_c||k'\rangle_r \eta^{S'}_{kk'} \langle k||Q_{c'}||k'\rangle_{r'} && (5.29)\\
&\times \left(\frac{1}{\omega - E_{kk'} + i\eta} - \frac{(-)^{S+S'}}{\omega + E_{kk'} + i\eta} \right),\\
\mathcal{R}^0_{\rm corr} &= \sum_{k\le k'} \frac{1}{1+\delta_{kk'}} \langle k||Q_c||k'\rangle_r \langle k||Q_{c'}||k'\rangle_{r'} && (5.30)\\
&\times \left\{ \frac{v_k^2}{\omega - (E_k + \varepsilon_{k'} - \lambda) + i\eta} - \frac{v_k^2 (-)^{S+S'}}{\omega + (E_k + \varepsilon_{k'} - \lambda) + i\eta} \right.\\
&+ \left. \frac{v_{k'}^2}{\omega - (E_{k'} + \varepsilon_k - \lambda) + i\eta} - \frac{v_{k'}^2 (-)^{S+S'}}{\omega + (E_{k'} + \varepsilon_k - \lambda) + i\eta} \right\},
\end{aligned}$$

The indices k and k' run only over the partially occupied states below the continuum limit ($\varepsilon_k < 0$). All the particle states in the positive energy continuum and all the states in the Dirac sea do not participate here, since they are completely taken into account in the continuum part $\mathcal{R}^0_{\rm cont}(r, r'\,\omega)$.

Concluding, the free response function will be simply the sum of the above separated terms, namely:

$$\mathcal{R}^0 = \mathcal{R}^0_{\rm cont} + \mathcal{R}^0_{\rm 2qp} + \mathcal{R}^0_{\rm corr} \qquad (5.31)$$

The calculation of the above free response function is all one needs in order to give an appropriate description of the collective excitations for open-shell nuclei. However, in

order to be fully self-consistency with the ground state calculated in the RMF+BCS approach, also the residual pairing interaction (dynamical pairing) should be taken into account.

5.3 Dynamical Pairing

It is well known that the exact Hamiltonian commutes with the particle number operator, i.e. the particle number N is a conserved quantity. Hence, the state associated with nucleon number conservation should have zero excitation energy [101], i.e. a Goldstone mode should appear, similar to the one, associated with the translational symmetry in the isoscalar dipole mode. The quantum number of this new spurious state should be $J^\pi = 0^+$, since the number operators has these quantum numbers.

Earlier versions of QRPA had been suffering the common problem of violating the sum rules of the resonance excitations. It was soon realized that this violation was directly connected to the Goldstone modes, which, in non self-consistent calculations are not orthogonal to the physical states. It is also known that this orthogonality and a precise decoupling from the normal modes is achieved, if the RPA theory treats the inherent symmetries of the problem consistently. In other words, the sum rule is satisfied when pairing is consistently treated not only in the mean field Hamiltonian (RMF level) with the proper inclusion of the occupation numbers, but also in the residual interaction (RPA level). This interaction should then include, apart from the particle-hole (ph) channel (5.21), an additional particle-particle (pp) channel, i.e. the effective interaction considered in the response equation should also contain an effective pairing force obtained from the second derivative to the pairing energy with respect to the pairing density κ

$$V_{pp}^{jj'} = \frac{\delta^2 E_{\text{pair}}}{\delta\kappa\delta\kappa} \tag{5.32}$$

Since the pairing interaction in the seniority model does not depend on density, there are no rearrangement terms in the pairing channel and we find

$$V_{pp}^{jj'} = -\frac{G}{2}(S_j^\dagger S_{j'} + S_j S_{j'}^\dagger). \tag{5.33}$$

where j, j' run over all the neutron (or proton) shells participating in pairing. The two-particle transfer operators $\hat{S}^\dagger$ and $\hat{S}$ defined in Eq. (5.5) are not Hermitian, and therefore it is convenient to introduce the Hermitian (and anti-Hermitian) operators:

$$S_+^j = \frac{1}{2}(S_j^\dagger + S_j), \qquad S_-^j = \frac{1}{2}(S_j^\dagger - S_j), \tag{5.34}$$

so that the pairing interaction is finally described by:

$$V_{pp}^{jj'} = -G(S_+^j S_+^{j'\,\dagger} + S_-^{j'} S_-^{j\,\dagger}). \tag{5.35}$$

In the following, we will use the index d to describe the two pairing interaction channels corresponding to the operators S_+ and S_-. Overall, the index $d = (\pm)$ will have two possible values (in case that we have both protons and neutrons in open shells there are four possible values). That means that in general the dimension of the full residual interaction will be extended by only four additional discrete channels, as shown in Table 5.1, which presents now super-matrix of dimension $(N + 4) \times (N + 4)$.

	$Q_{c'}(r')$	S^n_+	S^n_-	S^n_+	S^n_-
$Q_c(r)$	$v_{cc'}(r')$	0	0	0	0
S^n_+	0	$-G_n/2$	0	0	0
S^n_-	0	0	$-G_n/2$	0	0
S^p_+	0	0	0	$-G_p/2$	0
S^p_-	0	0	0	0	$-G_p/2$

Table 5.1: Vertices and quantum numbers of the different channels in Eq. (3.57). The indices n and p refer to protons and neutrons. For semi-magic nuclei we have only two discrete channels.

Of course we also have to extend the reduced free response in Eq. Eq.(5.23) by two (or four) discrete pairing channels. By expanding $S_\pm$ in terms of the Bogoliubov operators and performing the calculations of Eq.(5.23) to (5.26) one finds for the pp-matrix elements:

$$\langle BCS|S_\pm|kk'\rangle = (u_k u_{k'} - (-)^S v_k v_{k'})\langle k|S_\pm|k'\rangle = \xi^S_{kk'}\langle k|S_\pm|k'\rangle$$

where we have now the factor $\xi^S_{kk'}$ instead of the factor $\eta^S_{kk'}$ for the two quasiparticle matrix element (5.26) in the ph-interaction. Finally we find for the free response function:

$$R^0_{dd} = \sum_{kk'} \frac{1}{1+\delta_{kk'}} \xi^S_{kk}\xi^{S'}_{kk} |\langle\, k|S_d|k\rangle|^2 \left(\frac{1}{\omega - 2E_k + i\eta} - \frac{(-)^{S+S'}}{\omega + 2E_k + i\eta}\right) \tag{5.36}$$

and for the mixed terms

$$R^0_{cd} = \sum_{kk'} \frac{1}{1+\delta_{kk'}} \eta^S_{kk}\langle k||Q_c||k\rangle \xi^{S'}_{kk}\langle\, k|S_d|k\rangle \left(\frac{1}{\omega - 2E_k + i\eta} - \frac{(-)^{S+S'}}{\omega + 2E_k + i\eta}\right) \tag{5.37}$$

where the *pp*-matrix element is simply:

$$\langle\, k|S_d|k'\rangle = \delta_{kk'}\sqrt{j_k + \frac{1}{2}}(-)^{j_k+1/2}, \quad \text{and} \quad \xi^S_{kk'} = u_k u_{k'} - (-)^S v_k v_{k'}. \tag{5.38}$$

From this relations one can see that the p-p terms of the response function are non-zero only when $k = k'$, i.e. when the transition undergoes within the same single particle orbital. In addition, we have to mention here that the spin indices S and S' of the pp components are different from the ones of the ph components, (Eq. 5.28). Here they get the values 1 and -1 according to whether the corresponding operator is $\hat{S}+$ or $\hat{S}_-$ (Eq. 5.34) respectively.

5.4 CQRPA Calculations and the Spurious State

One of the most interesting characteristics of the BCS model appears in the monopole $J = 0$ excitation, where the spurious state can be successfully separated from the normal vibrations of the system once we work in a fully-self consistent framework, i.e. when dynamical pairing is properly taken into account. This can be proven using the following arguments.

Suppose that there is no particle-hole term of the interaction, i.e. all the excitation modes are subject to the particle-particle pairing force. We want to see if $\omega = 0$ is a possible solution of the full response function:

$$\mathcal{R}(\omega) = \frac{\mathcal{R}^0_{dd'}(\omega)}{1 - \mathcal{R}^0_{dd'}(\omega)V_{pp}}. \tag{5.39}$$

for isoscalar monopole mode. $R(\omega)$ must diverge at this energy, which is of course satisfied, only if

$$\left[1 - \mathcal{R}^0_{dd'}(\omega)V_{pp}\right]_{\omega=0} = 0 \tag{5.40}$$

By substituting Eq.(5.36) and V_{pp} in Eq.(5.40), the requirement $\omega = 0$ simply leads to

$$\frac{2}{G} = \sum_k \frac{1}{E_k}. \tag{5.41}$$

which is exactly the gap equation (5.18) we derived in the RMF+BCS model. In other words, the initial assumption that the spurious state is at exactly zero energy should be valid, as long as the gap equation is satisfied.

However this does not happen always. The reason is that the smooth pairing window which is usually introduced in the RMF level is far beyond the continuum limit, e.g. at E_p close to 20 MeV, as we show in the upper case of Fig. 5.2. The fulfillment of the gap equation requires of course the inclusion of all the pairing active states, even those which have $\varepsilon_k > 0$. Any truncation of these states would lead to $2/G > \sum k1/E_k$. This is exactly the situation in the Eqs. (5.28); the free response function takes into account only bound states ($\varepsilon_k < 0$). As a consequence, the gap equation is satisfied only up to 60-70 %, leading to a solution of $\omega \neq 0$.

This drawback can be overtaken in a relatively simple way. In principle, continuum QRPA states that all states which lie in the continuum shall not contribute to the gap equation. In the language of BCS that means that all states above $E = 0$ must have zero occupation probability. This can numerically be achieved, if we set the pairing window at $E_p = +|\mu|$, where μ is the chemical potential. In addition, one has to make the pairing window stiff so that no state contributes partially.

In Fig. 5.2 the pairing factor f_k of Eq. (5.19) is given with respect to the single particle energy, while the drop lines correspond to the occupation probability of each state.

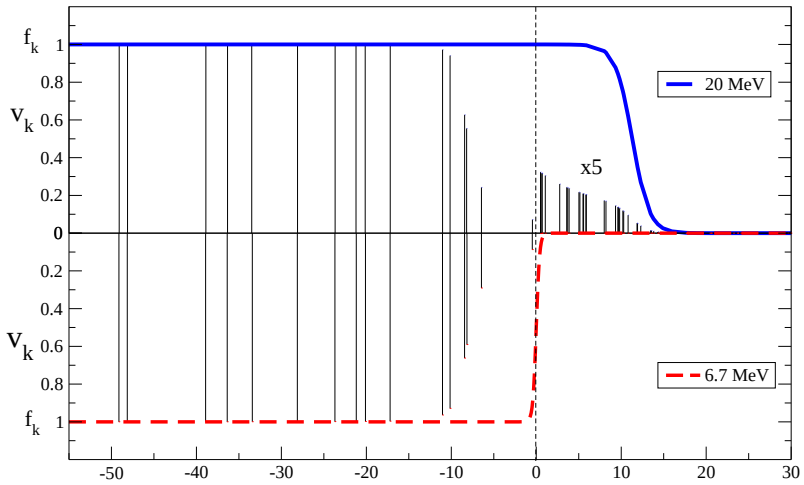

Figure 5.2: *The cut-off factor f_i is given for the two different pairing windows ($E_p = 20$ MeV and $E_p = 6.7$ MeV). At the same time, the occupation numbers of each single particle state are given with respect to the corresponding s.p. energy. In both cases, the occupation probabilities of the continuum states ($E > 0$) are multiplied by a factor of 5 for guiding the eye. The present example is deduced from calculations on ^{116}Sn and with constant gap $G = 23$ MeV.*

In the lower case we see that we have produced a spectrum, where all the states in the continuum have zero occupation number and thus the pairing active area can be restricted to only bound states.

Since in the lower case of Fig. 5.2 the the gap equation is fulfilled up to 100% for the bound states, we expect that the spurious state is at $\omega = 0$. In Fig. 5.3 we show the isoscalar monopole distribution for the spherical open shell nucleus ^{116}Sn, using Continuum RQRPA. For this problem, we make use of two external operators $\hat{F}$ having $J = 0$, that is the monopole 0^+ operator and the particle number operator $\hat{N}$. The reason is that $\hat{N}$ is an operator with a pure $\Delta N = 0$, while 0^+ contains also $\Delta N = 0$ excitations. We clearly see that the calculations which take the full pairing into account (solid lines) and therefore are fully self-consistent, bring the position of the spurious state at exactly zero energy. On the other hand, if the dynamical pairing is excluded, the spurious state is mixed with the physical states, resulting in finite strength distribution at energies below 2 MeV. The peak which appears at $\omega = 3.2$ MeV is of a pure ph character.

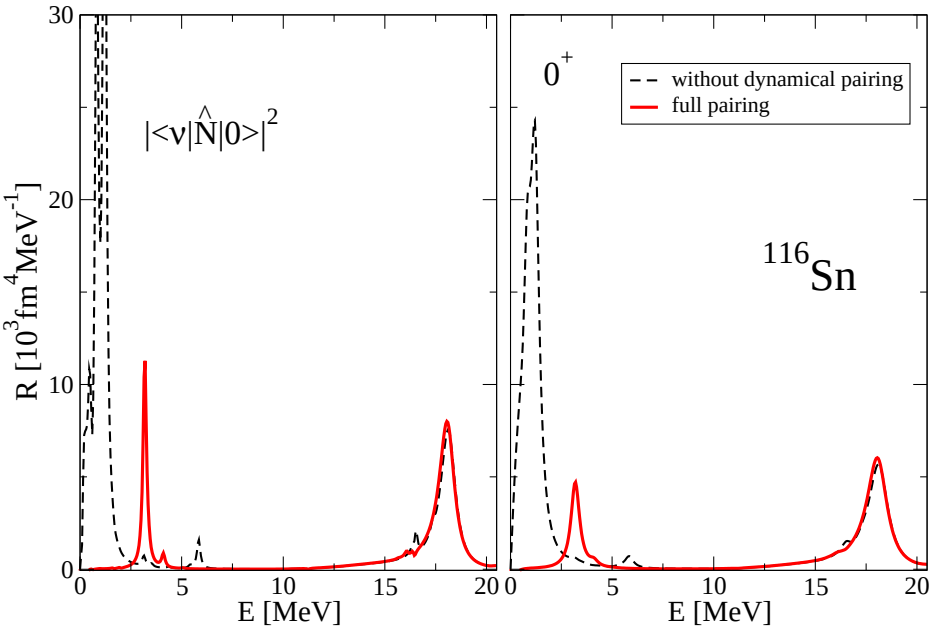

Figure 5.3: *The strength function the partricle number operator (left) and the isoscalar strength function for the monopole operator (right) in ^{116}Sn. The curves corespond to Continuum RQRPA calculations with full pairing (red solid line) and without dynamical pairing (black dashed line).*

5.4.1 Tin Isotopes

The continuum RQRPA gives us the oportunity to study isotopic chains of nuclei where most of the isotopes are open shell nuclei and require treatment of pairing correlations. In the following we show the ISGMR and IVGDR results for a chain of neighbor nuclei, such as the Sn isotopes. Despite the fact that in our continuum RQRPA calculations the spurious state associated with the particle number conservation is properly separated from the physical spectrum, we often concentrate in excitation energies $\omega\epsilon[10.5, 20.5]$ MeV with the corresponding sum rules to be defined in the same energy region.. The reason is that we want to compare our results with other models which do not successfully decompose the spurious state and they restrict their calculations only within this range.

In the Fig. 5.4 the ISGMR excitation energies are compared with the experimental data, taken from [160]. One finds a very nice agreement not only in the slightly descending trend but also in the absolute values.

In Fig. 5.5 the isovector dipole strength distributions for the Sn isotopes are revealed. In this analysis, we have extended the calculations also in the region of extreme neutron rich nuclei, i.e. to isotopes close to the neutron drip line. For the cases that we can

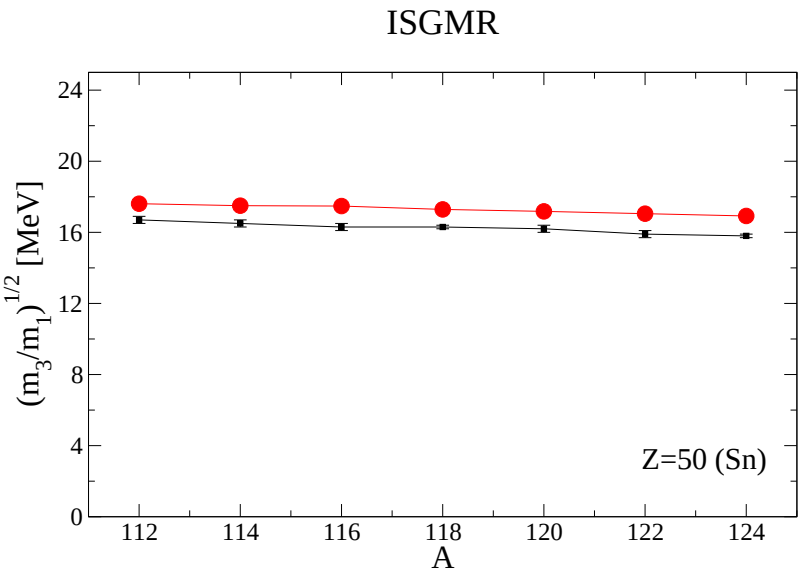

Figure 5.4: *The ISGMR energies for the Sn isotopes using PC-F1, as compared to the experimental results [160]*

compare with the experimental data (^{116}Sn,^{120}Sn and ^{124}Sn), we see that the agreement is wonderful. The general picture however is that the low-lying strength becomes larger as we move to heavier nuclei, without losing the strong collective character of the giant dipole resonance.

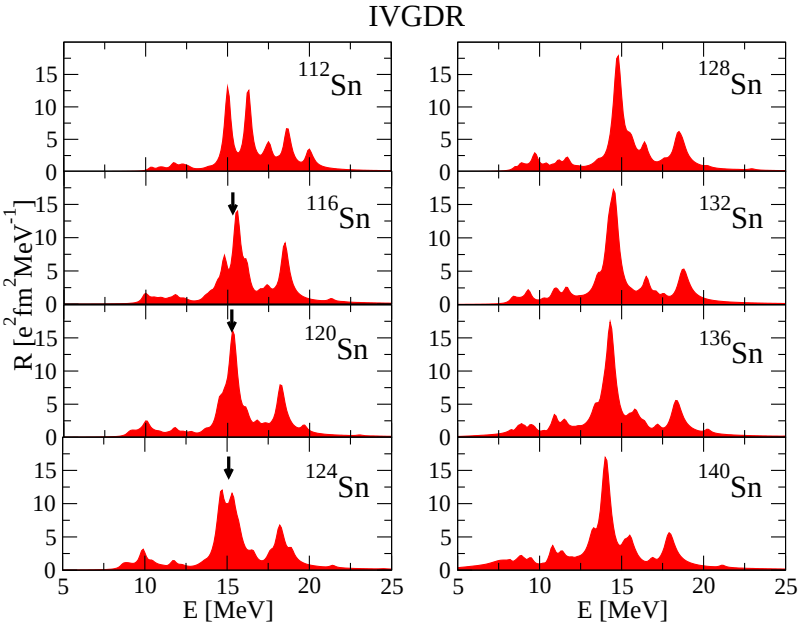

Figure 5.5: *The IVGDR strength disributions for the Sn isotopes using PC-F1. The arrows indicate the experimental excitation energy.*

Chapter 6

Conclusion and outlook

In this work we have outlined a fully relativistic method to study the nuclear collective phenomena, such as giant resonances in a variety of nuclei along the periodic table. Starting from a point coupling Lagrangian, we have used the non-spectral relativistic RPA approach to examine the corresponding excitation spectra and we have compared the results with spectral calculations based on the same Lagrangian. Our main contribution is that we have formulated a continuum RPA method, where the coupling to the continuum is taken into account in an explicit way. This RPA approach is built on the basis of a relativistic Point-Coupling RMF using the phenomenological parameter sets PCF1 and DDPC1. By further including BCS approximation, the RMF model provides a unified description of mean field and pairing correlations, making it a ideal tool for the study of spherical nuclei over the entire nuclear chart.

The Quasiparticle CRPA model employed in this work is fully self-consistent. The same interaction is used in both the RMF equations and in the linear response equations of the RPA. As it has been shown, this self-consistency feature is of vital importance for the fulfillment of current conservation and the decoupling of spurious modes.

In Conventional RPA approaches, where the continuum is discretized, the Dirac sea of negative energy states were included in the configuration space, increasing considerably the numerical effort. However, in the continuum RPA formalism and due to the non-spectral representation of the Green's function, the antiparticle states do not appear in the model. In this way, a considerable decrease in numerical effort is achieved, although the entire configuration space in the 1p-1h picture is included explicitly. This is of paramount importance for the decoupling of spurious states, as well as for the proper description of the collective giant resonances.

A great deal of effort and time was spent in the construction and validation of a computer code written in FORTRAN 77 for solving the continuum RPA equations in the linear response theory. Through extensive testing, the correctness of the implemented

numerical solution has been proved. In particular, the decoupling of the spurious modes associated with the broken translational symmetry is accomplished without further adjustments in the interaction.

We have applied the CRPA framework to the study of the multipole giant resonances in spherical nuclei, in particular the Isoscalar Giant monopole and Isovector Giant dipole modes where we have shown an excellent agreement with the discrete RPA methods. In the case of heavy nuclei, the total energy weighted sum rule agrees with the TRK sum rule almost 100% in the case of ISGMR and up to an enhancement factor of roughly 30% for the IVGDR.

Furthermore, a prominent peak at excitation energies between $7-10\,MeV$ was expected in the isovector dipole resonance. This is identified as the pygmy mode, which faces a considerable interest over the last years. Using CRRPA, we have indeed shown the appearance of a soft collective mode in this energy region, specially for ^{132}Sn and ^{208}Pb exhausting around 5% of the total energy weighted sum rule. Its structure resembles that of a pygmy excitation mode, and hints that its interpretation as an oscillation of a proton-neutron core against a neutron skin is valid in heavy spherical nuclei. It has been also found that the position of these soft collective modes are quite sensitive to the model in use, since CRPA calculations do not fully agree with the discrete RRPA ones, anlike for example to the giant dipole state. It possibly has to do with the fact that in the discrete methods, the configuration space is truncated and this cause a shift of the position of the states, specially for the low-lying ones. However, further study in the direction including better experimental data are necessary to draw final conclusions.

We would also like to give a brief outlook of future extensions and improvements of the Continuum RRPA, planned or already under development, which show the direction, scope and possibilities that such a framework offers. These include:

i) Improving parameter sets. Systematic differences in the performance of the three static models (non linear terms, density dependencies, point coupling) discussed in chapter 2 have been identified and studied under the relatively small scope of the sample applications presented in this document. It has been discussed that the parameter set PC-F1 of Buervenich et al. [46] although successful in reproducing bulk properties and excitation phenomena of closed shell nuclei, it is not as much powerful when one goes to spherical open shell or even deformed nuclei. The set DD-PC1 on the other hand behaves exactly the other way around, since it has been adjusted to open shell and deformed nuclei. Thus, the development of future energy functionals that give a better quantitative agreement with the experimental data must be a task of the future.

In addition, the implementation of meson exchange interaction into out CRPA code would certainly lead to an overall better description and understanding of nuclear phenomena, since it has been seen that the density dependent set DD-ME2 has proven itself one of the best phenomenological forces available.

ii) Better treatment of pairing. A better treatment of pairing correlations opens the door to the study of exotic nuclei close to the drip lines, where new nuclear structure is being reported in recent experimental and theoretical results. Within this work, we have used the BCS model with constant pairing gap deduced from experimental information. In addition to the RMF level, we have applied the BCS model also in RPA by the dynamical pairing in the (pp) channel. This simple approach, although capable of reproducing the properties of the giant resonances in nuclei close to the beta-stability line, it fails to apply on nuclei close to the drip lines, where occupied states may lie in the continuum. Therefore, a proper implementation of the relativistic Hartree Bogoliubov or Hartree Fock Bogoliubov within our Continuum RPA method is a very important and challenging task in order to predict nuclear structure phenomena in exotic nuclei, where experiments are missing. In addition, it would be useful to count with a pairing interaction that does not depend on the experimental knowledge of the gaps.

iii) Applications to astrophysics. A direct and natural extension to this work is the inclusion of proton-neutron RPA. Gamow-Teller and isobaric analog resonances play a very important role in astrophysics. Electroweak interactions such as scattering and absorption of electrons and neutrinos are strongly influenced by these resonances. They play an essential role during many stages in the evolution of stellar objects. The knowledge of such reaction rates provides a crucial input for the modeling of supernova explosions as well as accretion processes in binary systems. Nuclear network calculations for the description of nucleosynthesis are of particular importance in the understanding of heavy element abundances in the universe, and require a precise knowledge of such reaction rates.

iv) Inclusion of more complex configuration of the RPA excitations. The present approach is based on the main RPA including only $1p1h$-configurations which are the main contributors to the collective phenomena. As a result, only the escape width of the resonances can be reproduced properly within CRPA. Unfortunately, this partial width alone is not enough. The width resulting from a coupling to more complex configurations, such as 2p-2h is very important, specially for heavy nuclei. In fact, such couplings have been introduced successfully in the relativistic scheme using the spectral representation in Refs. [111, 112]. On the non-relativistic side such techniques have also been used in the context of the non-spectral representation without [161, 106] and with [162] pairing. So far, however, fully self-consistent relativistic applications including complex configurations with a proper treatment of the continuum are still missing.

In conclusion, the relativistic CQRPA represents a significant new theoretical tool for a realistic description of excitation phenomena in large regions of the nuclear chart. Its development, and the few sample applications presented in this document, show that its future use in nuclear structure and astrophysics will provide an valuable insight into very important, and still open, questions about the nature of the nuclear interaction,

collective response, deformation effects, heavy element abundances and cross sections relevant in astrophysical processes.

Appendix A

Rearrangement terms of the residual Interaction

In this Appendix we write explicitly the full expression of the two-body residual interaction, as it is defined after the inclusion of the rearrangement terms, due to the higher order terms of the density dependance. These rearrangement terms are essential for a fully self consistent relativistic RPA implementation. Only when their contribution is treated properly in the matrix elements of the residual interaction it is possible to reproduce reasonably well the excitation spectrum of giant multipole resonances.

The basic idea is to include all the non-linear terms of the lagrangian density (2.36) into a density dependent coupling constant which then applies on the linear term. A different coupling constant is of course expected for the various covariant terms of the field.

In general, the density functional $E(\hat{\rho})$ is the starting point to derive the mean field hamiltonian:

$$\hat{h} = \frac{\delta E}{\delta \hat{\rho}} \tag{A.1}$$

as well as the RPA-interaction, in the small amplitude limit *:

$$\hat{V} = \frac{1}{2}\frac{\delta^2 E}{\delta\hat{\rho}\delta\hat{\rho}}. \tag{A.4}$$

*The factor $\frac{1}{2}$ comes from the fact that

$$\hat{\rho} = \hat{\rho}_0 + \delta\hat{\rho} \tag{A.2}$$

and thus

$$E(\hat{\rho}) = E(\hat{\rho}_0 + \delta\hat{\rho}) = E(\hat{\rho}_0) + \frac{1}{2}\sum_{kk'll'} V_{kl',k'l}\delta\rho^*_{kk'}\delta\rho_{ll'}. \tag{A.3}$$

The above energy functional (without exchange terms) can be written as:

$$E_{pot} = \frac{1}{2}\sum_{\alpha_1\alpha_1'}\sum_{\alpha_2\alpha_2'}\int d^3r_1 d^3r_2 \psi^*_{\alpha_1}(\mathbf{r}_1)\Gamma^{\dagger}_{\alpha_1\alpha_1'}\psi_{\alpha_1'}(\mathbf{r}_1)V(\mathbf{r}_1,\mathbf{r}_2)\psi^*_{\alpha_2}(\mathbf{r}_2)\Gamma_{\alpha_2\alpha_2'}\psi_{\alpha_2'}(\mathbf{r}_2) \quad (A.5)$$

$$= \frac{1}{2}\int d^3r_1 d^3r_2 \mathrm{Tr}(\Gamma^{\dagger}\hat{\rho}(\mathbf{r}_1))V(\mathbf{r}_1,\mathbf{r}_2)\mathrm{Tr}(\Gamma\hat{\rho}(\mathbf{r}_2)). \quad (A.6)$$

A.1 PC-F1

We concentrate here in the cases where the interaction part of the Lagrangian has an explicit density dependance $G_i f(\Gamma_i\hat{\rho})$ on all the civariant densities, i.e. not exclusively on the baryon density. For instance, in the Lagrangian of Buervenich et al. [46] the isoscalar scalar functional depends on the scalar density $\rho_s = \gamma_0\rho$. In any case, the potential energy functional becomes:

$$E_i = \langle\Phi|V_i|\Phi\rangle = \frac{1}{2}G_i\int d^3r \int d^3r' \mathrm{Tr}(\Gamma_i\hat{\rho}(\mathbf{r}))f_i[\rho_i(\mathbf{r})]\delta(\mathbf{r}-\mathbf{r}')\mathrm{Tr}(\Gamma_i\hat{\rho}(\mathbf{r}')), \quad (A.7)$$

where the trace runs over:

$$\mathrm{Tr}(\Gamma\hat{\rho}(\mathbf{r})) = \sum_{i=1}^{A}\langle\psi_i(\mathbf{r})|\Gamma|\psi_i(\mathbf{r})\rangle = \rho_i(\mathbf{r}) \quad (A.8)$$

and i runs over the interaction terms, namely $i = \{S, V, TV\}$. One has to mention here that the density $\hat{\rho}(\mathbf{r})$ is the local (diagonal) part of the full relativistic single particle density matrix $\hat{\rho}(\mathbf{r},\mathbf{r}')$. Using the fact that $\hat{\rho}$ is Hermitian, i.e.

$$\mathrm{Tr}(\Gamma^{\dagger}\hat{\rho}(\mathbf{r})) = \mathrm{Tr}(\Gamma^*\hat{\rho}^*(\mathbf{r}))$$

and that the derivative of this trace with respect to the density is:

$$\frac{\delta\mathrm{Tr}(\Gamma^*_i\rho^*(\mathbf{r}_1,\mathbf{r}_1'))}{\delta\rho^*_i(\mathbf{r},\mathbf{r}')} = \Gamma^*_i\delta(\mathbf{r}-\mathbf{r}_1)\delta(\mathbf{r}'-\mathbf{r}_1')$$

one can calculate the self energies:

$$\Sigma_i(\mathbf{r},\mathbf{r}') = \frac{\delta E_{pot}}{\delta\rho^*(\mathbf{r},\mathbf{r}')}$$

$$= \delta(\mathbf{r}-\mathbf{r}')G\int d^3r_2\Gamma^*_i f[\rho_i(\mathbf{r})]\rho_i(\mathbf{r}_2) + \frac{1}{2}\rho^*_i(\mathbf{r}_1)\frac{\delta f[\rho_i(\mathbf{r}_1,\mathbf{r}_2)]}{\delta\rho^*(\mathbf{r},\mathbf{r}')}\rho_i(\mathbf{r}_2). \quad (A.9)$$

The derivative of the functional $f[\rho_i]$ is:

$$\frac{\delta f(\rho_i(\mathbf{r}_1,\mathbf{r}_2))}{\delta\rho^*(\mathbf{r},\mathbf{r}')} = f_i'[\rho_i(\mathbf{r}_1,\mathbf{r}_2)]\frac{\delta\rho_i(\mathbf{r}_1,\mathbf{r}_2)}{\delta\rho^*(\mathbf{r},\mathbf{r}')}$$

$$= f_i'[\rho_i(\mathbf{r}_1,\mathbf{r}_2)]\Gamma_i\delta(\mathbf{r}-\mathbf{r}_1)\delta(\mathbf{r}'-\mathbf{r}_2) \quad (A.10)$$

and thus we obtain for Eq. (A.9:

$$\Sigma_i(\mathbf{r},\mathbf{r}') = \delta(\mathbf{r}-\mathbf{r}')G_i\left(f_\sigma[\rho_i(\mathbf{r})]\Gamma_i^*\rho(\mathbf{r}) + \frac{1}{2}f_i'[\rho_i(\mathbf{r})]\Gamma_i\rho_i^*(\mathbf{r})\rho_i(\mathbf{r})\right). \tag{A.11}$$

For the second derivative we find

$$V(\mathbf{r}_1,\mathbf{r}_2',\mathbf{r}_1',\mathbf{r}_2) = \frac{\delta\Sigma_i(\mathbf{r}_1,\mathbf{r}_1')}{\delta\rho(\mathbf{r}_2,\mathbf{r}_2')} = I_1 + I_2 + I_3 + I_4 \tag{A.12}$$

with the normal term

$$I_1 = \delta(\mathbf{r}_1-\mathbf{r}_1')\delta(\mathbf{r}_2-\mathbf{r}_2')G_i f_i[\rho_i(\mathbf{r}_1))\Gamma_i^{(1)}\delta(\mathbf{r}_1-\mathbf{r}_2)\Gamma_i^{(2)} \tag{A.13}$$

and

$$\begin{aligned} I_2 &= \delta(\mathbf{r}_1-\mathbf{r}_1')G_i f_i'[\rho_i(\mathbf{r}_1)]\frac{\delta\rho_i(\mathbf{r}_1,\mathbf{r}_1')}{\delta\rho(\mathbf{r}_2,\mathbf{r}_2')}\Gamma_i^{*(1)}\rho_i(\mathbf{r}_1') \\ &= \delta(\mathbf{r}_1-\mathbf{r}_1')G_i f_i'[\rho_i(\mathbf{r}_1))\Gamma_i^{(2)}\delta(\mathbf{r}_1-\mathbf{r}_2)\delta(\mathbf{r}_1'-\mathbf{r}_2')\Gamma_i^{*(1)}\rho_i(\mathbf{r}_1') \\ &= \delta(\mathbf{r}_1-\mathbf{r}_1')\delta(\mathbf{r}_2-\mathbf{r}_2')\delta(\mathbf{r}_1-\mathbf{r}_2)G_i f_i'[\rho_i(\mathbf{r}_1)]\rho_i(\mathbf{r}_1)\Gamma_i^{*(1)}\Gamma_i^{(2)} \end{aligned} \tag{A.14}$$

and

$$I_3 = \delta(\mathbf{r}_1-\mathbf{r}_1')\delta(\mathbf{r}_2-\mathbf{r}_2')\delta(\mathbf{r}_1-\mathbf{r}_2)G_i f_i'[\rho_i(\mathbf{r}_1)]\rho_i(\mathbf{r}_1)\Gamma_i^{*(1)}\Gamma_i^{(2)} \tag{A.15}$$

and finally

$$I_4 = \frac{1}{2}G_i f_i''[\rho_i(\mathbf{r}_1)]\Gamma_i^{(1)}\Gamma_i^{(2)}\delta(\mathbf{r}_1^-\mathbf{r}_1')\delta(\mathbf{r}_2-\mathbf{r}_2')\delta(\mathbf{r}_1-\mathbf{r}_2)\rho_i^*(\mathbf{r}_1)\delta(\mathbf{r}_1-\mathbf{r}_1')\rho_i(\mathbf{r}_1) \tag{A.16}$$

$$= \frac{1}{2}\delta(\mathbf{r}_1-\mathbf{r}_1')\delta(\mathbf{r}_2-\mathbf{r}_2')\delta(\mathbf{r}_1-\mathbf{r}_2)G_i f_i''[\rho_i(\mathbf{r}_1)]\rho_i^*(\mathbf{r}_1)\rho_i(\mathbf{r}_1)\Gamma_i^{(1)}\Gamma_i^{(2)}. \tag{A.17}$$

Therefore we find for the interaction with the rearrangement terms in short hand notation

$$\boxed{\hat{V}_i(\mathbf{r}_1-\mathbf{r}_2) = \delta(\mathbf{r}_1-\mathbf{r}_2)G_i[f_i[\rho_i] + 2f_i'[\rho_i]\rho_i + \frac{1}{2}f_i''[\rho_i]\rho_i^2]\Gamma_i^{(1)}\Gamma_i^{(2)}} \tag{A.18}$$

- **Isoscalar-scalar term**

  Looking at the isoscalar-scalar part of the Lagrangian we find:

  $$\mathcal{L}_s = -\frac{1}{2}\alpha_s(\bar{\psi}\psi)^2 - \frac{1}{3}\beta_s(\bar{\psi}\psi)^3 - \frac{1}{4}\gamma_s(\bar{\psi}\psi)^4 \tag{A.19}$$

  and the Dirac operator is $\Gamma_s = \gamma_0$. Neglecting exchange terms we find

  $$E_s = \langle\Phi|\mathcal{L}_s|\Phi\rangle = \frac{1}{2}\int d^3r\left[\alpha_s\rho_s^2 + \frac{2}{3}\beta_s\rho_s^3 + \frac{1}{2}\gamma_s\rho_s^4\right] \tag{A.20}$$

  $$= \frac{1}{2}\alpha_s\int d^3r(\bar{\psi}\psi)\left[1 + \frac{2}{3}\frac{\beta_s}{\alpha_s}\rho_s + \frac{1}{2}\frac{\gamma_s}{\alpha_s}\rho_s^2\right](\bar{\psi}\psi) \tag{A.21}$$

  $$= \alpha_s\int d^3r\int d^3r'\mathrm{Tr}(\gamma_0\hat{\rho}(\mathbf{r}))f_s[\rho_s(\mathbf{r})]\delta(\mathbf{r}-\mathbf{r}')\mathrm{Tr}(\gamma_0\hat{\rho}(\mathbf{r}')), \tag{A.22}$$

where the trace reads:

$$\mathrm{Tr}(\gamma_0\hat{\rho}(\mathbf{r})) = \sum_{i=1}^{A}\langle\psi_i(\mathbf{r})|\gamma_0|\psi_i(\mathbf{r})\rangle = \rho_s(\mathbf{r}). \tag{A.23}$$

The function f describes exactly the density dependence of the interaction, and it is given by the polynomial expression:

$$f_s[\rho_s] = 1 + \frac{2}{3}\frac{\beta_s}{\alpha_s}\rho_s + \frac{1}{2}\frac{\gamma_s}{\alpha_s}\rho_s^2, \qquad G_s = \alpha_s. \tag{A.24}$$

Following the method of calculating the first and second derivative of the energy functional (A.5) in the simple case of only linear terms, we do the same here, but we need to keep in mind that the function $f_s[\hat{\rho}]$ has a finite derivative.

Finally, one gets the isoscalar-scalar part of the interaction with the rearrangement terms included:

$$\hat{V}_s(\mathbf{r}_1 - \mathbf{r}_2) = \delta(\mathbf{r}_1 - \mathbf{r}_2)\alpha_s[f_s[\rho_s] + 2f_s'(\rho_s)\rho_s + \frac{1}{2}f_s''[\rho_s]\rho_s^2]\gamma_0^{(1)}\gamma_0^{(2)}. \tag{A.25}$$

We recall that for the same interaction without the rearrangement terms, one would have:

$$\hat{V}_s(\mathbf{r}_1 - \mathbf{r}_2) = \delta(\mathbf{r}_1 - \mathbf{r}_2)\alpha_s\gamma_0^{(1)}\gamma_0^{(2)} \tag{A.26}$$

which means that the density dependent expression

$$F_s[\rho_s] = f_s[\rho_s] + 2f_s'[\rho_s]\rho_s + \frac{1}{2}f_s''[\rho_s]\rho_s^2 \tag{A.27}$$

is missing out.

- **Isoscalar-vector term**

  In the isoscalar-vector channel we have $\Gamma_V = \gamma_0\gamma^\mu = (1, \alpha)$ and using

  $$j^\mu(\mathbf{r}) = Tr(\gamma_0\gamma^\mu\hat{\rho}(\mathbf{r})) \tag{A.28}$$

  we get for the density functional:

  $$f_v[x] = 1 + \frac{1}{2}\frac{\gamma_v}{\alpha_v}x^2 \tag{A.29}$$

  with $x = \sqrt{j^\mu j_\mu}$, i.e.

  $$f_v = 1 + \frac{1}{2}\frac{\gamma_v}{\alpha_v}j^\mu j_\mu, \qquad G_v = \alpha_v. \tag{A.30}$$

  In the static case of even-even nuclei the spatial parts of the currents are vanishing (only for RPA in rotating nuclei we have spatial currents already in the static solution). However, in the RPA level, the currents terms are non zero.

Using the second derivation, we get for the conventional term of Eq. (A.12):

$$I_1 = G_v\delta(\mathbf{r}_1-\mathbf{r}_2)f_s[x](\gamma_0\gamma^\mu)^{(1)}(\gamma_0\gamma_\mu)^{(2)} \tag{A.31}$$

$$= G_s\delta(\mathbf{r}_1-\mathbf{r}_2)f_s[x](\mathbf{1}^{(1)}\mathbf{1}^{(2)}-\alpha^{(1)}\alpha^{(2)}), \tag{A.32}$$

where the rearrangement terms are:

$$I_2 = G_v\delta(\mathbf{r}_1-\mathbf{r}_2)\frac{\delta\, f_v[x(\mathbf{r}_2)]}{\delta\rho(\mathbf{r}_2)}(\gamma_0\gamma^\mu)^{(1)}\rho_v(\mathbf{r}_1). \tag{A.33}$$

Neglecting spatial currents this means

$$I_2 = G_v\delta(\mathbf{r}_1-\mathbf{r}_2)\rho_v(\mathbf{r}_1)\ \mathbf{1}^{(1)}\frac{\delta f_v[x(\mathbf{r}_2)]}{\delta\rho(\mathbf{r}_2)}. \tag{A.34}$$

The derivative term can be analyzed into:

$$\frac{\delta f_v[x(\mathbf{r})]}{\delta\rho(\mathbf{r})} = f_v'[x]\frac{\delta x}{\delta\rho} = \frac{1}{2x}f_v'[x]\frac{\delta x^2}{\delta\rho} = \frac{1}{2x}f_v'[x]\frac{\delta(j^\nu j_\nu)}{\delta\rho}, \tag{A.35}$$

i.e.

$$\frac{\delta f_v[x(\mathbf{r})]}{\delta\rho(\mathbf{r})} = \frac{1}{x}f_v'[x]\rho_v(\mathbf{r})(\gamma_0\gamma_\nu)^{(2)} = \frac{1}{x}f_v'[x]j^\nu(\mathbf{r})(\gamma_0\gamma_\nu)^{(2)}. \tag{A.36}$$

In the static case where $j^u=(\rho_v,0,0,0)$, it is $x=\rho_\nu$ and therefore

$$\frac{\delta f_v[x(\mathbf{r})]}{\delta\rho(\mathbf{r})} = f_v'[x]\mathbf{1}^{(2)}. \tag{A.37}$$

Finally , this yields for I_2:

$$I_2 = G_v\delta(\mathbf{r}_1-\mathbf{r}_2)f_v'[\rho_v]\rho_v\ \mathbf{1}^{(1)}\mathbf{1}^{(2)}. \tag{A.38}$$

Next we consider the term I_3

$$I_3 = G_v\delta(\mathbf{r}_1-\mathbf{r}_2)\frac{\delta\, f_v[x(\mathbf{r}_1)]}{\delta\rho^*(\mathbf{r}_1)}\rho_v\mathbf{1}^{(2)} \tag{A.39}$$

and using Eq. (A.37) we obtain in short hand notation

$$I_3 = G_v\delta(\mathbf{r}_1-\mathbf{r}_2)f_v'[\rho_v]\rho_v\mathbf{1}^{(1)}\mathbf{1}^{(2)} = I_2. \tag{A.40}$$

For the last term I_4 in Eq. (3.64), we can again neglect the spatial currents after forming the derivatives and obtain

$$I_4 = \frac{1}{2}G_v\delta(\mathbf{r}_1-\mathbf{r}_2)\frac{\delta^2 f_v[x(\mathbf{r}_2)]}{\delta\rho^*(\mathbf{r}_2)\delta\rho(\mathbf{r}_2)}\rho_v^2(\mathbf{r}_1). \tag{A.41}$$

Next, we calculate the second derivative. Using Eq. (A.36) we obtain using that $(\gamma_0\gamma_\nu)$ is Hermitian and that we can neglect the spatial currents after forming the derivative$\frac{1}{x}f_\omega'[x]j^\nu(\mathbf{r})(\gamma_0\gamma_\nu)^{(2)}$

$$\frac{\delta^2 f_v[x(\mathbf{r})]}{\delta\rho^*(\mathbf{r})\delta\rho_{\alpha_2\alpha_2'}(\mathbf{r})} = \frac{\delta}{\delta\rho(\mathbf{r})}[\frac{1}{x}f_v'[x]\rho_v(\mathbf{r})(\gamma_0\gamma_\nu)^{(1)}] \tag{A.42}$$

$$= \frac{\delta(\frac{1}{x}f_v'[x])}{\delta\rho(\mathbf{r})}\rho_v\mathbf{1}^{(1)} + \frac{1}{x}f_v'[x](\gamma_0\gamma_\nu)^{(1)}(\gamma_0\gamma^\nu)^{(2)}. \tag{A.43}$$

Using Eq. (A.37) we get:

$$\frac{\delta(\frac{1}{x}f_v'[x])}{\delta\rho(\mathbf{r})} = (\frac{1}{x}f_v''[x] - \frac{1}{x^2}f_v')[x]\mathbf{1}^{(2)}. \tag{A.44}$$

Again, using Eq. (A.36) and replacing f by $\frac{1}{x}f'$ we find in short hand notation:

$$\frac{\delta^2 f[x(\mathbf{r})]}{\delta\rho^*(\mathbf{r})\delta\rho(\mathbf{r})} = (f_v''[x] - \frac{1}{x}f_v')[x]\mathbf{1}^{(1)}\mathbf{1}^{(2)} + \frac{1}{x}f_v'[x](\mathbf{1}^{(1)}\mathbf{1}^{(2)} - \alpha^{(1)}\alpha^{(2)}) \tag{A.45}$$

$$= f_v''[\rho_v]\mathbf{1}^{(1)}\mathbf{1}^{(2)} - \frac{1}{x}f_v'[\rho_v]\alpha^{(1)}\alpha^{(2)}. \tag{A.46}$$

This yields in short hand notation

$$I_4 = \frac{1}{2}G_v\delta(\mathbf{r}_1 - \mathbf{r}_2)[\rho_v^2 f_v''[\rho_v]1^{(1)}1^{(2)} - \rho_v f_v'[\rho_v]\alpha^{(1)}\alpha^{(2)}]. \tag{A.47}$$

Summarizing we find for the isoscalar-vector channel

$$\hat{V}_v(\mathbf{r}_1,\mathbf{r}_2) = G_v\delta(\mathbf{r}_1 - \mathbf{r}_2)[(f_v[\rho_v] + 2\rho_v f_v'[\rho_v] + \frac{1}{2}\rho_v^2 f_v''[\rho_v])1^{(1)}1^{(2)}$$
$$- (f_v + \frac{1}{2}\rho_v f_v'[\rho_v])\alpha^{(1)}\alpha^{(2)}]. \tag{A.48}$$

- **Isovector-vector term**

  In the isovector-vector channel we have $\Gamma_{TV} = \gamma_0\gamma^\mu\vec{\tau} = (\vec{\tau}, \alpha\vec{\tau})$ and using

$$\vec{j}^\mu(\mathbf{r}) = Tr(\gamma_0\gamma^\mu\vec{\tau}\hat{\rho}(\mathbf{r})) \tag{A.49}$$

$$f_{TV}[x] = 1 + \frac{1}{2}\frac{\gamma_{TV}}{\alpha_{TV}}x^2 \tag{A.50}$$

  with $x = \sqrt{\vec{j}^\mu\vec{j}_\mu}$, i.e.

$$f_{TV} = 1 + \frac{1}{2}\frac{\gamma_{TV}}{\alpha_{TV}}\vec{j}^\mu\vec{j}_\mu, \qquad G_{TV} = \alpha_{TV}. \tag{A.51}$$

  In the static case the spatial parts of the currents are vanishing and because of charge conservation we have only τ_3 and ρ_3. The rest runs in full analogy to the ω-channel

  For the conventional term we find:

$$I_1 = G_{TV}\delta(\mathbf{r}_1 - \mathbf{r}_2)f_{TV}[x](\gamma_0\gamma^\mu\tau_3)^{(1)}(\gamma_0\gamma_\mu\tau_3)^{(2)} \tag{A.52}$$

$$= G_{TV}\delta(\mathbf{r}_1 - \mathbf{r}_2)f_{TV}(1^{(1)}1^{(2)} - \alpha^{(1)}\alpha^{(2)})\tau_3^{(1)}\tau_3^{(2)} \tag{A.53}$$

  while for the rearrangement terms one gets:

$$I_2 = G_{TV}\delta(\mathbf{r}_1 - \mathbf{r}_2)\rho_3\ \tau_3^{(1)}\frac{\delta f_{TV}[x(\mathbf{r}_2)]}{\delta\rho(\mathbf{r}_2)} \tag{A.54}$$

and

$$I_2 = I_3 = G_{TV}\delta(\mathbf{r}_1 - \mathbf{r}_2) f'_{TV}[\rho_3]\rho_3 \ \tau_3^{(1)}\tau_3^{(2)}. \tag{A.55}$$

Finally, for the term I_4 we get:

$$I_4 = \frac{1}{2} G_{TV}\delta(\mathbf{r}_1 - \mathbf{r}_2)[\rho_3^2 f''_{TV}[\rho_3]1^{(1)}1^{(2)} - \rho_3 f'_\rho[\rho_3]\alpha^{(1)}\alpha^{(2)}]\tau_3^{(1)}\tau_3^{(2)}. \tag{A.56}$$

Summarizing the isovector-vector channel is expressed in the form:

$$\begin{aligned}\hat{V}_{TV}(\mathbf{r}_1, \mathbf{r}_2) = G_{TV}\delta(\mathbf{r}_1 - \mathbf{r}_2)[(f_{TV}[\rho_3] + 2\rho_3 f'_{TV}[\rho_3] + \frac{1}{2}\rho_3^2 f''_{TV}[\rho_3])1^{(1)}1^{(2)} \\ - (f_{TV}[\rho_3] + \frac{1}{2}\rho_3 f'_{TV}[\rho_3])\alpha^{(1)}\alpha^{(2)}](\tau_3^{(1)}\tau_3^{(2)}).\end{aligned} \tag{A.57}$$

A.2 DD-PC1

The Lagrangian parametrization DD-PC1 is quite different from the PC-F1, as we discussed in Section (2.4), not only because the density dependent function $f_i[\rho]$ has a different non-polynomial structure, but mainly because it depends on the baryon density $\rho = \rho_v$ only, regardless the covariant field i under consideration.

$$G_i f_i[\rho] = a_i + (b_i + c_i x)e^{-d_i x}, \qquad x = \rho/\rho_{sat} \tag{A.58}$$

where ρ_{sat} is the saturation density of nuclear matter. Here, G_i can be chosen to be $G_i = 1$ or $G_i = 1/f_i[\rho_{sat}]$. Eventually, the second derivative of the energy functional will lead to off-diagonal terms in isospin space, as we will find out in the following.

For the interaction we obtain the usual conventional term:

$$I_1 = G_i\delta(\mathbf{r}_1 - \mathbf{r}_2) f[\rho(\mathbf{r}_1)]\Gamma^{\dagger(1)}\Gamma^{(2)} \tag{A.59}$$

and the rearrangement terms

$$I_2 = G_i\delta(\mathbf{r}_1 - \mathbf{r}_2)\frac{\delta f_i[\rho(\mathbf{r}_2)]}{\delta\rho(\mathbf{r}_2)}\Gamma^{\dagger(1)}\rho_i(\mathbf{r}_1) \tag{A.60}$$

and

$$I_3 = G_i\delta(\mathbf{r}_1 - \mathbf{r}_2)\frac{\delta f_i[\rho(\mathbf{r}_2)]}{\delta\rho^*(\mathbf{r}_2)}\Gamma^{(2)}\rho_i(\mathbf{r}_1)^* \tag{A.61}$$

and

$$I_4 = \frac{1}{2} G_i\delta(\mathbf{r}_1 - \mathbf{r}_2)\frac{\delta^2 f_i[\rho(\mathbf{r}_2)]}{\delta\rho^*(\mathbf{r}_2)\delta\rho(\mathbf{r}_2)}\rho_i(\mathbf{r})^*\rho_i(\mathbf{r}). \tag{A.62}$$

Since all the coupling constants depend on the same baryon density alone and the functional forms of $f_s[\rho]$, $f_v[\rho]$, and $f_{TV}[\rho]$ are different. Since all the arguments are ρ we une in the following only the abbreviations

$$f_s = f_s[\rho(\mathbf{r})], \qquad f'_s = \frac{d}{d\rho}f_s[\rho(\mathbf{r})], \qquad f''_s = \frac{d^2}{d\rho^2}f_s[\rho(\mathbf{r})] \quad . \tag{A.63}$$

Using

$$\frac{\delta\rho(\mathbf{r}_1)}{\delta\rho(\mathbf{r})^*} = \left(\frac{\delta\rho_i(\mathbf{r}_1)}{\delta\rho(\mathbf{r})}\right)^* = 1\delta(\mathbf{r}-\mathbf{r}_1) \tag{A.64}$$

we obtain

$$I_2 = G_i f_i' \delta(\mathbf{r}_1-\mathbf{r}_2)\Gamma^{\dagger(1)}1^{(2)}\rho_i(\mathbf{r}_1) \tag{A.65}$$
$$I_3 = G_i f_i' \delta(\mathbf{r}_1-\mathbf{r}_2)1^{(1)}\Gamma^{(2)}\rho_i(\mathbf{r}_1) \tag{A.66}$$
$$I_4 = G_i f_i'' \delta(\mathbf{r}_1-\mathbf{r}_2)1^{(1)}1^{(2)}\rho_i(\mathbf{r}_1)^*\rho_i(\mathbf{r}_1). \tag{A.67}$$

Summarizing we obtain for the interaction in the various channels1:

- **Isoscalar-scalar term**

$$\hat{V}_s(\mathbf{r}_1,\mathbf{r}_2) = G_s\delta(\mathbf{r}_1-\mathbf{r}_2)[f_s\gamma_0^{(1)}\gamma_0^{(2)} + \rho_s f_s'(\gamma_0^{(1)}1^{(2)} + 1^{(1)}\gamma_0^{(2)}) + \frac{1}{2}\rho_s^2 f_s''1^{(1)}1^{(2)}], \tag{A.68}$$

- **Isoscalar-vector term**

$$\hat{V}_v(\mathbf{r}_1,\mathbf{r}_2) = G_v\delta(\mathbf{r}_1-\mathbf{r}_2)[(f_v + 2\rho f_v' + \frac{1}{2}\rho^2 f_v'')1^{(1)}1^{(2)} - f_v\alpha^{(1)}\alpha^{(2)}], \tag{A.69}$$

- **Isovector-vector term**

$$\begin{aligned}\hat{V}_{TV}(\mathbf{r}_1,\mathbf{r}_2) &= G_{TV}\delta(\mathbf{r}_1-\mathbf{r}_2)[f_{TV}(1^{(1)}1^{(2)} - \alpha^{(1)}\alpha^{(2)})\vec{\tau}^{(1)}\vec{\tau}^{(2)} \\ &+ \rho_3 f_{TV}'(\tau_3^{(1)}1^{(2)} + 1^{(1)}\tau_3^{(2)}) + \frac{1}{2}\rho_3^2 f_{TV}''1^{(1)}1^{(2)}].\end{aligned} \tag{A.70}$$

As a consequence, the rearrangement terms in the set DD-PC1 would occupy also off-diagonal terms of the interaction matrix, as we summarize in the Table 3.2 of Chapter 3.

Appendix B

Derivative Terms in the Point-Coupling Interaction

At first, we show how the gradient operator applies in the conventional RPA approach. The corresponding interaction matrix element will be written as:

$$\hat{V}^D_{1234} = \int_0^\infty \int_0^\infty d^3r_1 d^3r_2 \bar{\psi}_1(\mathbf{r}_1)\psi_3(\mathbf{r}_1)V_D(\mathbf{r}_1,\mathbf{r}_2)\bar{\psi}_2(\mathbf{r}_2)\psi_4(\mathbf{r}_2)$$

But $V_D(\mathbf{r}_1,\mathbf{r}_2) = \delta_s \frac{\delta(r_1-r_2)}{r_1 r_2}\nabla_r^2$ with $\nabla_r^2 = \frac{\partial^2}{\partial r^2} + \frac{2}{r}\frac{\partial}{\partial r} - \frac{l(l+1)}{r^2}$, so that:

$$\begin{aligned}\hat{V}^D_{1234} &= \delta_s \int_0^\infty r^2 dr\, \bar{\psi}_1(r)\psi_3(r)\left(\frac{\partial^2}{\partial r^2}\right)\bar{\psi}_2(r)\psi_4(r) \\ &+ \delta_s \int_0^\infty r^2 dr\, \bar{\psi}_1(r)\psi_3(r)\left(\frac{2}{r}\frac{\partial}{\partial r}\right)\bar{\psi}_2(r)\psi_4(r) - \delta_s \int_0^\infty r^2 dr\, \bar{\psi}_1(r)\psi_3(r)\left(\frac{l(l+1)}{r^2}\right)\bar{\psi}_2(r)\psi_4(r\end{aligned}$$

This integral can be much simplified if we solve the integrations by part and at the same time consider the relation $\int_0^\infty f(r)\frac{dg}{dr}dr = [f(r)g(r)]_{r=0}^{r=\infty} - \int_0^\infty \frac{df}{dr}g(r)dr = -\int_0^\infty \frac{df}{dr}g(r)dr$. After doing that, one gets:

$$\hat{V}^D_{1234} = -\delta_s \int_0^\infty r^2 dr(\bar{\psi}_1(r)\psi_3(r)\left(\frac{\overleftarrow{\partial}}{\partial r}\frac{\overrightarrow{\partial}}{\partial r} + \frac{l(l+1)}{r^2}\right)\bar{\psi}_2(r)\psi_4(r) \tag{B.1}$$

In other words, the gradient operator in the A-B formalism can be substituted by the much simpler

$$\nabla_r^2 = \frac{\overleftarrow{\partial}}{\partial r}\frac{\overrightarrow{\partial}}{\partial r} - \frac{l(l+1)}{r^2} \tag{B.2}$$

Gradient in Linear response equations

The gradient expression is somehow different if we try to apply it in the linearized Bethe-Salpeter equation:

$$R(r,r') = R^0(r,r') + \int_0^\infty dr_1 dr_2 R^0(r,r_1) V_D(r_1,r_2) R(r_2,r'). \tag{B.3}$$

Here, R^0 is a function of the radial wave functions $U(r) = r \cdot \psi(r)$. This is the reason why the terms r_1^2 and r_2^2 are absent from the Eq. (B.3). This is important, because the integration by parts do not lead to the operator B.2.

The integrant part of the Bethe-Salpeter equation will then be:

$$\begin{aligned} R^0(r,r') - R^0(r,r') = I &= \int_0^\infty dr_1 dr_2 R^0(r,r_1) \frac{\delta(r_1-r_2)}{r_1 r_2} \nabla_r^2 R(r_2,r') \\ &= \int_0^\infty dr_1 R^0(r,r_1) \nabla_r^2 \left(\frac{1}{r_1^2} R(r_1,r') \right) \end{aligned} \tag{B.4}$$

$$\tag{B.5}$$

Now, if we expand the gradient operator into its constituents, we get:

$$\begin{aligned} I &= \int_0^\infty dr_1 R^0(r,r_1) \left(\frac{\partial^2}{\partial r_1^2} \right) \left(\frac{1}{r_1^2} R(r_1,r') \right) \\ &+ \int_0^\infty dr_1 R^0(r,r_1) \left(\frac{2}{r_1} \frac{\partial}{\partial r_1} \right) \left(\frac{1}{r_1^2} R(r_1,r') \right) - \int_0^\infty dr_1 R^0(r,r_1) \left(\frac{L(L+1)}{r_1^2} \right) \left(\frac{1}{r_1^2} R(r_1,r') \right) \end{aligned} \tag{B.6}$$

where L is the total angular momentum of the system, which equals the angular momentum J of the excitation mode. Using again the property $\int_0^\infty f(r) \frac{dg}{dr} dr = -\int_0^\infty \frac{df}{dr} g(r) dr$, we continue the simplifying:

$$\begin{aligned} I &= -\left\{ \int_0^\infty dr_1 \left(\frac{\partial}{\partial r_1} \right) R^0(r,r_1) \left(\frac{\partial}{\partial r_1} \right) \left(\frac{1}{r_1^2} R(r_1,r') \right) \right\} \\ &+ \left\{ 2 \int_0^\infty dr_1 R^0(r,r_1) \frac{1}{r_1^3} \frac{\partial R}{\partial r_1} - 4 \int_0^\infty dr_1 R^0(r,r_1) \frac{1}{r_1^4} R(r_1,r') \right\} \\ &- \left\{ \int_0^\infty dr_1 R^0(r,r_1) \left(\frac{J(J+1)}{r_1^2} \right) \frac{1}{r_1^2} R(r_1,r') \right\} \end{aligned} \tag{B.7}$$

or

$$\begin{aligned} I &= -\left\{ \int_0^\infty dr_1 \frac{\partial R^0}{\partial r_1} \frac{1}{{r_1}^2} \frac{\partial R)}{\partial r_1} - 2 \int_0^\infty dr_1 \frac{\partial R^0}{\partial r_1} \frac{1}{{r_1}^3} R(r_1,r') \right\} \\ &+ \left\{ -2 \int_0^\infty dr_1 \frac{\partial}{\partial r_1} \left[R^0(r,r_1) \frac{1}{r_1^3} \right] R(r_1,r') \right\} \\ &- \left\{ \int_0^\infty dr_1 R^0(r,r_1) \left(\frac{J(J+1)+4}{r_1^4} \right) R(r_1,r') \right\} \end{aligned} \tag{B.8}$$

or

$$\begin{aligned} I &= -\int_0^\infty dr_1 \frac{\partial R^0}{\partial r_1}\frac{1}{{r_1}^2}\frac{\partial R}{\partial r_1} + 2\int_0^\infty dr_1 \frac{\partial R^0}{\partial r_1}\frac{1}{{r_1}^3}R(r_1,r') \\ &- 2\int_0^\infty dr_1 \frac{\partial R^0}{\partial r_1}\frac{1}{r_1^3}R(r_1,r') + 6\int_0^\infty dr_1 R^0(r,r_1)\frac{1}{r_1^4}R(r_1,r') \\ &- \int_0^\infty dr_1 R^0(r,r_1)\left(\frac{J(J+1)+4}{r_1^4}\right)R(r_1,r') \end{aligned} \tag{B.9}$$

or finally

$$\begin{aligned} R^0(r,r') - R^0(r,r') &= -\int_0^\infty dr_1 \frac{\partial R^0}{\partial r_1}\frac{1}{{r_1}^2}\frac{\partial R}{\partial r_1} - \int_0^\infty dr_1 R^0(r,r_1)\left(\frac{J(J+1)-2}{r_1^2}\right)\frac{1}{r_1^2}R(r_1,r') \\ &= -\int_0^\infty dr_1 R^0(r,r_1)\left[\frac{\overleftarrow{\partial}}{\partial r_1}\frac{1}{r_1^2}\frac{\overrightarrow{\partial}}{\partial r_1} + \frac{J(J+1)-2}{r_1^4}\right]R(r_1,r'). \end{aligned} \tag{B.10}$$

The big advantage here is that the gradient and the linear part of the interaction can be included in the same interaction channel. So, for instance, for the isoscalar-scalar part (counterpart of the isoscalar-scalar term) we will have:

$$R(r,r') = R^0(r,r') + \int_0^\infty dr_1 R^0(r,r_1)V_s(r_1)R(r_1,r') \tag{B.11}$$

where

$$V_s(r) = \left[\alpha_s F_s[\rho_s(r)]\frac{1}{r^2} - \delta_s\frac{\overleftarrow{\partial}}{\partial r}\frac{1}{r^2}\frac{\overrightarrow{\partial}}{\partial r} - \delta_s\frac{J(J+1)-2}{r^4}\right] \tag{B.12}$$

with α_s and δ_s being the coupling constants of the linear and the gradient term of the isoscalar scalar field respectively.

Numerically, $R^0(r,r_1)$ with fixed r, is an array in r_1 of dimension N. Similar is the situation for $R(r_1,r')$ where r' is fixed. The interaction $V_s(r)$ however, is a $N\times N$ matrix with only diagonal terms in the case of $\alpha_s\frac{1}{r^2}$ and $-\delta_s\frac{J(J+1)+4}{r^4}$ but with more complicated structure in the case of $-\delta_s\frac{\overleftarrow{\partial}}{\partial r}\frac{1}{r^2}\frac{\overrightarrow{\partial}}{\partial r}$. In total, the integral will be a sum over N points for the quantity:

$$I = \sum_{k=1}^{N}\bar{R}_i^0 V_{i,k}R_k\cdot h$$

with

$$V_{ik} = \left[\alpha_s - \delta_s\frac{J(J+1)-2}{r_i^2}\right]\frac{h}{r_i^2}\cdot\hat{I}_{ik} - \delta_s h\cdot\hat{D}_{ik}$$

For the numerical derivation we can use any of the methods prescribed in the literature, but we prefer the 3-points formula:

$$\frac{df(r)}{dr} = \frac{-3f(r)+4f(r+h)-f(r+2h)}{2h}$$

because in this way one describes the endpoints ($i=1$ and $i=n_{max}$) with better accuracy.

Definition from tensor derivation

One can get the same result in a much simpler way, if one make use of the fact that the radial part of the gradient operator can be also written as:

$$\Delta = -\overleftarrow{\nabla}\,\overrightarrow{\nabla}$$

We must have in mind that these two derivative terms are vectors and thus they would apply not only on the spatial but also on the angular part of the response function:

$$R(\mathbf{r},\mathbf{r}') = R(r,\mathbf{r}')\mathbf{Y}_{LM}(\Omega). \tag{B.13}$$

so that the vector harmonics $\mathbf{Y}_{LM}$ cannot be excluded from the problem. Instead, one has to apply the properties:

$$\begin{aligned}\nabla(f(r)Y_{lm}(\Omega)) = &- \sqrt{\frac{l+1}{2l+1}}\left(\frac{df}{dr} - l\frac{f(r)}{r}\right)Y_{l+1\,m}(\Omega)\\ &+ \sqrt{\frac{l}{2l+1}}\left(\frac{df}{dr} + \frac{l+1}{r}f(r)\right)Y_{l-1\,m}(\Omega)\\ &= \mathcal{U}(r)\cdot Y_{l+1\,m}(\Omega) + \mathcal{V}(r)\cdot Y_{l-1\,m}(\Omega)\end{aligned} \tag{B.14}$$

of the vector gradient operators [163]. After some calculations, we receive the following four parts:

$$\begin{aligned}I_1 &= \int_0^\infty d\Omega_1 \left[R^0(r,r_1)\overleftarrow{\mathcal{U}}(r)\overrightarrow{\mathcal{U}}(r)R(r_1,r')\right]Y_{L+1}(\Omega_1)Y^*_{L+1}(\Omega_1)\\ I_2 &= \int_0^\infty d\Omega_1 \left[R^0(r,r_1)\overleftarrow{\mathcal{U}}(r)\overrightarrow{\mathcal{V}}(r)R(r_1,r')\right]Y_{L+1}(\Omega_1)Y^*_{L-1}(\Omega_1)\\ I_3 &= \int_0^\infty d\Omega_1 \left[R^0(r,r_1)\overleftarrow{\mathcal{V}}(r)\overrightarrow{\mathcal{U}}(r)R(r_1,r')\right]Y_{L-1}(\Omega_1)Y^*_{L+1}(\Omega_1)\\ I_4 &= \int_0^\infty d\Omega_1 \left[R^0(r,r_1)\overleftarrow{\mathcal{V}}(r)\overrightarrow{\mathcal{V}}(r)R(r_1,r')\right]Y_{L-1}(\Omega_1)Y^*_{L-1}(\Omega_1)\end{aligned}$$

where of course only the first and the forth one survive, following the orthogonality relation $\int_0^\infty Y_L Y^*_{L'} d\Omega = \delta_{LL'}$. Finally, the radial part that results is equal to

$$V_D(r) = \overleftarrow{\mathcal{U}}(r)\overrightarrow{\mathcal{U}}(r) + \overleftarrow{\mathcal{V}}(r)\overrightarrow{\mathcal{V}}(r),$$

or after applying Eq. (B.14:

$$\begin{aligned}V_D(r) &= \delta_s\left[\frac{\overleftarrow{\partial}}{\partial r}\frac{1}{r^2}\frac{\overrightarrow{\partial}}{\partial r} + \frac{J(J+1)+4}{r^4} - \left(\frac{\overleftarrow{\partial}}{\partial r}\frac{2}{r^3} + \frac{2}{r^3}\frac{\overrightarrow{\partial}}{\partial r}\right)\right]\\ &= \delta_s\left[\frac{\overleftarrow{\partial}}{\partial r}\frac{1}{r^2}\frac{\overrightarrow{\partial}}{\partial r} + \frac{J(J+1)-2}{r^4}\right]\end{aligned} \tag{B.15}$$

which is exactly the same result with the one we got in Eq. (B.10) when we made use of $\Delta = \nabla^2$.

Bibliography

[1] S. Fritsch, N. Kaiser, and W. Weise, Nucl. Phys. **A750**, 259 (2005).

[2] R. B. Wiringa, V. G. Stoks, and R. Schiavilla, Phys. Rev. **C51**, 38 (1995).

[3] R. B. Wiringa, S. C. Pieper, J. Carlson, and V. R. Pandharipade, Phys. Rev. **C62**, 014001 (2000).

[4] S. C. Pieper, V. R. Pandharipade, R. B. Wiringa, and J. Carlson, Phys. Rev. **C64**, 014001 (2001).

[5] D. R. Entem and R. Machleidt, Phys. Rev. **C68**, 041001 (2003).

[6] P. Navratil, S. Quaglioni, I. Stetcu, and B. R. Barrett, J. Phys. **G36**, 083101 (2009).

[7] G. Hagen, D. J. Dean, M. Hjorth-Jensen, T. Papenbrock, and A. Schwenk, Phys. Rev. **C76**, 044305 (2007).

[8] E. Caurier, G. Martínez-Pinedo, F. Novacki, A. Poves, and A. P. Zuker, Rev. Mod. Phys. **77**, 427 (2005).

[9] T. Otsuka, M. Honma, T. Mizusaki, N. Shimizu, and Y. Utsuno, Prog. Part. Nucl. Phys. **47**, 319 (2001).

[10] W. Kohn and L. J. Sham, Phys. Rev. **137**, A1697 (1965).

[11] W. Kohn and L. J. Sham, Phys. Rev. **140**, A1133 (1965).

[12] P. Hohenberg and W. Kohn, Phys. Rev. **136**, B864 (1964).

[13] J. Goldstone, Proc. Roy. Soc. **98**, 267 (1957).

[14] K. A. Brueckner, J. L. Gammel, and H. Weitzner, Phys. Rev. **110**, 431 (1958).

[15] D. Vautherin and D. M. Brink, Phys. Rev. **C5**, 626 (1972).

[16] J. Dechargé and D. Gogny, Phys. Rev. **C21**, 1568 (1980).

[17] H. P. Dürr, Phys. Rev. **103**, 469 (1956).

[18] J. D. Walecka, Ann. Phys. (N.Y.) **83**, 491 (1974).

[19] B. D. Serot and J. D. Walecka, Adv. Nucl. Phys. **16**, 1 (1986).

[20] M. Mayer-Goeppert and J. H. D. Jensen, *Elementary Theory of Nuclear Shell Structure* (John Wiley & Sons, New York, 1955).

[21] J. D. Walecka, Ann. Phys. (N.Y.) **83**, 491 (1974).

[22] C. J. Horowitz and B. D. Serot, Phys. Lett. **B140**, 181 (1984).

[23] K. T. Hecht and A. Alder, Nucl. Phys. **A137**, 129 (1969).

[24] A. Arima, M. Harvey, and K. Shimizu, Phys. Lett. **B30**, 517 (1969).

[25] J. N. Ginocchio, Phys. Rev. Lett. **78**, 436 (1997).

[26] J. N. Ginocchio, Phys. Rep. **414**, 165 (2005).

[27] U. Hofmann and P. Ring, Phys. Lett. **B214**, 307 (1988).

[28] W. Koepf and P. Ring, Nucl. Phys. **A511**, 279 (1990).

[29] A. V. Afanasjev, S. Frauendorf, and P. Ring, in *Proc. NATO Advanced Research Workshop on "The Nuclear Many-Body Problem 2001", Brijuni, Pula, Croatia 2001*, edited by W. Nazarewicz and D. Vretenar (Kluver Academic Publishers, Dordrecht, 2002), Vol. 53, p. 103.

[30] A. V. Afanasjev and P. Ring, Phys. Rev. **C62**, 031302(R) (2000).

[31] M. M. Sharma, G. A. Lalazissis, and P. Ring, Phys. Lett. **B317**, 9 (1993).

[32] J. Boguta and A. R. Bodmer, Nucl. Phys. **A292**, 413 (1977).

[33] P.-G. Reinhard, Rep. Prog. Phys. **52**, 439 (1989).

[34] B. D. Serot, Rep. Prog. Phys. **55**, 1855 (1992).

[35] P. Ring, Prog. Part. Nucl. Phys. **37**, 193 (1996).

[36] *Lecture Notes in Physics*, edited by G. A. Lalazissis, P. Ring, and D. Vretenar (Springer-Verlag, Heidelberg, 2004), Vol. 641.

[37] D. Vretenar, A. V. Afanasjev, G. A. Lalazissis, and P. Ring, Phys. Rep. **409**, 101 (2005).

[38] J. Meng, H. Toki, S.-G. Zhou, S.-Q. Zhang, W.-H. Long, and L.-S. Geng, Prog. Part. Nucl. Phys. **57**, 470 (2006).

[39] R. Brockmann and H. Toki, Phys. Rev. Lett. **68**, 3408 (1992).

[40] P. Finelli, N. Kaiser, D. Vretenar, and W. Weise, Nucl. Phys. **A735**, 449 (2004).

[41] T. Nikšić, D. Vretenar, P. Finelli, and P. Ring, Phys. Rev. **C66**, 024306 (2002).

[42] T. Nikšić, D. Vretenar, and P. Ring, Phys. Rev. **C66**, 064302 (2002).

[43] G. A. Lalazissis, T. Nikšić, D. Vretenar, and P. Ring, Phys. Rev. **C71**, 024312 (2005).

[44] P. Manakos and T. Mannel, Z. Phys. **A330**, 223 (1989).

[45] P. Manakos and T. Mannel, Z. Phys. **A334**, 481 (1989).

[46] T. Bürvenich, D. G. Madland, J. A. Maruhn, and P.-G. Reinhard, Phys. Rev. **C65**, 044308 (2002).

[47] S. T. Belyaev, Nucl. Phys. **24**, 322 (1961).

[48] N. Tajima, Prog. Theor. Phys. **Suppl. 142**, 265 (2001).

[49] T. Gonzales-Llarena, J. L. Egido, G. A. Lalazissis, and P. Ring, Phys. Lett. **B379**, 13 (1996).

[50] M. Serra and P. Ring, Phys. Rev. **C65**, 064324 (2002).

[51] E. Litvinova and P. Ring, Phys. Rev. **C73**, 044328 (2006).

[52] D. Vretenar, H. Berghammer, and P. Ring, Nucl. Phys. **A581**, 679 (1995).

[53] P. Ring, Z.-Y. Ma, N. Van Giai, D. Vretenar, A. Wandelt, and L.-G. Cao, Nucl. Phys. **A694**, 249 (2001).

[54] Z.-Y. Ma, A. Wandelt, N. Van Giai, D. Vretenar, P. Ring, and L.-G. Cao, Nucl. Phys. **A703**, 222 (2002).

[55] D. Vretenar, T. Nikšić, and P. Ring, Phys. Rev. **C68**, 024310 (2003).

[56] Z.-Y. Ma, N. Van Giai, A. Wandelt, D. Vretenar, and P. Ring, Nucl. Phys. **A686**, 173 (2001).

[57] D. Vretenar, N. Paar, T. Nikšić, and P. Ring, Phys. Rev. Lett. **91**, 262502 (2003).

[58] D. Vretenar, P. Ring, G. A. Lalazissis, T. Nikšić, P. Finelli, and N. Paar, AIP Conf. Proc. **656**, 221 (2003).

[59] D. Vretenar, G. A. Lalazissis, R. Behnsch, W. Pöschl, and P. Ring, Nucl. Phys. **A621**, 853 (1997).

[60] D. Vretenar, N. Paar, P. Ring, and G. A. Lalazissis, Phys. Rev **E60**, 308 (1999).

[61] D. Vretenar, P. Ring, G. A. Lalazissis, and N. Paar, Nucl. Phys. **A649**, 29c (1999).

[62] Y. K. Gambhir, P. Ring, and A. Thimet, Ann. Phys. (N.Y.) **198**, 132 (1990).

[63] S.-G. Zhou, J. Meng, and P. Ring, Phys. Rev. **C68**, 034323 (2003).

[64] S. Shlomo and G. F. Bertsch, Nucl. Phys. **A243**, 507 (1975).

[65] T. Nakatsukasa and K. Yabana, Prog. Theor. Phys. Suppl. **146**, 447 (2002).

[66] J.E.Harriman, Phys. Rev. **A24**, 680 (1981).

[67] N. Argaman and G. Makov, Amer. J. Phys. **68**, 69 (2000).

[68] J. W. Negele, Phys. Rev. **C1**, 1260 (1970).

[69] T. H. R. Skyrme, Proc. Phys. Soc. (London) **A70**, 433 (1957).

[70] P. Quentin and H. Flocard, Ann. Rev. Nucl. Sci. **28**, 523 (1978).

[71] P. Bonche, H. Flocard, P.-H. Heenen, S. J. Krieger, and M. S. Weiss, Nucl. Phys. **A443**, 39 (1985).

[72] J. F. Berger, M. Girod, and D. Gogny, Comp. Phys. Comm. **61**, 365 (1991).

[73] H. P. Dürr and E. Teller, Phys. Rev. **101**, 494 (1956).

[74] H. P. Dürr, Phys. Rev. **109**, 117 (1958).

[75] M. Bender, P.-H. Heenen, and P.-G. Reinhard, Rev. Mod. Phys. **75**, 121 (2003).

[76] J. Engel, Phys. Rev. **C75**, 014306 (2007).

[77] B. G. Giraud, Phys. Rev. **C77**, 014311 (2008).

[78] N. Barnea, Phys. Rev. **C76**, 067302 (2007).

[79] J. G. Valatin, Phys. Rev. **122**, 1012 (1961).

[80] H. Kucharek and P. Ring, Z. Phys. **A339**, 23 (1991).

[81] T. Hartmann, J. Enders, P. Mohr, K. Vogt, S. Volz, and A. Zilges, Phys. Rev. Lett. **85**, 274 (2000).

[82] S. A. Chin and J. D. Walecka, Phys. Lett. **B52**, 24 (1974).

[83] D. A. Wasson, Phys. Lett. **B210**, 41 (1988).

[84] Z. Y. Zhu, H. J. Mang, and P. Ring, Phys. Lett **B254**, 325 (1991).

[85] Y. Sugahara and H. Toki, Nucl. Phys. **A579**, 557 (1994).

[86] M. Haidari and M. Sharma, Nucl. Phys. **802**, 159 (2008).

[87] P.-G. Reinhard, M. Rufa, J. Maruhn, W. Greiner, and J. Friedrich, Z. Phys. **A323**, 13 (1986).

[88] M. M. Sharma, M. A. Nagarajan, and P. Ring, Phys. Lett. **B312**, 377 (1993).

[89] G. A. Lalazissis, J. König, and P. Ring, Phys. Rev. **C55**, 540 (1997).

[90] G. A. Lalazissis, S. Karatzikos, R. Fossion, D. P. Arteaga, A. V. Afanasjev, and P. Ring, Phys. Lett. **B671**, 36 (2009).

[91] C. Fuchs, H. Lenske, and H. H. Wolter, Phys. Rev. **C52**, 3043 (1995).

[92] F. Hofmann, C. M. Keil, and H. Lenske, Phys. Rev. **C64**, 034314 (2001).

[93] F. de Jong and H. Lenske, Phys. Rev. **C57**, 3099 (1998).

[94] S. Typel and H. H. Wolter, Nucl. Phys. **A656**, 331 (1999).

[95] T. Nikšić, D. Vretenar, P. Finelli, and P. Ring, Phys. Rev. **C66**, 024306 (2002).

[96] G. A. Lalazissis, T. Nikšić, D. Vretenar, and P. Ring, Phys. Rev. **C71**, 024312 (2005).

[97] R. J. Furnstahl, B. D. Serot, and H.-B. Tang, Phys. Rev. **C36**, 441 (1997).

[98] T. Nikšić, D. Vretenar, G. A. Lalazissis, and P. Ring, Phys. Rev. **C78**, 034318 (2008).

[99] D. Bohm and D. Pines, Phys. Rev. **92**, 609 (1953).

[100] H. Berghammer, D. Vretenar, and P. Ring, Comp. Phys. Comm. **88**, 293 (1995).

[101] P. Ring and P. Schuck, *The Nuclear Many-Body Problem* (Springer-Verlag, Berlin, 1980).

[102] O. Bohigas, A. M. Lane, and J. Martorell, Phys. Rep. **52**, 267 (1979).

[103] T. Nikšić, D. Vretenar, and P. Ring, Phys. Rev. **C72**, 014312 (2005).

[104] N. Paar *et al*, Phys. Rev. **C67**, 034312 (2003).

[105] D. Vretenar, T. Nikšić, N. Paar, and P. Ring, Nucl. Phys. **A731**, 281 (2004).

[106] S. P. Kamerdzhiev, J. Speth, and G. Y. Tertychny, Phys. Rep. **393**, 1 (2004).

[107] K. Hagino and H. Sagawa, Nucl. Phys. **A695**, 82 (2001).

[108] E. Tamura, Phys. Rev. **B45**, 3271 (1992).

[109] W. Greiner, *Relativistic Quantum Mechanics* (Springer Verlag, Berlin, 1990), textbook.

[110] M. Abramowitz and I. A. Stegun, *Handbook of Mathematical Functions* (Dover Publications, New York, 1970).

[111] E. Litvinova, P. Ring, and V. I. Tselyaev, Phys. Rev. **C75**, 064308 (2007).

[112] E. Litvinova, P. Ring, and V. I. Tselyaev, Phys. Rev. **C78**, 014312 (2008).

[113] *Electric and Magnetic Giant Resonances in Nuclei*, edited by J. Speth (World Scientific, Singapore, 1991), Vol. 7.

[114] M. N. Harakeh and A. van der Woude, *Giant Resonances* (Oxford University Press, Oxford, 2001).

[115] W. Bothe and W. Gentner, Z. Phys. **106**, 236 (1937).

[116] G. C. Baldwin and G. S. Klaiber, Phys. Rev. **71**, 3 (1947).

[117] M. Goldhaber and E. Teller, Phys. Rev. **74**, 1046 (1948).

[118] P. Ring and J. Speth, Nucl. Phys. **A235**, 315 (1974).

[119] J. P. Blaizot, Nucl. Phys. **A649**, 61c (1999).

[120] G. Coló and P. F. Bortignon, Nucl. Phys. **A696**, 427 (2001).

[121] J. Piekarewicz, Phys. Rev. **C62**, 051304(R) (2000).

[122] J. Piekarewicz, Phys. Rev. **C64**, 024307 (2001).

[123] G. Coló and N. Van Giai, Nucl. Phys. **A731**, 15 (2004).

[124] J. Piekarewicz, Phys. Rev. **C76**, 064310 (2007).

[125] D. H. Youngblood, Y.-W. Lui, H. L. Clark, B. John, Y. Tokimoto, and X. Chen, Phys. Rev. **C69**, 034315 (2004).

[126] D. Vretenar, A. Wandelt, and P. Ring, Phys. Lett. **B487**, 334 (2000).

[127] R. Mohan, M. Danos, and L. C. Biedenharn, Phys. Rev. **C3**, 1740 (1971).

[128] Y. Suzuki, K. Ikeda, and H. Sato, Prog. Theor. Phys. **83**, 180 (1990).

[129] N. Ryezayeva, T. Hartmann, Y. Kalmykov, H. Lenske, P. von Neumann-Cosel, V. Y. Ponomarev, A. Richter, A. Shevchenko, S. Volz, and J.Wambach, Phys. Rev. Lett. **89**, 272502 (2002).

[130] A. Zilges, M. Babilon, T. Hartmann, D. Savran, and S. Volz, Prog. Part. Nucl. Phys. **55**, 408 (2005).

[131] D. Vretenar, N. Paar, P. Ring, and G. A. Lalazissis, Phys. Rev. **C63**, 047301 (2001).

[132] G. A. Lalazissis, J. König, and P. Ring, Phys. Rev. **C55**, 540 (1997).

[133] J. Ritman, F.-D. Berg, W. Kühn, V. Metag, R. Novotny, M. Notheisen, P. Paul, M. Pfeiffer, O. Schwalb, H. Löhner, L. Venema, A. Gobbi, N. Herrmann, K. D. Hildenbrand, J. Mösner, R. S. Simon, K. Teh, J. P. Wessels, and T. Wienold, Phys. Rev. Lett. **70**, 533 (1993).

[134] N. Paar, T. Nikšić, D. Vretenar, and P. Ring, Phys. Lett. **B606**, 288 (2005).

[135] J. Piekarewicz, Phys. Rev. **C73**, 044325 (2006).

[136] V. V. Varlamov, Yad. Konst. **1**, 52 (1993).

[137] H. Beil, R. Bergere, P. Carlos, A. Lepretre, A. de Miniac, and A. Veyssiere, Nucl. Phys. **A227**, 427 (1974).

[138] B. F. Davis, U. Garg, W. Reviol, M. Harakeh, A. Bacher, G. P. A. Berg, C. C. Foster, E. J. Stephenson, Y. Wang, J. Jnecke, K. Pham, D. Roberts, H. Akimune, M. Fujiwara, and J. Lisantti, Phys. Rev. Lett. **79**, 609 (1997).

[139] H. Clark, Y.-W. Lui, D. Youngblood, K. Bachtr, U. Garg, M. Harakeh, and N. Kalantar-Nayestanaki, Nucl. Phys. **A649**, 57c (1999).

[140] M. Uchida, H. Sakaguchi, M. Itoh, M. Yosoi, T. Kawabata, Y. Yasuda, H. Takeda, T. Murakami, S. Terashima, S. Kishi, U. Garg, P. Boutachkov, M. Hedden, B. Kharraja, M. Koss, B. K. Nayak, S. Zhu, M. Fujiwara, H. Fujimura, H. P. Yoshida, K. Hara, H. Akimune, and M. N. Harakeh, Phys. Rev. **C69**, 051301(R) (2004).

[141] G. Coló, N. Van Giai, P. F. Bortignon, and M. R. Quaglia, Phys. Lett. **B485**, 362 (2000).

[142] H. L. Clark, Y.-W. Lui, and D. H. Youngblood, Phys. Rev. **C63**, 031301(R) (2001).

[143] D. Vretenar, N. Paar, P. Ring, and T. Nikšić, Phys. Rev. **C65**, 021301 (2002).

[144] V. Dubovik and A. Cheshkov, Sov. J. Part. Nucl. **5**, 318 (1975).

[145] V. Dubovik and L. Tosunyan, Sov. J. Part. Nucl. **14**, 504 (1983).

[146] S. I. Bastrukov, S. Misicu, and V. Sushkov, Nucl. Phys. **A562**, 191 (1993).

[147] S. Misicu, Phys. Rev. **C73**, 024301 (2006).

[148] N. V. Giai and H. Sagawa, Nucl. Phys. **A371**, 1 (1981).

[149] J. F. Dawson and R. J. Furnstahl, Phys. Rev. **C42**, 2009 (1990).

[150] I. Hamamoto, H. Sagawa, and X. Z. Zhang, Phys. Rev. **C57**, R1064 (1998).

[151] G. G. Coló, N. Van Giai, P. R. Bortignon, and M. R. Quaglia, Phys. Lett. **B485**, 362 (2000).

[152] S. Shlomo and A. I. Sanzhur, Phys. Rev. **C65**, 044310 (2002).

[153] N. Paar, D. Vretenar, E. Khan, and G. Coló, Rep. Prog. Phys. **70**, 691 (2007).

[154] R. Pittan and T. Walcher, Phys. Lett. **B36**, 563 (1971).

[155] M. B. Lewis and F. E. Bertrand, Nucl. Phys. **A196**, 337 (1972).

[156] D. H. Youngblood, P. Bogucki, J. D. Bronson, U. Garg, Y. W. Lui, and C. M. Rozsca, Phys. Rev. **C23**, 1997 (1981).

[157] S. Kamerdzhiev, R. J. Liotta, E. Litvinova, and V. I. Tselyaev, Phys. Rev. **C58**, 172 (1998).

[158] J. Dobaczewski, H. Flocard, and J. Treiner, Nucl. Phys. **A422**, 103 (1984).

[159] I. Hamamoto and H. Sagawa, Phys. Rev. **C66**, 044315 (2002).

[160] T. Li, U. Garg, Y. Liu, R. Marks, B. Nayak, P. M. Rao, M. Fujiwara, H. Hashimoto, K. Kawase, K. Nakanishi, S. Okumura, M. Yosoi, M. Itoh, M. Ichikawa, R. Matsuo, T. Terazono, M. Uchida, T. Kawabata, H. Akimune, Y. Iwao, T. Murakami, H. Sakaguchi, S. Terashima, Y. Yasuda, J. Zenihiro, and M. Harakeh, Phys. Rev. Lett. **99**, 162503 (2007).

[161] S. P. Kamerdzhiev, G. Y. Tertychny, and V. I. Tselyaev, Phys. Part. Nucl. **28**, 134 (1997).

[162] E. V. Litvinova and V. I. Tselyaev, Phys. Rev. **C75**, 054318 (2007).

[163] A. R. Edmonds, *Angular Momentum in Quantum Mechanics* (University Press, Princeton, 1957).